I. DEVELOPMENT OF FACILE ROUTE TO FLUORIDE-MEDIATED, PURE-SILICA ZEOLITE THIN FILMS

II. REMOVAL OF STRUCTURE-DIRECTING AGENTS FROM MOLECULAR SIEVES VIA THE USE OF PHOTOLABILE STRUCTURE-DIRECTING AGENTS

Thesis by

Heather K. Hunt

In Partial Fulfillment of the Requirements for the

Degree of

Doctor of Philosophy

CALIFORNIA INSTITUTE OF TECHNOLOGY

Pasadena, California

2010

(Defended 28 September 2009)

© 2010

Heather K. Hunt

All Rights Reserved

Acknowledgments

The time I have spent at Caltech has been equally the most challenging and the happiest of all of my life, and I know that I will always remember Caltech and the wonderful people that I have met here with great affection. Over the last five years, I have been privileged to interact and work with truly inspiring and talented educators, researchers, mentors, authors, and administrators, and I am sincerely grateful to all of them for their guidance and support. This thesis is the culmination of several years of effort that would not have been possible without them.

First and foremost, I would like to thank my advisor, Professor Mark E. Davis, for all of his support, financial and otherwise, throughout my time here. I have been very fortunate to work in his lab, and this work would not have been possible without his efforts, suggestions, and patience when not everything worked perfectly the first time. (Or even the second or third time.) I will always be grateful to him for giving me this opportunity. I would also like to thank the members of my Candidacy and Thesis Committees, Professor Richard Flagan, Dr. Stacey Zones, Professor Yushan Yan, and Professor Julia Greer for their suggestions, support, and kindness. Professor Flagan has always been ready to discuss research problems and suggest solutions to them. Dr. Zones, at Chevron, has provided steady support and guidance, despite his busy schedule, and has led me to a deeper understanding of zeolite science. Professor Yan, at University of California, Riverside, has been like a secondary advisor to me, and has provided me with not only a group full of talented and helpful graduate students to collaborate with, but has also given me excellent suggestions on the direction of my zeolite films research and manuscript

preparation. Lastly, but certainly not least, Professor Greer has provided me with encouragement, support, and advice, in addition to access to her lab. To all of you, thank you.

In addition to my committee, I would also like to thank Dr. Allen Burton, at Chevron, for his help with modeling, zeolite identification, and synthetic suggestions. Many an unusual behavior or result would remain unexplained if not for him. I would also like to thank Dr. Sonjong Hwang, our resident solid-state NMR expert, for his help with the NMR equipment, and his advice on interpreting NMR spectra. Dr. Dongchan Jang in the Greer group was very helpful in his explanation of and instruction on the mechanical testing of the zeolite films I prepared. Additionally, in the Yan group, two students, Minwei Sun and Chris Lew, were extremely helpful in the synthesis and characterization of the zeolite films and powders we studied; Chris was especially dedicated, running capacitance measurements on sample after sample, and always sending me detailed and thoughtful explanations of the results. Lastly, I would like to thank all the members of the Davis group, past and present, who have made my time here at Caltech both educational and entertaining. Specifically, I would like to thank Dr. Eric Margelefsky for his help with organic synthesis, and for always listening when I needed someone to complain to or someone to give encouragement. His willingness especially to escape lab for ice cream was very helpful. I would also like to thank Dr. Ray Archer, for our discussions on zeolite science, and Dr. John Carpenter, my long-suffering office mate, who put up with five years of my incessant nattering about any subject under the sun without once asking me to get a

grip. These three have broadened my research horizons, helped me fix any number of equipment problems in the lab, and were always willing to help me open autoclaves.

I would also like to thank the administrators of the Women's Center, the Women Mentoring Women program, and the Caltech Animal Team, for their support. These include Dr. Felicia Hunt, Portia Harris, Dr. Candace Rypisi, Linda Taddeo, and Dr. Mike Hucka. Being involved in these organizations has allowed me to serve the Caltech community, to organize events from seminars to socials, to interact with a variety of people outside my division, and to form what I know will be lasting friendships with truly caring people. I have greatly enjoyed my time on the boards of these organizations, as well as my time in other student organizations, such as the Caltech Project for Effective Teaching, and the Caltech Dance Club.

I would also like to thank my friends for their constant support, and their willingness to drop anything if I needed help. My classmates, Shelby Hutchens, Heather McCaig, Arwen Brown, and Lisa Hochrein, have all been the best friends, partners in crime, and ardent supporters that I could have asked for when I came to graduate school. They have listened in sympathy and in laughter, and have always had time for tea. From them, I have learned a great deal about other research fields, and have been allowed to use equipment I never would have touched otherwise. With them, I have experienced all the joys and anguish of life and research at Caltech. Finally, I thank my husband, Nick Thurwanger, and my parents, Richard and Jennifer Hunt. Without their encouragement, their support, their patience, and in Nick's case, willingness to move halfway across the country, I would not

have made it to Caltech, let alone enjoyed my time here. To the three of you, I owe a debt of gratitude that I can only hope I can repay.

God bless all of you.

Abstract

This thesis consists of two projects related to the development of new routes to zeolite films. In an effort to expand the known library of pure-silica zeolites accessible in planar conformation, Part I details the development of a new synthetic technique, the vapor phase transport of fluoride, to produce pure-silica zeolite films with the LTA, CHA, STT, ITW and –SVR topologies. The films are characterized by X-ray diffraction, field emission scanning electron microscopy, X-ray energy dispersive analyses, and mechanical testing. Such pure-silica zeolite films could be useful in a variety of applications, due to their porosity, crystallinity, and general stability. For example, these materials could be employed as low dielectric constant materials, which are needed for microprocessors as the feature size is continually reduced. Upon investigation of the aforementioned zeolite powders and films, we find that the materials with the LTA topology have the lowest dielectric constant of all the pure-silica zeolites. Additionally, all the zeolites investigated, except STT, give *k*-values lower than predicted from their structures using the Bruggeman effective medium model, which has been commonly employed and found able to predict dielectric constants of amorphous silicas.

The second part of this thesis presents the development of an alternative method to thermal combustion to remove organics from zeolite pores, which can degrade zeolite films, using a photolabile structure-directing agent that can be removed from the zeolite pore space using UV photolysis. Here, the synthesis, photocleavage, and structure-directing ability of two different photolabile molecules (8,8-dimethyl-2-(2-nitrophenyl)-1,4-dioxa-8-azoniaspiro[4.5]decane hydroxide (P-SDA 1) and 1-(2-nitrobenzyl)-1H-

imidazole (P-SDA 2)), are presented and discussed. Cleavage of the photolytic P-SDA 1 is demonstrated in a homogeneous solution, and intercalated into a dealuminated zeolite FAU. The structure-directing ability of P-SDA 1 is evaluated via attempts to synthesize silicate and aluminosilicate zeolites, resulting in the formation of amorphous and layered materials. The structure-directing ability of P-SDA 2 is evaluated via attempts to produce aluminophosphate zeolites, resulting in several unknown crystalline phases, in addition to dense and hydrated phases. Lastly, complete photocleavage of P-SDA 2 within the crystalline, aluminophosphate materials is also demonstrated.

Table of Contents

Acknowledgements……..iii
Abstract……...vii
Table of Contents……ix
List of Tables……..xii
List of Figures……xiii

Part 1: Development of Facile Route to Fluoride-Mediated, Pure-Silica Zeolite Thin Films……1

Chapter 1: Introduction and Organization of Thesis Presentation……2
1.1 Introduction to Zeolites and Molecular Sieves.....2
1.2 Synthesis and Formation of Zeolites……...5
1.3 Zeolite Applications……...9
1.4 Thesis Organization……..10
1.5 References……12

Chapter 2: Introduction to Part I of Thesis 20
2.1 Introduction 20
2.2 Zeolite Film and Membrane Synthetic Strategies 23
2.2.1 Support Choice and Modification 24
2.2.2 Synthetic Strategies 25
2.2.2.1 Hydrothermal Techniques.....26
2.2.2.2 Non-hydrothermal Techniques 32
2.2.3 Characterization Techniques 34
2.2.4 Defect Elimination.....35
2.3 Development of New Synthetic Techniques 36
2.4 References 38

Chapter 3: In Situ Crystallization of Fluoride-Mediated, Pure-Silica Zeolite Thin Films……... 44
Abstract 44
3.1 Introduction 45
3.2 Results and Discussion.....51
3.2.2 Seeding and Diluting the Zeolite Precursor Gel 51
3.2.3 Vapor Phase Transport of Fluoride.....56
3.3 Conclusions.....67
3.4 Experimental.....68
3.4.1 Synthesis of Structure-Directing Agent (4-methyl-2,3,6,7-tetrahydro-1H,5H-pyrido [3.2.1-ij] quinolinium hydroxide).....68
3.4.2 Synthesis of ITQ-29 (LTA) Films and Powder Via Seeding / Diluting.....69
3.4.3 Synthesis of ITQ-29 (LTA) Films and Powder Via Vapor Phase Transport of Fluoride.....70

3.4.4 Characterization 72
3.5 References 73

Chapter 4: Investigation of Dielectric Properties of Fluoride-Mediated, Pure-Silica Zeolite Thin Films 77
Abstract 77
4.1 Introduction 78
4.2 Results and Discussion 90
4.3 Conclusions 104
4.4 Experimental 105
4.4.1 Synthesis of Structure-Directing Agent A (1,2,3-trimethylimidazolium hydroxide) 105
4.4.2 Synthesis of Structure-Directing Agent B (N,N,N-trimethyl-1-adamantylammonium hydroxide) 105
4.4.3 Synthesis of Structure-Directing Agent C (Hexamethylene-1,6-bis-(N-methyl-N-pyrrolidinium) hydroxide) 106
4.4.4 Surface Modification of the Substrates 107
4.4.5 Synthesis of Fluoride-Mediated, Pure-Silica Zeolite Films and Powder 107
4.4.6 Characterization 109
4.5 References 111

Part II: Removal of Structure-Directing Agents from Molecular Sieves Via the Use of Photolabile Structure-Directing Agents 115

Chapter 5: Introduction to Part II of Thesis 116
5.1 Introduction 116
5.2 Photolabile Structure-Directing Agents 124
5.3 Photochemical Protecting Groups in Organic Synthesis 126
5.3.1 2-Nitrobenzyl Family 127
5.3.2 Benzyloxycarbonyl Family 130
5.3.3 3-Nitrophenyl Family 131
5.3.4 Phenacyl Family 132
5.4 Photofunctional Zeolites 133
5.5 Development of a Photolabile Structure-Directing Agent 135
5.6 References .....

Chapter 6: Photolabile Structure-Directing Agents for Zeolite Synthesis 142
Abstract 142
6.1 Introduction 142
6.2 Results and Discussion 145
6.2.1 P-SDA 1 Synthesis 145
6.2.2 Photolysis of P-SDA 1 150
6.2.3 Zeolite Synthesis Using P-SDA 1 155
6.3 Conclusions 160

6.4 Experimental 161
6.4.1 Synthesis of P-SDA 1 161
6.4.1.1 Ketalization Reaction 161
6.4.1.2 Amine Quaternization Reaction 162
6.4.2 Photocleavage of P-SDA 1 163
6.4.2.1 Homogeneous Cleavage of P-SDA 1 163
6.4.2.2 Photocleavage of P-SDA 1 Intercalated within Tosoh 390-HUA, a Dealuminated Zeolite X (Structure Code FAU) 163
6.4.3 Zeolite Synthesis with P-SDA 1 164
6.4.4 Characterization 166
6.5 References 167

Chapter 7 : An Imidazole-Based, Photolabile Structure-Directing Agent for the Synthesis of Aluminophosphate Zeolites 170
Abstract 170
7.1 Introduction 171
7.2 Results and Discussion 175
7.2.1 P-SDA 2 Synthesis 175
7.2.2 Aluminophosphate Zeolite Synthesis Using SDA 2 179
7.2.3 Aluminophosphate Zeolite Synthesis Using P-SDA 2 184
7.2.4 Photocleavage of P-SDA 2 within Aluminophosphate Material .. 190
7.3 Conclusions 196
7.4 Experimental 197
7.4.1 Synthesis of P-SDA 2 197
7.4.2 Synthesis of Aluminophosphate Zeolites with SDA 2 and P-SDA 2 198
7.4.3 Synthesis of Metal-Substituted Aluminophosphate Zeolites with SDA 2 and P-SDA 2 198
7.4.4 Photocleavage of P-SDA 2 in As-Made Aluminophosphate and Metal-Substituted Aluminophosphate Materials 199
7.4.5 Characterization 200
7.5 References 200

Chapter 8: Summary and Conclusions 203
1. Summary and Conclusions 203
2. Future Directions 211

List of Tables

Chapter 3

Table 3.1 Energy dispersive spectrometry (EDS) data of the amorphous precursor film supported on OH-(100) Si demonstrates that the film is pure-silica, with the carbon content appearing due to the TMAOH and SDA in the precursor gel. EDS data for the calcined sample indicates that the carbon content has been completely removed. 65

Chapter 4

Table 4.1 Dielectric constant (k) of various pure-silica zeolite powders measured at 2 GHz 98
Table 4.2 Synthesis conditions for zeolite films and powders..... 109

Chapter 6

Table 6.1 Synthesis conditions for zeolite synthesis using P-SDA 1 as the structure-directing agent 158

Chapter 7

Table 7.1 Results of $AlPO_4$ syntheses attempted with SDA 2 (A = amorphous, DP = dense phase, #1 = ATS / unknown phase, #2 = AFI / tridymite)..... 180
Table 7.2 Results of magnesium-substituted aluminophosphate runs using SDA 2 at 150, 175, and 200 °C (A = Amorphous) 182
Table 7.3 Results of attempted aluminophosphate zeolite syntheses with P-SDA 2 as the structure-directing agent (3 = unknown hydrated phase, 4 = unknown phase, 5 = unknown phase, 6 = ATS / unknown phase, 7 = ATV / dense phase, DP = dense phase) 185
Table 7.4 Results of attempted metal-substituted, aluminophosphate zeolite syntheses with P-SDA 2 as the structure-directing agent..... 190

List of Figures

Chapter 2

Figure 2.1 Schematic representation of the three categories of nanostructured, planar zeolite and zeolite-based configurations 22
Figure 2.2 Synthetic strategies for the formation of zeolite and zeolite-based films and membranes 26
Figure 2.3 Models of zeolite and zeolite-based film formation for in situ synthetic techniques 28
Figure 2.4 Silicalite (MFI) polycrystalline film grown via *in situ* techniques showing a loose layer of MFI crystals on the surface 29
Figure 2.5 Schematic of the vapor phase transport method for film formation ... 31

Chapter 3

Figure 3.1 Schematic of the synthesis process of fluoride-mediated zeolite films by the seeding / diluting modification to in situ crystallization 49
Figure 3.2 Schematic of the synthesis process of fluoride-mediated, pure-silica zeolite LTA films by the vapor phase transport of fluoride 50
Figure 3.3 PSZ ITQ-29 (LTA) film synthesis attempts using various substrates, seed amounts, and dilutions 53
Figure 3.4 Al-free ITQ-29 (LTA) film synthesis attempts using various substrates, seed amounts, and dilutions 54
Figure 3.5 (a) Substrate submerged in ITQ-29 precursor gel of appropriate molar composition, (*i*) Stir to hydrolize the TEOS; (b) Substrate subjected to dip-coating, (*ii*) Dip-coat substrates, 5x, in the hydrolyzed gel to create amorphous precursor film; (c) Coated substrate and bulk precursor gel placed inside vacuum desiccator, (*iii*) Evaporate ethanol produced during hydrolysis and excess H_2O; (d) Amorphous precursor film and solid (dry) gel; (e) Introduce dry gel into Teflon®-lined Parr Autoclave after addition of HF (aq) to dry gel, introduce coated substrate (no HF present in amorphous film) into autoclave on elevated Teflon® platform, and crystallize via VPTM 57
Figure 3.6 X-ray diffraction patterns of as-made, calcined and polished PSZ LTA film samples on OH-(100) Si demonstrates phase crystallization of the precursor film using the VPTM of fluoride 62
Figure 3.7 FE SEM micrographs of (a) surface of calcined PSZ LTA film; (b) a thin section of calcined PSZ LTA film showing ~ 115 μm thick film; (c) surface of calcined PSZ LTA film after mechanical polishing; (d) a thin section of calcined PSZ LTA film after polishing showing ~ 1.7 μm thick film 64
Figure 3.8 Load / displacement curves for the PSZ ITQ-29 films on (100) Si wafers indicate that different elastic moduli are obtained at different indentation sites 66

Chapter 4

Figure 4.1 Cartoon of a parallel-plate capacitor with a dielectric medium polarized by an electric field, E 80
Figure 4.2 (a) Metal-insulator-metal structures used for parallel-plate capacitance measurements; (b) Schematic of a time-domain reflectometer (TDR) coupled with transmission line for dielectric measurements of powder samples (used with permission)[7] 81
Figure 4.3 (a) LTA framework, viewed along the [001] axis; (b) CHA framework, viewed normal to the [001] axis; (c) STT framework, viewed normal to the [100] axis; (d) ITW framework, viewed along the [100] axis;[37] (e) -SVR framework, viewed along the [001] axis (courtesy of A. Burton, Chevron) 89
Figure 4.4 X-ray diffraction patterns of calcined and polished (a) PSZ CHA films on (100) Si; (b) PSZ STT films on (100) Si; (c) PSZ ITW films on (100) Si; (d) PSZ -SVR films on (100) Si..... 91
Figure 4.5 FE SEM micrographs of (a) surface of calcined PSZ CHA film; (b) surface of calcined PSZ STT film; (c) surface of PSZ CHA / STT intergrowth; (d) calcined, polished PSZ STT film; (e) surface of calcined PSZ ITW film; (f) surface of calcined PSZ -SVR film; (g) surface of calcined, polished PSZ -SVR film; (h) thin section of a typical PSZ STT film after mechanical polishing, showing ~ 1.7 μm thick film with variable height..... 94
Figure 4.6 *k*-values obtained for PSZ thin film of *MRE, MFI, BEA*, and LTA topologies made by *in situ* (MFI and BEA*) and vapor phase transport methods (*MRE and LTA) 96
Figure 4.7 Effective dielectric constant of pure-silica CHA measured over a range of frequencies..... 98
Figure 4.8 Effective dielectric constant of pure-silica STT measured over a range of frequencies..... 99
Figure 4.9 Effective dielectric constant of pure-silica ITW measured over a range of frequencies..... 99
Figure 4.10 Effective dielectric constant of pure-silica -SVR measured over a range of frequencies..... 100
Figure 4.11 *k*-values obtained for fluoride-mediated, PSZ powders of MFI, ITW, FER, -SVR, STT, CHA, and LTA topologies via TDR 103

Chapter 5

Figure 5.1 Schematic representation of the results of thermal stresses on zeolite films during calcination: (a) cracking at film / substrate interface if film is not well-adhered to substrate, (b) cracking within film if film is well-adhered to substrate 118
Figure 5.2 Schematic of zeolite film patterning using UV / ozonolysis photochemical “calcination” treatment to remove occluded organics.....120
Figure 5.3 Cleavage reaction of ketal-containing structure-directing agent into smaller fragments[21] 122

Figure 5.4 Recyclable structure-directing agent route – (1) zeolite synthesis; (2) cleavage of the organic molecules inside the zeolite pores; (3) removal of the cleaved fragments; (4) recombination of the fragments into the original SDA molecule[2] 122
Figure 5.5 Various acid-cleavable ketal structure-directing agents [21] 123
Figure 5.6 Examples of the 2-nitrobenzyl family of photochemical protecting groups: (a) 2-nitrobenzyl group, (b) 2-nitrobenzyloxycarbonyl, and (c) 2-nitrophenylethyleneglycol 128
Figure 5.7 Schematic of the 2-nitrobenzyl group cleavage mechanism via hydrogen abstraction 130
Figure 5.8 Examples of the benzyloxycarbonyl family of photochemical protecting group: (a) benzyloxycarbonyl group, and (b) 3,5-dimethoxybenzyloxycarbonyl 131
Figure 5.9 Examples of the 3-nitrophenyl photochemical protecting group: (a) 3-nitrophenylhydroxide, and (b) 3-nitrophenyloxycarbonyl 132
Figure 5.10 The phenacyl photochemical protecting group family.....132
Figure 5.11 P-SDA 1, 8,8-dimethyl-2-(2-nitrophenyl)-1,4-dioxa-8-azoniaspiro[4.5] decane 136
Figure 5.12 P-SDA 2, 1-(2-nitrobenzyl)-1H-imidazole.....137

Chapter 6

Figure 6.1 (a) Acid-cleavable structure-directing agent 8,8-dimethyl-2-phenyl-1,4-dioxa-8-azoniaspiro[4,5]decane hydroxide; (b) potential photolabile structure-directing agent, 8,8-dimethyl-2-(2-nitrophenyl)-1,4-dioxa-8-azoniaspiro[4.5]decane hydroxide 145
Figure 6.2 Proposed synthetic route for the preparation of P-SDA 1: (*i*) ketalization reaction; (*ii*) quaternization of the secondary amine; (*iii*) ion exchange of the quaternary amine counter-ion.....146
Figure 6.3 ^{1}H NMR spectrum of P-SDA 1 in its iodide salt form.....148
Figure 6.4 TGA data of P-SDA 1 prior to conversion of quaternary ammonium iodide salt form to quaternary ammonium hydroxide material.....149
Figure 6.5 Photolysis mechanism of P-SDA 1, generating 2-hydroxy-1-(2-nitrosophenyl)ethanone and 1,1-dimethyl-4-oxopiperidinium.....151
Figure 6.6 ^{13}C CPMAS NMR spectra of: (a) P-SDA 1 in the iodide salt form; (b) P-SDA 1 intercalated into the pure-silica zeolite with the FAU structure; (c) results of initial attempts to photocleave P-SDA 1 intercalated into the pure-silica FAU material demonstrate that cleavage did not occur, as the NMR data did not change 153
Figure 6.7 TGA data of P-SDA 1 intercalated in pure-silica zeolite FAU.....154
Figure 6.8 IR spectra of (a) P-SDA 1; (b) P-SDA 1 subjected to photolysis while intercalated in pure-silica zeolite FAU 155
Figure 6.9 Schematic representation of P-SDA 1 in zeolite BEA* (docking calculations performed by A. Burton at Chevron).....156

Figure 6.10 ^{13}C CPMAS NMR spectrum of P-SDA 1 in materials containing MFI crystals shows the molecule is still intact 159

Chapter 7

Figure 7.1 (a) 1-(2-nitrobenzyl)-1H-imidazole (P-SDA 2) ; (b) 1-benzyl-1H-imidazole (SDA 2) 173
Figure 7.2 Photolysis of P-SDA 2 proceeds via an intramolecular hydrogen abstraction from the carbon-hydrogen bond ortho to the nitro group to yield carbonyl and nitroso groups in the ortho position 173
Figure 7.3 IR absorbance spectrum of P-SDA 2 176
Figure 7.4 ^{13}C CP MAS NMR spectrum of P-SDA 2 at a spin rate of 6,000 177
Figure 7.5 TGA data for P-SDA 2 178
Figure 7.6 XRD patterns of aluminophosphate zeolites made with SDA 2: (bottom) ATS / unknown phase; (top) AFI / tridymite dense phase 180
Figure 7.7 Framework schematic of the aluminophosphate zeolites phases: (a) ATS, viewed along the [001] axis; (b) AFI, viewed along the [001] axis with projection down the [001] axis on the upper right[18] 181
Figure 7.8 XRD pattern of the ATS phase from the compositions in Table 7.2 ...183
Figure 7.9 XRD patterns of as-made aluminophosphate materials produced using P-SDA 2 as the structure-directing agent: (a) phase 3; (b) phase 4; (c) phase 5; (d) phase 6; and calcined phase 5: (e) ATV / dense phase 186
Figure 7.10 ^{13}C CPMAS NMR spectrum of the as-made, crystalline, aluminophosphate phase 5 produced using P-SDA 2 as the structure-directing agent 187
Figure 7.11 TGA data of the as-made, aluminophosphate phase 5, produced using P-SDA 2 as the structure-directing agent 188
Figure 7.12 ^{13}C CPMAS NMR spectrum of as-made, aluminophosphate material produced using P-SDA 2 as the structure-directing agent, after UV irradiation 191
Figure 7.13 TGA data of the cleaved and extracted aluminophosphate material .192
Figure 7.14 XRD patterns of: (bottom) the as-made phase 5 sample; (top) the photocleaved phase 5 sample 193
Figure 7.15 IR spectra of photocleaved and extracted phase 5 sample 193
Figure 7.16 SEM micrographs of: (a) photocleaved phase 5 crystals and aggregates; (b) calcined ATV / dense phase material crystals and aggregates 195
Figure 7.17 Synthesis of P-SDA 2 via photochemical protection of the amino functionality of the imidazole 197

Part I:

Development of Facile Route to Fluoride-Mediated, Pure-Silica Zeolite Thin Films

Chapter 1: Introduction and Organization of Thesis Presentation

1. Introduction to Zeolites and Molecular Sieves

Zeolites and molecular sieves comprise a class of microporous (0.2–2 nm pore size), crystalline oxide minerals whose structure arises from a three-dimensional network of atoms such as Si, Al, Ga, Ge, Zn, Be, etc. These tetrahedrally coordinated atoms, or T-atoms, are coordinated to four oxygen atoms and are linked to other T-atoms by sharing each oxygen with a neighboring T-atom tetrahedron.[1,2] This results in a framework ratio of oxygen to T-atoms of two. While pure silica materials have a neutral electronic structure due to the Si^{4+} ion, other oxide compositions, such as the aluminosilicates, have an overall charge resulting from the tetrahedral coordination of the Al^{3+} ions.[3] This requires the introduction of extra-framework cations to balance the net charge on the framework; the number of these cations depends on the amount of Al T-atoms in the material. Typically, these cations are protons, inorganic cations such as alkali and alkaline earth metals, ammonium ions, and / or organic cations. The general empirical formula for the composition of a zeolite is: $Al_2O_3 \bullet x\ SiO_2 \bullet y\ H_2O \bullet M_{2/n}O$, where M is a cation. The ratio of silica (SiO_2) to alumina (Al_2O_3) is variable, but because aluminum tetrahedra do not sit in adjacent positions due to the bond angle strain that would impose, it is always equal to or greater than two. The various combinations of tetrahedral SiO_4 and AlO_4^- units form a wide array of topologies with one-, two-, and / or three-dimensional pores. The pore architecture can be interconnected, with cages and channels fronted by rings of T-atoms of different sizes and shapes, and can contain water molecules and cations in the interior of the architecture. It is this crystalline pore structure that gives zeolites their unique and inherent ability to selectively adsorb

molecules based on shape and size; for this reason, zeolites are referred to as "molecular sieves".[4]

The traditional definition of a zeolite is a crystalline, microporous *aluminosilicate*. A distinction is then made between zeolites and molecular sieves: while all zeolites are molecular sieves, not all molecular sieves are zeolites. As mentioned above, molecular sieve materials can have a wide array of chemical compositions based on framework ion substitution (not necessarily isoelectronic substitution, however), while still maintaining the structural aspects of zeolites. For instance, purely siliceous molecular sieves can be made with framework topologies analogous to aluminosilicates, but these would not be technically zeolites (although they are often referred to as "pure-silica zeolites"). Other framework substitutions may be made, generating classes of materials with aluminophosphate, metalloaluminate, metallosilicate, germanosilicate, etc., compositions, each resulting in different chemical properties. For instance, neutral frameworks, such as the silicates, are more hydrophobic than charged frameworks, and exhibit low ion exchange capacity, since cations are not required to stabilize the framework. All, however, maintain the unique crystalline structure that gives rise to both the molecular sieving action and the improvement in mechanical strength over amorphous materials. More recent definitions of zeolites focus more on their pore structure and guest-host molecular interactions, rather than their chemical composition, resulting in a broader definition of zeolites with an empirical formula of $C_x[Si_{(1-y)}T_yO_{(2+x)}]A_v \bullet wM$, where C represents the nonframework cations, A the anions, M the neutral species, and T the

atoms that structurally replace the silicon atoms in the framework.[5] In this thesis, we will refer to zeolites using this broader definition.

Zeolite nomenclature can be particularly complex, as each new zeolite composition and topology synthesized may be given use-names or trade-names based on the research group, the composition, the topology, etc. For instance, Linde type D describes a zeolite with the chabazite structure (a natural zeolite) made by Union Carbide. Additionally, there are many more zeolites that can be synthesized, in terms of composition and structure, in a laboratory than in nature. Natural zeolites are given typical mineral names, such as ferrierite, barrerite, mordenite, etc., which are not usually named based on structure or composition, but rather the place the mineral was found or the scientist who found it. When a zeolite is synthesized that is isostructural with a natural zeolite, it can be named based on that zeolite or modified to represent synthetic conditions, but when a zeolite with a new topology is created, how is it named? In response to this problem, the International Union of Pure and Applied Chemistry (IUPAC) Commission on Zeolite Nomenclature and the International Zeolite Association (IZA) have developed a series of rules governing the naming of zeolite structures using three letter structure codes. All zeolites, natural or synthetic, can be described in terms of their topology using these designations. To date, the IZA has recognized 191 zeolite topologies, many with a variety of framework compositions.[6] For instance, the structure code "LTA" is based on the original trade-name of "Linde type A," and comes in a variety of aluminosilicate, silicate, and germanosilicate compositions. In its aluminosilicate composition, it can also have various cation guests. Therefore, in literature reports, zeolites with the LTA

structure can be denoted as zeolite A, NaA (for the sodium cation), 5A (for the pore size), pure-silica zeolite A, ITQ-29 (for the university that created the silicate and germanosilicate compositions), etc., each of which defines something different about the composition or synthetic conditions. The physicochemical properties of a given zeolite, with a defined composition and pore architecture, may be tailored by framework substitution, as mentioned earlier, dealumination / realumination, ion exchange of the charge-balancing cations, insertion of catalytically active guest molecules, such as transition metal ions, metal complexes, basic alkali metals, and metal oxide clusters, through guest-host interactions, and functionalization of the interior and / or exterior of the zeolite surface. For instance, Jones and Davis prepared pure-silica zeolite of the BEA* topology that contained sulfonic acid via silica functionalization techniques to study the synthesis of 2,2-pentamethylene-1,3-dioxolane via the acid catalyzed reaction of cyclohexane with ethylene glycol.[7] Functionalization and insertion of guest molecules can also be used to modify the accessible portions of the pore architecture, or to decrease the size of the pore channels and cages; this technique has been used extensively in the design of mesoporous, non-zeolite materials.[8] The ability to tailor zeolites in these ways makes them ideal candidates for the development of novel, porous materials.

2. Synthesis and Formation of Zeolites

Zeolites are generally synthesized hydrothermally from a precursor gel containing T-atom precursors, inorganics or organic cations, mineralizing agents, and water. T-atom precursors include, but are not limited to, (a) silica sources such as fumed silica, tetraethylorthosilicate (TEOS), colloidal silica, and dried silica gels, (b) alumina sources

such as aluminum metal, aluminum hydroxide gels, and sodium aluminate, and (c) heteroatom (B, Zn, Ga, Ge, etc.) sources such as nitrates, acetates, and oxides. Inorganic cations can be introduced as strong bases, such as NaOH and KOH, or as fluoride-containing acids, such as HF or NH_4F, which also introduces sources for the mineralizing agent. The mineralizing agent, either OH^- or F^-, cleaves Si-O bonds. Organic cations, which are referred to as "structure-directing agents", are typically quaternary ammonium compounds, such as tetrapropylammonium hydroxide. The selection of the gel composition plays an important role in determining the final structure of the zeolite.

For instance, the structure-directing agent, or SDA, can direct the formation of a specific crystalline structure, but it does not generally act as a true template (imposing its shape on the final pore structure of the zeolite). The effects of the SDA on the resulting zeolite depend more on the shape and size of the molecule than its inherent chemical properties, and for small SDAs in zeolites undergoing hydrothermal crystallization at high temperatures, the shape itself is not critical, as thermal motions of the SDA can mask the shape.[9] The potential for size and shape dependence can be seen through the synthesis of ZSM-48 (structure code *MRE) and ZSM-5 (structure code MFI). Both zeolites contain 10-membered rings (that is, pores structures enclosed by rings containing 10 T-atoms linked together), but ZSM-48 has a one-dimensional pore structure, where ZSM-5 has a three-dimensional structure. ZSM-48 is formed using either linear molecules, such as diethylamine or dipropylamine as the SDA, while ZSM-5 is formed using tripropylamine or triethylamine; thus, the presence of a branched SDA produces the three-dimensional pore architecture of ZSM-5.[9] The choice of heteroatom affects the bond lengths and

angles (Si-O-X, where X is a heteroatom), resulting in different "building blocks", or combinations of tetrahedral units, and therefore the overall pore structure. The presence or absence of alkali metal cations, such as Na and K, accelerates the nucleation and growth of crystals, probably through the polymerization reactions of the silicate species in solution.[10] The choice of mineralizing agent can affect the final crystal size, defect density (concentration of silanols sites, Si-O-H), and framework density attainable. For instance, using F^- as the mineralizing agent has been shown to stabilize the formation of open-framework (low density), pure-silica zeolites with very low framework density. It also tends to produce large (~ 10 μm) crystallites.[11,12,13] All of these precursor gel choices affect the final synthetic result.

In addition to the gel chemistry, the choice of reaction conditions plays a role in determining the final crystalline structure. These include reaction time, reaction temperature, presence of seeds, aging of the precursor gel, and static vs. rotating crystallization conditions. Zeolites are generally crystallized at temperatures ranging between 100 – 200 °C and for times of a few hours to several months. Because zeolites are not the thermodynamic product of synthesis (this is dense quartz for pure-silica zeolites), but are instead kinetically trapped phases, the selection of lower temperature conditions favors the selection of more open-framework, or less dense, structures. Additionally, the use of pre-formed zeolite seeds can both encourage the formation of a specific crystalline structure in a gel that might otherwise form a mixture of zeolite topologies, and it can decouple the nucleation and growth steps of zeolite formation, leading to larger crystallites.[11,14] Lastly, longer reaction times can result in different

crystalline products from the same precursor gel; for instance, CIT-6 (structure code BEA*) and VPI-8 (structure code VET) crystallize in three and seven days, respectively, from the same zincosilicate gel.[15,16] By varying these conditions, novel zeolite structures may be obtained.

Despite the knowledge of how various gel and reaction conditions affect the final zeolite product, the mechanism for zeolite formation remains not fully understood. Studies of the synthesis of the pure-silica zeolite known as silicalite (structure code MFI), which is a simple model system whose precursor gel contains only tetraethylorthosilicate, tetrapropylammonium hydroxide (the SDA and mineralizing agent), and water, have provided some insight into zeolite formation.[17,18,19,20] These studies suggest that in the zeolite precursor gel, the hydrated SDA loses its hydration sphere and interacts with the inorganic silica species via van der Waals interactions. The increase in entropy in the gel is the driving force for the formation of aggregates from smaller building blocks (5 nm building blocks have been observed by small angle X-ray scattering experiments) or crystal nuclei. These aggregates grow into larger silicalite crystallites (50 – 100 nm), and continue to grow in size over the crystallization period, suggesting Ostwald ripening. The effects of nanoparticles and their formation has been shown to play a similar role in the production of aluminosilicates.[21] The implication of full understanding of the formation mechanism would be profound: with this knowledge, zeolites could be rationally designed even beyond our current modification capabilities by the proper selection of SDAs, heteroatoms, reaction conditions, etc., for their specific end use. This is the goal of a large selection of past and current zeolite research.

3. Zeolite Applications

Due to their compositional variety, uniform pore space, and structural symmetry, zeolites have high surface areas, the ability to sieve molecules based on size- and shape-selectivity, and internal physicochemical properties that can range from acidic to basic and hydrophobic to hydrophilic.[22] The unique, and tunable, physicochemical properties of zeolites have led to their use in a wide array of applications. For instance, due to (a) their high ion-exchange capacity if not created with a neutral framework, and (b) their ability to adsorb water and small molecules very easily, they have been used for gas purification, desiccation, and water softening. Because of (c) their shape and size selectivity, they are useful for separation processes; for example, ITQ-12 (structure code ITW) has been shown to selectively separate propane and propene from its mixtures.[23,24] Lastly, due to (d) the presence of Brønsted acid sites when a proton balances a negative charge of an alumina site is the basis for their use as a heterogeneous catalyst in applications such as catalytic cracking, hydrocracking, hydroisomerization, alkylation, methanol to gasoline conversion, NO_x reduction, etc. They may also be used as a shape- or size-selective catalyst, as total selectivity occurs when the gas molecules are similar in size to the pore apertures.[25] The combination of (c) and (d) makes them useful for combining reaction and separation operations, which could significantly reduce the operating and capital costs of industrial chemical syntheses by replacing thermal separation processes. This application makes use of the selectivity of the pore size, the chemical nature of the permeating molecules, and the adsorption properties of the zeolite to, for instance, selectively separate n-hexane from branched isomers in a

hydroisomerization membrane reactor using silicalite, the pure-silica composition of the zeolite with structure code MFI (linear alkanes are preferentially adsorbed and supplied to the catalyst).[26] While many of these applications use zeolites in compressed powder form, such as pellets or granules, more recent applications frequently use zeolites in planar (thin film or membrane) form. For instance, zeolites have been suggested for use as separation membranes[27,28,29,30,31,32], membrane reactors[25,33,34], adsorption coatings[35], catalytic coatings[36,37], heat pumps[38,39], chemical sensors[40,41,42,43,44], and low dielectric constant (*k*) materials for semiconductors.[45,46,47,48,49,50,51,52,53,54,55,56,57,58,59] For these reasons, the study and development of zeolites and their uses is of great importance scientifically and industrially.

4. Thesis Organization

This thesis consists of two separate pieces of research into zeolite science. Both, however, are rooted in the development of new synthetic routes to zeolite films.

Part I presents the development of a new methodology of producing fluoride-mediated, pure-silica zeolite films, primarily for low-*k* applications. Chapter 2 provides a general introduction into zeolite films and membranes. This chapter contains information on how films and membranes are created, including support choice, synthetic strategies, characterization techniques, defect identification and elimination, the development of novel synthetic techniques, and a short discussion of selecting methods based on application intent. Chapter 3 discusses the need for the development of new methods to synthesize fluoride-mediated, zeolite thin films, and examines two novel methods for this purpose. The first method utilizes a seeding and dilution modification to typical *in situ*

film syntheses, while the second applies the vapor phase transport method to the zeolite mineralizing agent, fluoride, to crystallize a precursor film deposited by dip-coating techniques. Both methods are evaluated via the synthesis of the silicate and germanosilicate compositions of the ITQ-29 zeolite (structure code LTA) thin films on a variety of substrates. The chapter also discusses film characterization to elucidate film quality, and suggests how the new methods could extend the current library of zeolite films available. Chapter 4 uses the methodology developed in Chapter 3 to demonstrate the film synthesis of the pure-silica zeolites with structure codes CHA, STT, ITW, and -SVR. Using these zeolites, as well as the pure-silica LTA from Chapter 3, we investigate their applicability for low-*k* materials using two different techniques for measuring the dielectric constant of the materials. Through this investigation, we demonstrate that these materials are appropriate for low-*k* applications, especially the LTA topology, which we found to have the lowest intrinsic dielectric constant of all the pure-silica zeolites. Additionally, we show that the Bruggeman effective medium correlation, which is a model for the behavior of a material's dielectric constant based on its porosity, is applicable to zeolites, but it does not take into account the effects of pore structure, which we show also plays a role in determining the dielectric constant of the material.

Part II is focused on the development of a new synthetic strategy for removing the structure-directing agent from the pores of zeolite films and membranes, a task usually accomplished via thermal calcination, which can structurally damage films and membranes. Here, we propose and test the use of a photo-cleavable structure-directing agents that can be disassembled through photolysis within the zeolite pore space and

removed after zeolite formation. Chapter 5 introduces the subject, and discusses the need for this new route, its potential compatibility with various zeolite applications, and the requirements for developing new structure-directing agents. Chapter 5 also contains a brief review of organic photo-protecting groups, which could be used to develop a photolabile structure-directing agent, including their stabilities, cleavage mechanisms and compatibility with zeolite syntheses. It concludes with a discussion of the 2-nitrobenzyl family of photo-protecting groups, which has the potential to be an appropriate choice for zeolite syntheses. Chapters 7 and 8 discuss attempts to synthesize zeolites (silicates, aluminosilicates, and aluminophosphates) using two different photolabile structure-directing agents, and demonstrate the feasibility of the photolabile structure-directing agent route. Chapter 9 concludes the thesis, summarizes Parts I and II, and discusses future opportunities for using the techniques developed here for novel applications, such as zeolite film patterning.

5. References

[1] Yan, Y. & Wang, H. in *Encyclopedia of Nanoscience and Nanotechnology* Vol. X (ed H. S. Nalwa) 1-19 (American Scientific Publishers, 2003).

[2] Szostak, R. *Molecular Sieves: Principles of Synthesis and Identification*. 2nd ed., (Blackie Academic & Professional, 1998).

[3] Davis, M. E. & Lobo, R. F. Zeolite And Molecular-Sieve Synthesis. *Chem. Mater.* **4**, 756-768 (1992).

[4] Davis, M. E. Ordered porous materials for emerging applications. *Nature* **417**, 813-821 (2002).

[5] Liebau, F. *Zeolites* **3** (1983).

[6] Baerlocher, C., Meier, W. M. & Olson, D. H. Vol. 2006 (International Zeolite Association, 2006).

[7] Jones, C. W., Tsuji, K., Takewaki, T., Beck, L. W. & Davis, M. E. Tailoring molecular sieve properties during SDA removal via solvent extraction. *Microporous Mesoporous Mat.* **48**, 57-64 (2001).

[8] Shylesh, S., Srilakshini, C., Singh, A. P. & Anderson, B. G. Bridging the gap between micropores and mesopores by the controlled transformation of bifunctional periodic mesoporous silicas. *Microporous Mesoporous Mat.* **108**, 29-40 (2008).

[9] Lobo, R. F., Zones, S. I. & Davis, M. E. Structure-Direction In Zeolite Synthesis. *J. Inclusion Phenom.* **21**, 47-78 (1995).

[10] Goepper, M., Li, H. X. & Davis, M. E. A Possible Role of Alkali-Metal Ions in the Synthesis of Pure-Silica Molecular Sieves. *J. Chem. Soc.-Chem. Commun.*, 1665-1666 (1992).

[11] Brigden, C. T. & Williams, C. D. The synthesis and characterization of Al-Beta and all-silica Beta formed in fluoride and caustic media. *Microporous Mesoporous Mat.* **100**, 118-127 (2007).

[12] Caullet, P., Paillaud, J. L., Simon-Masseron, A., Soulard, M. & Patarin, J. The fluoride route: a strategy to crystalline porous materials. *Comptes Rendus Chimie* **8**, 245-266 (2005).

[13] Zones, S. I. *et al.* The fluoride-based route to all-silica molecular sieves; a strategy for synthesis of new materials based upon close-packing of guest-host products. *Comptes Rendus Chimie* **8**, 267-282 (2005).

[14] Bouizi, Y., Paillaud, J. L., Simon, L. & Valtchev, V. Seeded synthesis of very high silica zeolite A. *Chem. Mater.* **19**, 652-654 (2007).

[15] Takewaki, T., Beck, L. W. & Davis, M. E. Synthesis of CIT-6, a zincosilicate with the (*)BEA topology. *Top. Catal.* **9**, 35-42 (1999).

[16] Takewaki, T., Beck, L. W. & Davis, M. E. Zincosilicate CIT-6: A precursor to a family of *BEA-type molecular sieves. *J. Phys. Chem. B* **103**, 2674-2679 (1999).

[17] Burkett, S. L. & Davis, M. E. Mechanism of Structure Direction in the Synthesis of Pure-Silica Zeolites. 2. Hydrophobic hydration and structural specificity. *Chem. Mater.* **7**, 1453-1463 (1995).

[18] Burkett, S. L. & Davis, M. E. Mechanisms of Structure Direction in the Synthesis of Pure-Silica Zeolites. 1. Synthesis of TPA/Si-ZSM-5. *Chem. Mater.* **7**, 920-928 (1995).

[19] Davis, M. E. in *Zeolites: A Refined Tool for Designing Catalytic Sites* Vol. 97 *Studies in Surface Science and Catalysis* (L. Bonneviot & S. Kaliaguine, eds.) 35-44 (1995).

[20] Davis, T. M. *et al.* Mechanistic principles of nanoparticle evolution to zeolite crystals. *Nat. Mater.* **5**, 400-408, doi:10.1038/nmat1636 (2006).

[21] Fedeyko, J. M., Egolf-Fox, H., Fickel, D. W., Vlachos, D. G. & Lobo, R. F. Initial stages of self-organization of silica-alumina gels in zeolite synthesis. *Langmuir* **23**, 4532-4540, doi:10.1021/la062808o (2007).

[22] Bein, T. Synthesis and applications of molecular sieve layers and membranes. *Chem. Mater.* **8**, 1636-1653 (1996).

[23] Barrett, P. A. *et al.* ITQ-12: a new microporous silica polymorph potentially useful for light hydrocarbon separations. *Chem. Commun.*, 2114-2115 (2003).

[24] Olson, D. H., Yang, X. B. & Camblor, M. A. ITQ-12: A zeolite having temperature dependent adsorption selectivity and potential for propene separation. *J. Phys. Chem. B* **108**, 11044-11048 (2004).

[25] McLeary, E. E., Jansen, J. C. & Kapteijn, F. Zeolite based films, membranes and membrane reactors: Progress and prospects. *Microporous Mesoporous Mat.* **90**, 198 (2006).

[26] McLeary, E. E., Buijsse, E. J. W., Gora, L., Jansen, J. C. & Maschmeyer, T. Membrane reactor technology for C-5/C-6 hydroisomerization. *Philos. Trans. R. Soc. A-Math. Phys. Eng. Sci.* **363**, 989-1000, doi:10.1098/rsta.2004.1533 (2005).

[27] Bai, C. S., Jia, M. D., Falconer, J. L. & Noble, R. D. Preparation And Separation Properties Of Silicalite Composite Membranes. *J. Membr. Sci.* **105**, 79-87 (1995).

[28] Lai, Z. P. *et al.* Microstructural optimization of a zeolite membrane for organic vapor separation. *Science* **300**, 456-460 (2003).

[29] Lin, X., Falconer, J. L. & Noble, R. D. Parallel pathways for transport in ZSM-5 zeolite membranes. *Chem. Mater.* **10**, 3716-3723 (1998).

[30] Morooka, S., Kuroda, T. & Kusakabe, K. in *Advances in Chemical Conversions for Mitigating Carbon Dioxide* Vol. 114 *Studies in Surface Science and Catalysis* (T. Inui *et al.,* eds.) 665-668 (1998).

[31] Sano, T., Yanagishita, H., Kiyozumi, Y., Mizukami, F. & Haraya, K. Separation Of Ethanol-Water Mixture By Silicalite Membrane On Pervaporation. *J. Membr. Sci.* **95**, 221-228 (1994).

[32] Yan, Y. S., Davis, M. E. & Gavalas, G. R. Preparation Of Zeolite Zsm-5 Membranes By In-Situ Crystallization On Porous Alpha-Al2o3. *Ind. Eng. Chem. Res.* **34**, 1652-1661 (1995).

[33] Salomon, M. A., Coronas, J., Menendez, M. & Santamaria, J. Synthesis of MTBE in zeolite membrane reactors. *Appl. Catal. A-Gen.* **200**, 201-210 (2000).

[34] Vanbekkum, H., Geus, E. R. & Kouwenhoven, H. W. in *Advanced Zeolite Science And Applications.* Vol. 85, *Studies In Surface Science And Catalysis,* 509-542 (1994).

[35] Davis, S. P., Borgstedt, E. V. R. & Suib, S. L. Growth of Zeolite Crystallites and Coatings on Metal-Surfaces. *Chem. Mater.* **2**, 712-719 (1990).

[36] Rebrov, E. V. *et al.* The preparation of highly ordered single layer ZSM-5 coating on prefabricated stainless steel microchannels. *Appl. Catal. A-Gen.* **206**, 125-143 (2001).

[37] Wan, Y. S. S., Chau, J. L. H., Gavriilidis, A. & Yeung, K. L. Design and fabrication of zeolite-based microreactors and membrane microseparators. *Microporous Mesoporous Mat.* **42**, 157-175 (2001).

[38] Erdem-Senatalar, A., Tatlier, M. & Urgen, M. Preparation of zeolite coatings by direct heating of the substrates. *Microporous Mesoporous Mat.* **32**, 331-343 (1999).

[39] Tatlier, M. & Erdem-Senatalar, A. in *Porous Materials in Environmentally Friendly Processes* Vol. 125 *Studies in Surface Science and Catalysis* (I. Kiricsi, G. PalBorbely, J. B. Nagy, & H. G. Karge, eds.) 101-108 (1999).

[40] Bein, T. *et al.* Microporous Assemblies For Chemical Recognition - Zeolite Layers And Sol-Gel-Derived Glass-Films On Sensors. *Abstr. Pap. Am. Chem. Soc.* **204**, 161-COLL (1992).

[41] Koegler, J. H. *et al.* in *Zeolites And Related Microporous Materials: State Of The Art 1994.* Vol. 84, *Studies In Surface Science And Catalysis,* 307-314 (1994).

[42] Mintova, S. & Bein, T. Nanosized zeolite films for vapor-sensing applications. *Microporous Mesoporous Mat.* **50**, 159-166 (2001).

[43] Yan, Y. G. & Bein, T. Molecular Recognition On Acoustic-Wave Devices - Sorption In Chemically Anchored Zeolite Monolayers. *J. Phys. Chem.* **96**, 9387-9393 (1992).

[44] Yan, Y. G. & Bein, T. Molecular Recognition Through Intercalation Chemistry - Immobilization Of Organoclays On Piezoelectric Devices. *Chem. Mater.* **5**, 905-907 (1993).

[45] Baklanov, M. R. & Maex, K. Porous low dielectric constant materials for microelectronics. *Philos. Trans. R. Soc. A-Math. Phys. Eng. Sci.* **364**, 201-215 (2006).

[46] Chen, Y. L. *et al.* Synthesis and characterization of pure-silica-zeolite Beta low-k thin films. *Microporous Mesoporous Mat.* **123**, 45-49, doi:10.1016/j.micromeso.2009.03.022 (2009).

[47] Larlus, O. *et al.* Silicalite-1/polymer films with low-k dielectric constants. *Appl. Surf. Sci.* **226**, 155 (2004).

[48] Lee, B. D. *et al.* Ultralow-k nanoporous organosilicate dielectric films imprinted with dendritic spheres. *Nat. Mater.* **4**, 147-U126 (2005).

[49] Lew, C. M. *et al.* Pure-Silica-Zeolite MFI and MEL Low-Dielectric-Constant Films with Fluoro-Organic Functionalization. *Adv. Funct. Mater.* **18**, 3454-3460 (2008).

[50] Lew, C. M. *et al.* Hydrofluoric-Acid-Resistant and Hydrophobic Pure-Silica-Zeolite MEL Low-Dielectric-Constant Films. *Langmuir* **25**, 5039-5044 (2009).

[51] Li, S. A., Li, Z. J. & Yan, Y. S. Ultra-low-k pure-silica zeolite MFI films using cyclodextrin as porogen. *Adv. Mater.* **15**, 1528 (2003).

[52] Li, Z. J. *et al.* Mechanical and dielectric properties of pure-silica-zeolite low-k materials. *Angew. Chem.-Int. Edit.* **45**, 6329-6332 (2006).

[53] Li, Z. J., Lew, C. M., Li, S., Medina, D. I. & Yan, Y. S. Pure-silica-zeolite MEL low-k films from nanoparticle suspensions. *J. Phys. Chem. B* **109**, 8652-8658 (2005).

[54] Liu, Y., Sun, M. W., Lew, C. M., Wang, J. L. & Yan, Y. S. MEL-type pure-silica zeolite nanocrystals prepared by an evaporation-assisted two-stage synthesis method as ultra-low-k materials. *Adv. Funct. Mater.* **18**, 1732-1738 (2008).

[55] Long, T. M. & Swager, T. M. Molecular design of free volume as a route to low-kappa dielectric materials. *J. Am. Chem. Soc.* **125**, 14113-14119 (2003).

[56] Maex, K. *et al.* Low dielectric constant materials for microelectronics. *J. Appl. Phys.* **93**, 8793-8841 (2003).

[57] Wang, Z. B., Mitra, A. P., Wang, H. T., Huang, L. M. & Yan, Y. H. Pure silica zeolite films as low-k dielectrics by spin-on of nanoparticle suspensions. *Adv. Mater.* **13**, 1463 (2001).

[58] Wang, Z. B., Wang, H. T., Mitra, A., Huang, L. M. & Yan, Y. S. Pure-silica zeolite low-k dielectric thin films. *Adv. Mater.* **13**, 746-749 (2001).

[59] Yan, Y., Wang, Z. & Wang, H. *Silica Zeolite Low-K Dielectric Thin Films*. U.S. Patent #6573131 (2003).

Chapter 2: Introduction to Part I of Thesis

1. Introduction

Zeolites and zeolite-based materials offer great potential for the development of nanostructured materials. This is due in large part to their crystallinity, structural symmetry, microporous uniformity, and topological variety, since these properties result in high surface areas, thermal stability, and the ability to sieve molecules based on size- and shape-selectivity.[1] Additionally, zeolites and zeolite-like materials can be synthesized in a range of chemical compositions, producing internal physicochemical properties that can range from acidic to basic and hydrophobic to hydrophilic.[2] Many of these properties can be modified by changing the synthesis conditions, leading to the potential to tailor the final characteristics to the zeolite's application.[3] Consequently, zeolites have been widely used in applications such as gas separation and absorption, catalysis, ion exchange, and have more recently been suggested for use as chemical sensors, membrane reactors, and low dielectric constant (k) materials for semiconductors.[1,4,5,6] Many of these applications would benefit from, and in the latter cases require, the development of zeolites in planar form (thin film or membrane).

Planar zeolites are generally classified as nanostructured materials whose lateral dimension is much greater than their thickness. Many zeolite single crystals with a plate- or sheet-like crystal habit are planar; however, these single crystals are typically very small (< 1 mm) and are therefore inappropriate for large-scale applications. Generally, planar zeolite and zeolite-based materials are polycrystalline, and can be categorized as

one of the following three types: layers, films, or membranes (Figure 2.1). Zeolite layers are comprised of individual crystals scattered discontinuously on a surface. Typically, these crystals are not fully intergrown, and are frequently adhered to the surface through electrostatic interactions, rather than through covalent bonding, although this can certainly be done.[7] Layers cannot be self-supported, although their supports can be porous. While molecular sieve layers are of limited use in applications requiring full intergrowth, such as electronic materials, they can be particularly useful in the development of chemical sensors, where their molecular selectivity could improve sensor performance.[8] Zeolite films consist of a continuous coverage of intergrown crystals or crystals imbedded in a composite matrix on the surface of a nonporous support. For the purposes of this chapter, we define films as supported materials, although they may be defined differently elsewhere. The use of a nonporous support restricts the use of zeolite films somewhat; as such, these materials can be used as coatings, whether adsorptive, catalytic, or corrosion-resistant, for applications such as chemical sensors, metal alloys, or low-*k* dielectrics.[2,4,9] Zeolite membranes, on the other hand, are used for separation processes. Membranes are either self-supported films or films on porous supports that act as a selective barrier to the transport of materials. Self-supported membranes are often referred to as “symmetric membranes”, while supported membranes are “asymmetric”.[10]

The quality of zeolite and zeolite-based films and membranes is determined by the surface coverage, continuity, and the number of defects in the material, which can be evaluated via microscopy techniques (see Section 2.3). For films and membranes, respectively, defects are defined as gaps in the substrate coverage, and transmembrane

pathways much larger than the intracrystalline zeolite pore network.[10] Depending on the application, other requirements for layers, films, and membranes may be imposed. For instance, applications such as chemical sensors require very thin films coating the sensors. Additionally, applications such as catalytic membrane reactors may require membranes with a high degree of selectivity, which could require a specific orientation of the zeolite structure within the membrane.[11,12] Lastly, applications that require thermal cycling, such as thermoelectrics, need film and membrane materials that are well-adhered to their substrates, and do not suffer from cracking or flaking on thermal treatment. For high temperature applications, this is especially a concern. If the coefficients of thermal expansion of the planar zeolite material and the substrate are dissimilar, rapid heating and cooling can lead to cracking and buckling of the planar material, resulting in the destruction of the surface.[11]

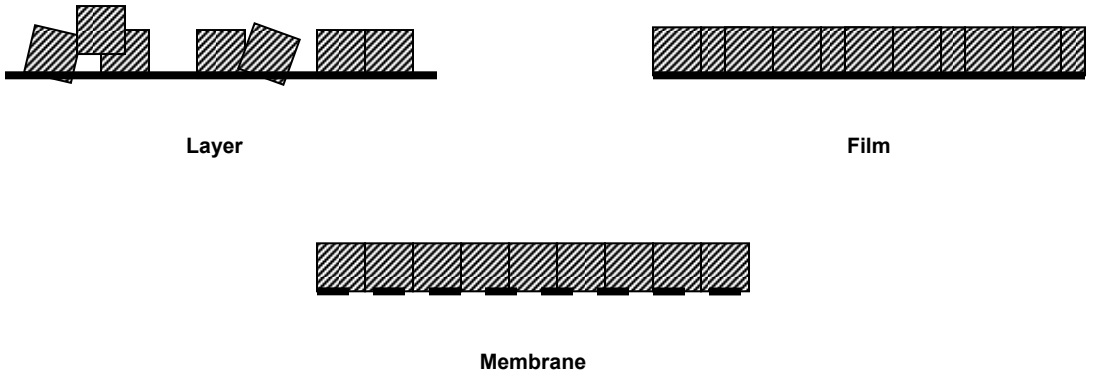

Figure 2.1 Schematic representation of the three categories of nanostructured, planar zeolite and zeolite-based configurations

There are several detailed reviews on the subject of zeolite films and membranes, as well as their applications.[2,10,11,13,14] This chapter provides a brief introduction into the common zeolite and membrane synthesis strategies, and discusses the advantages and disadvantages of each. Section 2 outlines the general process of creating planar zeolites, introducing in turn the selection of a proper support, the various methods of film and membrane production, the suggested models of film and membrane formation, characterization techniques, and lastly, defect elimination. Lastly, Section 3 discusses the necessity of pairing the synthetic technique to the application requirements, which often guides both the choice of synthetic strategy and the development of new strategies.

2. Zeolite Film and Membrane Synthetic Strategies

The synthesis of zeolite films and membranes is in many ways similar to the synthesis of zeolite powders, in that there is often a very specific set of requirements that must be met in order for the zeolite phase of interest to crystallize. Films and membranes, however, have the added requirement of crystallization on a surface. In some cases, this can be as simple as inserting a substrate into the zeolite precursor gel prior to crystallization, while in other cases, it can be as complex as preparing pre-formed zeolite seeds of a specific size in a colloidal suspension, electrochemically modifying a substrate, depositing the seeds on the substrate, and then inserting the substrate into another zeolite precursor gel to carry out a secondary growth procedure that seals the spaces between seed crystals.[15,16] The first step in preparing films and membranes is to determine the type of support needed.

2.1 Support Choice and Modification

There are myriad possibilities for the choice of substrate for a zeolite film or membrane.[10] For instance, metallic materials such as gold, copper, silver, platinum, and stainless steel have all been used to synthesize zeolite films and membranes, such as zeolite A (LTA topology with an aluminosilicate composition) and zeolite NaY (FAU topology with an aluminosilicate composition with a sodium counter-ion).[17,18] Additionally, ceramic and metal-oxide-based materials, like porous alumina, single-crystal silicon wafers, quartz, and glass, have been used as supports for ZSM-5 (MFI topology with an aluminosilicate composition), silicalite (MFI topology with a pure-silica composition), and Beta (BEA* topology with either an aluminosilicate or a pure-silica composition).[19,20,21,22,23,24] Lastly, organic polymer supports such as Teflon® and cellulose have been used (and then later removed) to create free-standing, or symmetric, membranes of ZSM-5.[25,26] In many cases, the choice of the support affects the final film or membrane properties. For instance, the substrate can influence the final orientation of the zeolite crystals, the final film thickness, the adhesion of the zeolite crystals to the surface, or the final crystal size.[14]

Substrates may be modified to accommodate the needs of a specific zeolite composition or synthetic technique. The most basic modification of a substrate is cleaning to remove organics that have accumulated on the surface and may prevent zeolite film formation. For instance, single-crystal silicon wafers have a native oxide layer and adsorbed organics on their surface that often need to be removed prior to use as a support. Cleaning may be accomplished through a variety of methods, including dips in aqueous hydrofluoric acid, and piranha solutions, and boiling in Alconox detergent.[27] Chemical

and mechanical polishing techniques may also be used to modify the surface roughness of the substrate, as thin films are less likely to adhere to rough surfaces than smooth.[11] Adhesion of the film to the substrate is generally a function of the hydrophilicity of the surface due to various van der Waals and hydrogen bonding interactions this enables, and can be improved by immersing the substrate in solutions of NaOH, which increases the number of surface hydroxyl groups and therefore the hydrophilicity of the surface. It also increases the number of potential nucleation sites.[11] More complicated techniques involve surface modification, such as the attachment of molecular coupling agents such as thiol alkylsilanes, which are used to either chemically adhere zeolite crystals to the surface, or the functionalization of surface silanols via vapor-phase silylation. Electrophoretic deposition can also be used to attach charged particles from colloidal suspensions to the surface during coating.[11] Lastly, the substrate can be patterned via lithographic techniques to guide zeolite crystallization into defined structures.[28,29,30]

2.2 Synthetic Strategies

The synthesis of zeolites in powder form is typically accomplished via hydrothermal or solvothermal conditions under autogeneous pressure at temperatures below 200 °C. Hydrothermal refers to the synthesis of zeolite using water as the gel solvent, whereas solvothermal indicates a non-aqueous (usually organic) solvent for the gel. Films and membranes, however, can be synthesized non-hydrothermally, as well as hydrothermally. The synthetic techniques for hydrothermal and non-hydrothermal film syntheses are often very similar in parts, and many of the synthetic techniques can be used for either category (Figure 2.2).

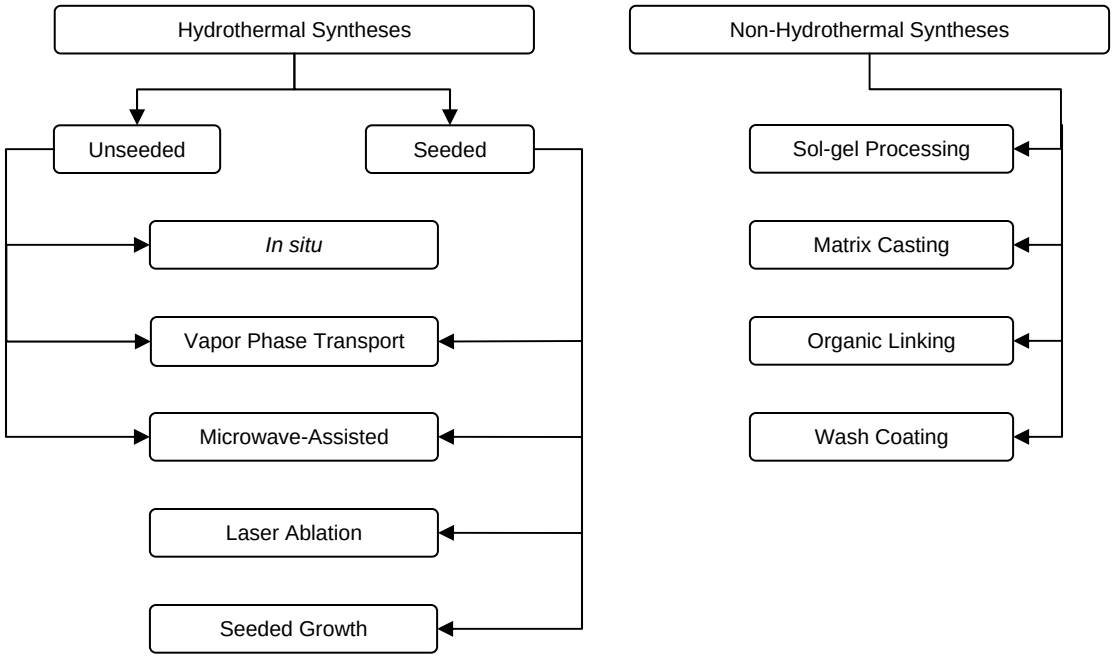

Figure 2.2 Synthetic strategies for the formation of zeolite and zeolite-based films and membranes

2.2.1 Hydrothermal Techniques

Hydrothermal film and membrane syntheses come in two varieties: seeded and unseeded. Seeded syntheses require the use of pre-formed zeolite crystals, typically nanocrystals of a uniform size, either to attach to the support or to seed the zeolite gel prior to crystallization. The main benefit of seeded syntheses over unseeded syntheses is that the nucleation (at high supersaturation) and growth (at low supersaturation) steps of zeolite crystallization can be decoupled, resulting in the suppression of secondary nucleation.[11] This can also render the effects of the surface on zeolite growth less important. Additionally, seeded methods can also be used to promote the crystallization of a single, pure phase when reaction conditions might tend towards producing a mixed phase, to grow large crystals, or to reduce the severity of reaction conditions, which might be necessary to induce nucleation but not to accommodate crystal growth.[29,31,32,33,34] The

disadvantage of seeded syntheses is that uniform and easily dispersed zeolite seeds must be made, which can be difficult to achieve. For instance, the zeolite particles may clump in solution and form large colloids, as opposed to a uniform suspension. In these cases, significant effort must be made to ensure that the zeolite crystals are well dispersed.[16] Also, nanocrystals of a uniform size may be difficult to obtain, as this can require stopping the synthesis prior to full crystallization and centrifuging for long times at high speeds to separate the amorphous bulk from the nanocrystals. In these cases, yields may be very low.

Hydrothermal, unseeded zeolite film and membrane syntheses are typically categorized as *in situ* crystallization procedures, referring to the formation of the zeolite film *in situ* during hydrothermal crystallization. In this method, the substrate is directly submerged into the zeolite precursor gel and the zeolite forms on both sides of the surface. Several models have been suggested for the formation of zeolite films via *in situ* procedures (Figure 2.3): (Model 1) homogeneous nucleation in the bulk gel, followed by either growth of the nuclei to crystals and then surface accumulation, or surface accumulation of the nuclei and then growth of the attached nuclei to crystals, (Model 2) diffusion of colloidal material to the surface of the substrate, followed by concentration at the surface and then nucleation of an amorphous gel layer on the surface to intergrown crystals, and (Model 3) direct nucleation at the surface, followed by crystal growth.[2,35,36,37] Any of these models are possible for the formation of zeolite films through *in situ* processes, however, homogeneous nucleation is very common for *in situ* crystallization.[36,37]

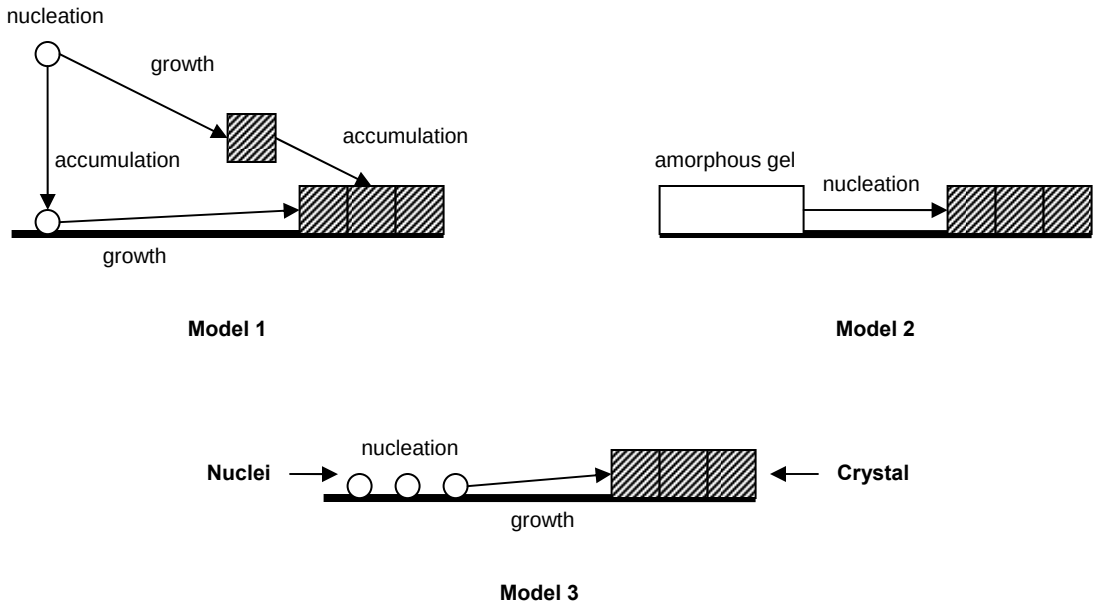

Figure 2.3 Models of zeolite and zeolite-based film formation for in situ synthetic techniques

In many *in situ* processes, the substrate itself may be partially consumed, or the gel conditions may lead to leaching of the substrate into the bulk gel.[10] For *in situ* processes which involve accumulation of nuclei or crystals at the substrate from the bulk gel, the accumulation process may be gravitationally or electrostatically driven, as in cases where the substrate has been modified to encourage good adhesion of the resulting film. There are many advantages to *in situ* film synthesis techniques: (1) since the substrate is fully submerged in the zeolite gel during crystallization, the gel can completely coat the surface of even complex surfaces, (2) since the technique involves only the insertion of a substrate, the procedures are much less complicated than other techniques, and (3) since

the synthesis requires no extra steps, the crystallization conditions frequently do not need to be modified to accommodate the film synthesis.[9] However, *in situ* techniques also have drawbacks. For instance, if heterogeneous nucleation occurs (in the bulk gel and at the substrate surface), the resulting polycrystalline film may have layers of scattered crystals on its surface from accumulation of bulk crystals after the film itself has crystallized (Figure 2.4). Additionally, *in situ* procedures call for the immersion of the substrate in, presumably, a clear solution or a dilute gel. Some zeolites, however, require very concentrated conditions to form. This is the case for most fluoride-mediated zeolite syntheses, where the zeolite precursor gel is almost a dry powder. In these cases, *in situ* techniques cannot be applied.

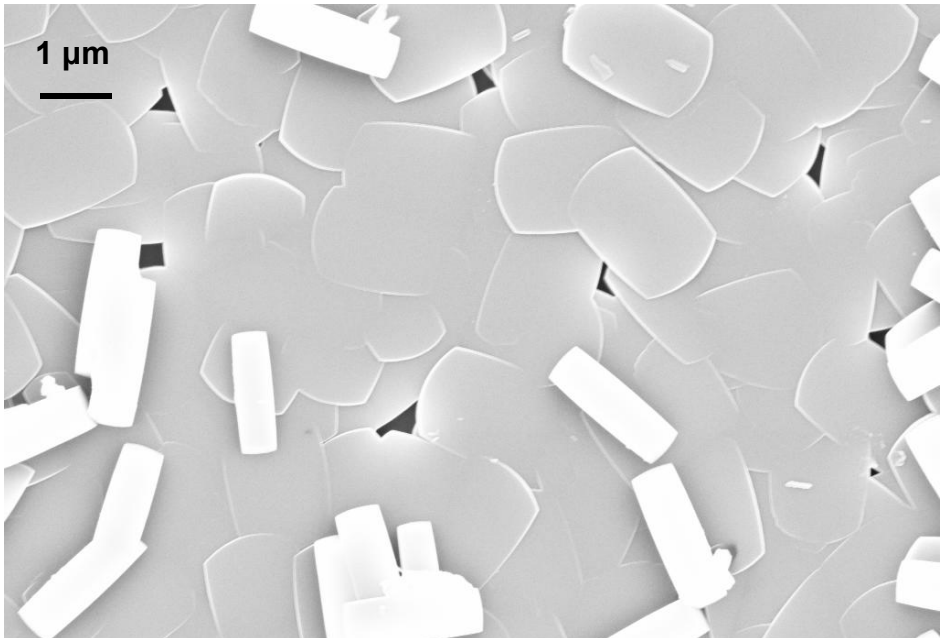

Figure 2.4 Silicalite (MFI) polycrystalline film grown via *in situ* techniques showing a loose layer of MFI crystals on the surface

For the cases where *in situ* techniques cannot be used, the vapor phase transport method may be used instead (Figure 2.5). In this method, a reactive gel layer is first applied to the substrate by submersion in a parent gel containing alumina, silica, water, and the mineralizing agent, and then the gel layer is crystallized hydrothermally in the presence of the structure-directing agent and water in the vapor phase (the remaining parent gel not used for coating is not crystallized).[2,35,38,39,40,41] More recently, Matsukata and co-workers have extended this approach by incorporating the silica source in the vapor phase, rather than the structure-directing agent and solvent.[42] The vapor phase transport method can be seeded or unseeded, in that the substrate or the precursor gel may be seeded prior to substrate coating. This method is convenient in that it decreases the use of the structure-directing agent, which can be quite expensive, and increases the number of films the reactive gel can make, since the bulk gel itself is not crystallized, but it is also a two-step process that requires the formation of a reactive gel layer, which may not be possible for every zeolite.

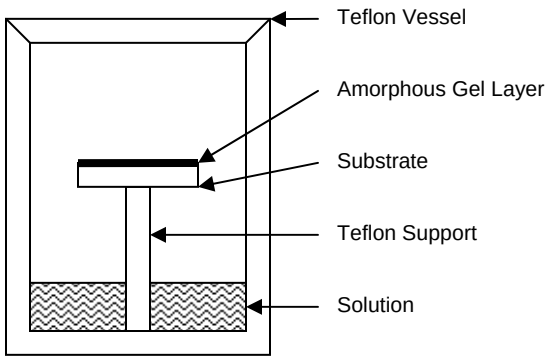

Figure 2.5 Schematic of the vapor phase transport method for film formation

Microwave-assisted crystallization is another hydrothermal synthetic procedure that uses laboratory microwaves to shorten the time required for crystallization. This is primarily a result of the fast heating of the autoclaves inside the microwave.[11] The high energy input also has some unusual affects on the formation of zeolite crystals: since the system heats very quickly to crystallization temperatures, the formation of nuclei is suppressed, leading to the growth of very large crystals. For film syntheses via microwave heating, the synthesis can proceed in a similar fashion to *in situ* crystallization; that is, the substrate may be fully submerged in the precursor gel. Alternatively, the substrate can be dip-coated in the zeolite precursor gel prior to crystallization and aged, which allows nuclei to form in the gel. In either case, the precursor gel or the substrate itself can be seeded to promote film growth. The advantage of this method is the very rapid crystallization time (a matter of hours as opposed to days), but it is limited in that uniform crystal growth is difficult to control.[11]

Lastly, hydrothermal synthesis may be carried out via laser ablation. Laser ablation uses preformed zeolite targets to coat the surface of a substrate with atoms, molecules, and clusters of the zeolitic material at low substrate temperatures.[2] Generally, this forms an amorphous layer of zeolite building-block materials on the surface of the substrate, which are crystallized during the ablation or during subsequent hydrothermal treatments. The main advantage of this method is that a typical zeolite gel is not required, however, the method also tends to result in the formation of zeolite crystals imbedded in an amorphous matrix, rather than a typical polycrystalline zeolite film.

2.2.2 Non-Hydrothermal Techniques

Non-hydrothermal, zeolite, and zeolite-based film and membrane synthetic techniques refer to processes of film formation that do not require a hydrothermal crystallization step; instead, these techniques make use of pre-formed zeolite seeds and a variety of binding agents. These techniques are collectively referred to as *ex situ* methods, and can be advantageous if the resulting surface coverage need not be fully intergrown, but rather fully covered, as *ex situ* syntheses allows the separation of the zeolite formation and film formation processes. It is also useful because it is a facile scheme of depositing a film on a surface. However, the final films can have gaps between crystals (thus qualifying the coating as a layer rather than a film), or the presence of a binder matrix in which the crystals are imbedded. For some applications, like low-*k* dielectrics, this can be favorable, as it can result in very smooth, completely interconnected films.[43] The presence of a permanent binding agent also results in a film with composite properties of the two materials. Lastly, as discussed for the hydrothermally seeded processes, obtaining seeds of appropriate size that can be easily dispersed can be very challenging. In general, non-hydrothermal techniques are a two-step process. First, the zeolite seeds are hydrothermally crystallized (not in the presence of the substrate). Second, the seeds are attached to the surface of the substrate via a binding agent, which can be an organic linker, an electrostatic linker (such as inducing a charge on the substrate), or a gel that contacts the surface. There are four primary processes by which zeolite crystals may be deposited on the surface of a material: sol-gel processing, matrix casting, organic linking, and wash coating.[2,13]

Sol-gel processing refers to the suspension of zeolite crystals in a solvent (the sol), typically tetraethylorthosilicate, followed by the formation of a gel through evaporative processes.[8] The substrate is contacted with the seeds via dip-coating, spin-coating, drop-coating, etc., and the substrate is then dried, hardening the film. In some cases, the sol is actually the original zeolite gel from which the seeds were hydrothermally crystallized. The benefits of this method are the ease with which any three-dimensional substrate can be coated, and the ability to tune the final thickness of the film based on the number of coats. Matrix casting is very similar to sol-gel processing, in that the binding agent is a solution, but here it is usually a polymeric solution, which is useful for its processability into a variety of self-supported shapes. For instance, the polymer / zeolite composite solution could be extruded into fibers, which could be woven into membranes for reverse osmosis water treatment, or it could be used to create flexible self-supported sheets.

Organic linking deposition methods present another interesting method to coat substrates.[2] In this process, the organic linker (generally a silylating agent) is attached to the zeolite crystals in solution, to the surface of the substrate, or to both, resulting in a covalent bond between the crystals and the surface. This method can help improve the dispersability of zeolites in solution, and can result in a substrate covered by only a single layer. However, this method results in a film which can be easily destroyed if the binding agent is removed, for instance, via high temperatures, since the crystals are not actually imbedded in or bonded to the substrate.

Wash coating is the last major method by which seeds can be deposited on a substrate. Here, the seeds are suspended in a binding agent to form a slurry, which is then used to coat the surface of the substrate.[13] The seeds are then bound to the surface via sintering at high temperatures. The primary disadvantage of this route is the high temperature process required for good adhesion of the crystals to the substrate.

2.3 Characterization Techniques

Zeolite films and membranes are characterized through a variety of techniques to ensure quality. X-ray diffraction (XRD) is used to determine the crystallinity and zeolite structure of the film. Microscopic techniques, such as scanning electron microscopy (SEM), and energy dispersive spectrometry (EDS), are used to determine film thickness, surface coverage, crystal size, crystal habit, degree of crystal intergrowth, defect quantity and type, and chemical composition of the film. These techniques are especially useful before and after calcination, as they show both that the structure-directing agent has been removed and that the film has not suffered from cracking. Typically, nitrogen adsorption experiments are used to determine the micropore volume and porosity of zeolite powders. However, this method is difficult to use for supported films, because the supports generally do not fit inside the sample tubes. An alternative method for the determination of porosity in thin films is the use of ellipsometric porosimetry, which uses *in situ* ellipsometry to observe the effects of adsorption of various organic vapors on the film via swelling and the change of refractive index.[44] Like nitrogen adsorption for powder samples, this method can determine average pore size, pore distribution, and porosity of the films. However, this method is limited in that only a very few of these setups have been made in the world. Ellipsometry, in general, is also a useful and non-destructive

technique for determining the film thickness of a sample.[45] In order to use this method, however, the films must have a very uniform thickness across the surface (which can be obtained through polishing), and must be reflective. Surface adhesion of the film to the substrate can be measured by laser spallation techniques (although early measurements consisted of the rough "sticky-tape test", where sticky tape was placed on the film and pulled off to determine how easily the film could be removed).[46] Mechanical testing of the films can also be carried out using standard nanoindentation techniques, which determine the films' hardness and modulus.[47,48,49] Capacitance testing of the films demonstrates its electronic properties, such as its dielectric constant and response to applied voltages.[50] This characterization method requires high quality (continuous, intergrown, and well-adhered) films with smooth surfaces to obtain consistent measurements using typical parallel-plate capacitance measurements. To obtain smooth, parallel surfaces, a high quality mechanical polisher is often needed, especially for film synthesis methods that do not directly yield a smooth surface (i.e., most hydrothermal syntheses). The use of these techniques, individually or in combination, demonstrates the type, quality, and physical properties of the resulting films. Other techniques, such as catalytic testing and separation ability, may also be applied if the end-use of the film or membrane requires it.

2.4 Defect Elimination

Zeolite films and membranes often have defects, discovered during characterization, which must be removed prior to their end use. For instance, cracks formed during calcination, or holes formed during crystallization, can often be sealed by soaking the

sample in a silica-containing gel and drying it, resulting in areas of the film with amorphous materials. Alternatively, the surface can be sealed using chemical vapor deposition techniques, such as vapor phase silylation, which can attack surface silanol groups (site defects in the crystal structure). This can also be used to attenuate the hydrophilicity of the film, since silanols promote water adsorption. When post-synthetic techniques cannot be used to fix the defects, defect elimination becomes an iterative process where the film preparation method itself must be adjusted to prevent defect formation. This can result in a change of substrate, the modification of a substrate, or changes in the crystallization or deposition conditions.

3. Development of New Synthetic Techniques

The choice of an appropriate film or membrane preparation technique is crucial to the development of a high-quality planar zeolite for a given application. If the application requires an ultra-thin film composed completely of intergrown zeolites, without the presence of a binder, a hydrothermal method such as vapor phase transport may be easiest. However, if the presence of a binder will not affect the end-use, a non-hydrothermal method such as sol-gel processing via spin-coating may be an easier choice. The zeolite crystallization conditions must also be taken into consideration, as must the choice of crystal size. If the film needs to be composed of very large crystals, seeded syntheses, which suppress nucleation, may be most appropriate. If the zeolite crystallizes at very concentrated gel conditions, an *in situ* synthesis would be inappropriate as the substrate cannot be submerged in the gel. In each case, the factors to consider are the end requirements of the film, the nature of the support, the zeolite gel

composition, the final zeolite topology, and the necessary crystallization conditions, such as aging time, crystallization time, and crystallization temperature. By examining these factors, it is generally possible to identify a synthetic technique that is appropriate for film preparation. In situations where this is not the case, new film and membrane preparation methods must be developed. It is through this process of pairing and modifying synthetic techniques that novel synthesis concepts are introduced, and the field of zeolite and zeolite-based nanostructures extended.

4. References

[1] Davis, M. E. Ordered porous materials for emerging applications. *Nature* **417**, 813-821 (2002).

[2] Bein, T. Synthesis and applications of molecular sieve layers and membranes. *Chem. Mater.* **8**, 1636-1653 (1996).

[3] Davis, M. E. in *Zeolites: A Refined Tool for Designing Catalytic Sites Studies in Surface Science and Catalysis* (L. Bonneviot & S. Kaliaguine, eds.) (Elsevier Science, 1995).

[4] Mintova, S. & Bein, T. Nanosized zeolite films for vapor-sensing applications. *Microporous Mesoporous Mat.* **50**, 159-166 (2001).

[5] Szostak, R. *Molecular Sieves: Principles of Synthesis and Identification*. 2nd ed., (Blackie Academic & Professional, 1998).

[6] Wang, Z. B., Wang, H. T., Mitra, A., Huang, L. M. & Yan, Y. S. Pure-silica zeolite low-k dielectric thin films. *Adv. Mater.* **13**, 746-749 (2001).

[7] Cho, G. *et al.* Ultra-thin zeolite films through simple self-assembled processes. *Adv. Mater.* **11**, 497 (1999).

[8] Bein, T. *et al.* Microporous Assemblies For Chemical Recognition - Zeolite Layers And Sol-Gel-Derived Glass-Films On Sensors. *Abstr. Pap. Am. Chem. Soc.* **204**, 161-COLL (1992).

[9] Cheng, X. L., Wang, Z. B. & Yan, Y. S. Corrosion-resistant zeolite coatings by in situ crystallization. *Electrochemical And Solid State Letters* **4**, B23-B26 (2001).

[10] Tavolaro, A. & Drioli, E. Zeolite membranes. *Adv. Mater.* **11**, 975-996 (1999).

[11] McLeary, E. E., Jansen, J. C. & Kapteijn, F. Zeolite based films, membranes and membrane reactors: Progress and prospects. *Microporous Mesoporous Mat.* **90**, 198 (2006).

[12] Saracco, G., Neomagus, H., Versteeg, G. F. & van Swaaij, W. P. M. High-temperature membrane reactors: potential and problems. *Chem. Eng. Sci.* **54**, 1997-2017 (1999).

[13] Yan, Y. & Wang, H. in *Encyclopedia of Nanoscience and Nanotechnology.* Vol. X, (H. S. Nalwa, ed.) 1-19 (American Scientific Publishers, 2003).

[14] Vanbekkum, H., Geus, E. R. & Kouwenhoven, H. W. in *Advanced Zeolite Science And Applications.*Vol. 85, S*tudies In Surface Science And Catalysis,* 509-542 (1994).

[15] Wang, Z. B. & Yan, Y. S. Oriented zeolite MFI monolayer films on metal substrates by in situ crystallization. *Microporous Mesoporous Mat.* **48**, 229-238 (2001).

[16] Boudreau, L. C., Kuck, J. A. & Tsapatsis, M. Deposition of oriented zeolite A films: in situ and secondary growth. *J. Membr. Sci.* **152**, 41-59 (1999).

[17] Davis, S. P., Borgstedt, E. V. R. & Suib, S. L. Growth of Zeolite Crystallites and Coatings on Metal-Surfaces. *Chem. Mater.* **2**, 712-719 (1990).

[18] Yan, Y. G. & Bein, T. Molecular Recognition On Acoustic-Wave Devices - Sorption In Chemically Anchored Zeolite Monolayers. *J. Phys. Chem.* **96**, 9387-9393 (1992).

[19] Lai, R., Yan, Y. S. & Gavalas, G. R. Growth of ZSM-5 films on alumina and other surfaces. *Microporous Mesoporous Mat.* **37**, 9-19 (2000).

[20] Lovallo, M. C., Gouzinis, A. & Tsapatsis, M. Synthesis and characterization of oriented MFI membranes prepared by secondary growth. *AIChE J.* **44**, 1903-1913 (1998).

[21] Lovallo, M. C. & Tsapatsis, M. Preferentially oriented submicron silicalite membranes. *AIChE J.* **42**, 3020-3029 (1996).

[22] Mitra, A. *et al.* Synthesis and evaluation of pure-silica-zeolite BEA as low dielectric constant material for microprocessors. *Ind. Eng. Chem. Res.* **43**, 2946-2949 (2004).

[23] Mitra, A. *et al.* Synthesis and corrosion resistance of high-silica zeolite MTW, BEA, and MFI coatings on steel and aluminum. *J. Electrochem. Soc.* **149**, B472-B478 (2002).

[24] Yan, Y. S., Tsapatsis, M., Gavalas, G. R. & Davis, M. E. Zeolite Zsm-5 Membranes Grown On Porous Alpha-Al2o3. *J. Chem. Soc.-Chem. Commun.*, 227-228 (1995).

[25] Sano, T. *et al.* Preparation And Characterization Of Zsm-5 Zeolite Film. *Zeolites* **11**, 842-845 (1991).

[26] Sano, T. *et al. J. Mater. Chem.* **2**, 141-142 (1992).

[27] Ljungberg, K., Jansson, U., Bengtsson, S. & Soderbarg, A. Modification of silicon surfaces with H2SO4:H2O2:HF and HNO3:HF for wafer bonding applications. *J. Electrochem. Soc.* **143**, 1709-1714 (1996).

[28] Yoon, K. B. Organization of zeolite microcrystals for production of functional materials. *Acc. Chem. Res.* **40**, 29-40 (2007).

[29] Caro, J. & Noack, M. Zeolite membranes - Recent developments and progress. *Microporous Mesoporous Mat.* **115**, 215-233 (2008).

[30] Caro, J., Noack, M., Kolsch, P. & Schafer, R. Zeolite membranes - state of their development and perspective. *Microporous Mesoporous Mat.* **38**, 3-24 (2000).

[31] Lai, S. M., Au, L. T. Y. & Yeung, K. L. Influence of the synthesis conditions and growth environment on MFI zeolite film orientation. *Microporous Mesoporous Mat.* **54**, 63-77 (2002).

[32] Lai, Z. P., Tsapatsis, M. & Nicolich, J. R. Siliceous ZSM-5 membranes by secondary growth of b-oriented seed layers. *Adv. Funct. Mater.* **14**, 716-729 (2004).

[33] Lin, J. C. & Yates, M. Z. Growth of oriented molecular sieve thin films from aligned seed layers. *Chem. Mater.* **18**, 4137-4141 (2006).

[34] Wong, W. C., Au, L. T. Y., Ariso, C. T. & Yeung, K. L. Effects of synthesis parameters on the zeolite membrane growth. *J. Membr. Sci.* **191**, 143-163 (2001).

[35] Matsukata, M. & Kikuchi, E. Zeolitic membranes: Synthesis, properties, and prospects. *Bull. Chem. Soc. Jpn.* **70**, 2341-2356 (1997).

[36] Li, S., Li, Z. J., Bozhilov, K. N., Chen, Z. W. & Yan, Y. S. TEM investigation of formation mechanism of monocrystal-thick b-oriented pure silica zeolite MFI film. *J. Am. Chem. Soc.* **126**, 10732-10737 (2004).

[37] Li, Y. S., Shi, J. L., Wang, J. Q. & Yan, D. S. in *Impact Of Zeolites And Other Porous Materials On The New Technologies At The Beginning Of The New Millennium, Pts. A And B.* Vol. 142, *Studies In Surface Science And Catalysis*, 1529-1536 (2002).

[38] Cho, Y. Pure Silica Zeolite Films Prepared by a Vapor Phase Transport Method. *Japanese Journal of Applied Physics. Parts 1 & 2* **47**, 8360-8363 (2008).

[39] Kikuchi, E., Yamashita, K., Hiromoto, S., Ueyama, K. & Matsukata, M. Synthesis of a zeolitic thin layer by a vapor-phase transport method: Appearance of a preferential orientation of MFI zeolite. *Microporous Mater.* **11**, 107-116 (1997).

[40] Kim, M. H., Jung, M. K. & Rhee, H. K. The Role Of Amines In The Synthesis Of Zeolites By Water-Organic Vapor-Phase Transport. *Korean J. Chem. Eng.* **12**, 410-415 (1995).

[41] Kim, M. H., Li, H. X. & Davis, M. E. Synthesis of zeolites by water-organic vapor-phase transport. *Microporous Mater.* **1**, 191-200 (1993).

[42] Mitra, A., Ichikawa, S., Kikuchi, E. & Matsukata, M. Hydrovapothermal conversion of tetraethoxysilane vapor to polycrystalline zeolite layer by in situ gelation. *Chem. Commun.*, 900-901 (2004).

[43] Li, Z. J., Lew, C. M., Li, S., Medina, D. I. & Yan, Y. S. Pure-silica-zeolite MEL low-k films from nanoparticle suspensions. *J. Phys. Chem. B* **109**, 8652-8658 (2005).

[44] Baklanov, M. R. & Mogilnikov, K. P. Characterization of porous dielectric films by ellipsometric porosimetry. *Opt. Appl.* **30**, 491-496 (2000).

[45] Hedlund, J., Schoeman, B. J. & Sterte, J. in *Progress In Zeolite And Microporous Materials, Pts. A-C.* Vol. 105, *Studies In Surface Science And Catalysis*, 2203-2210 (1997).

[46] Hu, L. L., Wang, J. L., Li, Z. J., Li, S. & Yan, Y. S. Interfacial adhesion of nanoporous zeolite thin films. *J. Mater. Res.* **21**, 505-511 (2006).

[47] Chen, X., Xiang, Y. & Vlassak, J. J. Novel technique for measuring the mechanical properties of porous materials by nanoindentation. *J. Mater. Res.* **21**, 715-724 (2006).

[48] Johnson, M., Li, Z. J., Wang, J. L. & Yan, Y. S. Mechanical characterization of zeolite low dielectric constant thin films by nanoindentation. *Thin Solid Films* **515**, 3164-3170 (2007).

[49] Xiang, Y., Chen, X., Tsui, T. Y., Jang, J. I. & Vlassak, J. J. Mechanical properties of porous and fully dense low-kappa dielectric thin films measured by means of nanoindentation and the plane-strain bulge test technique. *J. Mater. Res.* **21**, 386-395 (2006).

[50] Yan, Y., Wang, Z. & Wang, H. *Silica Zeolite Low-K Dielectric Thin Films*. U.S. Patent #6573131 (2003).

Chapter 3: In situ crystallization of fluoride-mediated, pure-silica zeolite thin films

Abstract

Two methods for the synthesis of fluoride-mediated, zeolite thin films were examined to determine if they could overcome the common limitations of fluoride-mediated zeolite syntheses, which are frequently incompatible with standard film synthesis techniques. The first method utilised a seeding and dilution modification to typical *in situ* film syntheses. The second method applied the vapor phase transport method to the zeolite mineralizing agent, fluoride, to crystallize a precursor film deposited by dip-coating techniques. With this method, we obtained thin films of silicate and germanosilicate zeolites with the LTA topology on a variety of substrates. The films were characterized by a combination of X-ray diffraction, field emission scanning electron microscopy, X-ray energy dispersive analyses, and mechanical testing via nanoindentation. The films were polycrystalline, inter-grown, continuous, and well-adhered to their substrates. The vapor phase transport of fluoride is a facile and general method for the synthesis of fluoride-mediated, zeolite thin films, specifically those with the pure-silica composition, and could extend the current library of zeolite films available.

Reproduced in part with permission from H. K. Hunt, C. M. Lew, M. Sun, Y. Yan and M. E. Davis, Pure-Silica Zeolite Thin Films by Vapor Phase Transport of Fluoride for Low-k Applications, *Microporous Mesoporous Mat.* © 2009 Elsevier.

1. Introduction

There is growing enthusiasm for the use of pure-silica zeolite (PSZ) films in applications such as chemical sensors, membrane reactors, and microelectronic devices.[1,2,3,4,5,6,7,8,9] For instance, the development of pure-silica zeolite thin films as low dielectric constant (low-*k*) materials is of particular interest to the semiconductor industry. Attempts to decrease feature size in microprocessors have been met with potential increases of cross-talk noise and energy dissipation. In order to overcome such limitations in an integrated circuit with feature sizes of 14 nm or smaller, an ultra-low-*k* material (between 2.3 – 2.6) must be developed to replace nonporous silica ($k = 4.0$) as the dielectric film insulating the wiring between transistors.[10] Typical approaches to the creation of low-*k* materials involve the introduction of porosity via methods such as sol-gel processing, surfactant-templating, and zeolite crystallization. Sol-gel-derived and surfactant-templated mesoporous silicas, however, tend to have low mechanical stiffness and high hydrophilicity.[11,12,13] In contrast, pure-silica zeolites are crystalline, porous structures with high mechanical strength, and high heat conductivity, as well as high thermal and chemical stability.[14,15] Additionally, the variety of zeolite topologies enables production of a tunable *k*-value by selecting topologies with different porosities. The porosity of a given zeolite is a function of its framework density (FD, the number of tetrahedrally-coordinated atoms per 1000 $Å^3$); for instance, the LTA topology first produced in pure-silica form by Corma et al. in 2004 has the lowest framework density (FD = 14.2) among all available pure-silica zeolites, and therefore could have the lowest dielectric constant.[16,17] For the reasons mentioned, the exploration of low-framework density pure-silica zeolites as low-*k* dielectric materials has generated great interest. However, these

efforts have been limited by the number of pure-silica zeolite materials that can be accessed via current zeolite thin film synthetic approaches, such as *in situ* crystallization, and the spin-on of zeolite nanoparticle suspensions. (*In situ* crystallization refers to a process where the zeolite film is grown *in situ* onto a bare substrate from a dilute precursor solution that is free from preformed crystals.) Indeed, of the 19 zeolite topologies with pure-silica compositions, only 4 (structure codes MFI (FD = 18.4, k = 2.7 via *in situ* crystallization and spin-coating), MEL (FD = 17.4, k = 1.9 via spin-coating, 1.51 via spin-coating followed by hydrofluoric acd-resistant modifications), *MRE (FD = 19.8, k = 2.7 via vapor phase transport), and BEA* (FD = 15.3, k = 2.3 via *in situ* crystallization, 2.07 via secondary growth)) have been prepared into films for zeolite low-k applications.[15,18,19,20,21,22]

Pure-silica zeolites can be synthesized from compositions that contain fluoride ions.[23,24] These fluoride-mediated syntheses produce the most promising candidates for low-k pure-silica zeolites materials, because they generally have low framework density and low silanol defect density when compared to pure-silica zeolites made using hydroxide as the mineralizing agent (such as the aforementioned films of MFI and MEL). However, the syntheses of fluoride-mediated zeolites have several features that are incompatible with current film *in situ* and spin-on deposition approaches. First, the extremely low H_2O / SiO_2 ratios (~ 2 – 7) required for crystallization prevents transport of reactants, such as the organic structure-directing agent (SDA) and mineralizing agent (F^-), from the bulk gel to the substrate through solvent mediation, and prevents good adhesion of material to the substrate. Second, the presence of the fluoride ion in the gel tends to cause severe

corrosion on direct contact with the substrate. Third, the synthesis conditions are not conducive to producing nanocrystals suitable for spin-on processes. When attempts are made to use *in situ* crystallization procedures to make films of fluoride-mediated zeolites, such as the pure-silica BEA*-type solids mentioned previously and aluminum-free LTA (the germanosilicate composition of LTA), the resulting films can suffer from poor adhesion to the substrate and are difficult to reproduce reliably. Similarly, seeded synthetic methods like secondary growth, such as the production of thin films of pure-silica BEA* may be limited by the production of zeolite nanocrystalts. The combination of these factors has made producing thin films of fluoride-mediated, pure-silica zeolites very difficult.

Resolving the aforementioned issues requires modification of current film synthesis techniques. To this end, we investigate two types of modifications to typical in situ crystallization routes that may overcome the limitations of fluoride-mediated syntheses: (1) the seeding and diluting of the zeolite precursor gel (Figure 3.1), and (2) the vapor phase transport of fluoride (Figure 3.2). Our interest is primarily in in situ techniques because these methods yield films of fully-intergrown crystals, which allows us to measure the intrinsic properties of the material, rather than the those of a composite material. To determine the viability of these two modifications, we applied them separately to the fluoride-mediated syntheses of zeolite LTA. Fluoride-mediated LTA was chosen as the test subject for this demonstration for the following reasons: (1) when made with fluoride, it can be made in both the pure-silica and the aluminum-free (germanosilicate) composition, which demonstrates whether the modifications are

applicable to a range of chemical compositions, (2) the synthesis of the pure-silica form requires the use of two structure-directing agents, making it one of the more difficult syntheses to reproduce, (3) the use of the LTA topology in its aluminosilicate form for its ion-exchange and water-softening properties represents the largest world-wide use of any zeolite, and (4) the pure-silica LTA structure has the lowest framework density of the known pure-silica zeolites and therefore, a film of this material could prove extremely useful for low-*k* applications. Additionally, a variety of *in situ* films techniques have been studied previously for the hydroxide-mediated, aluminosilicate LTA material, which provides insight into problems that might arise during film synthesis with the LTA structure. Therefore, the fluoride-mediated LTA materials are of great interest both in terms of end use and the difficulty of the synthesis. In this chapter, we discuss the results and effectiveness of these two modifications to the in situ film crystallization procedures.

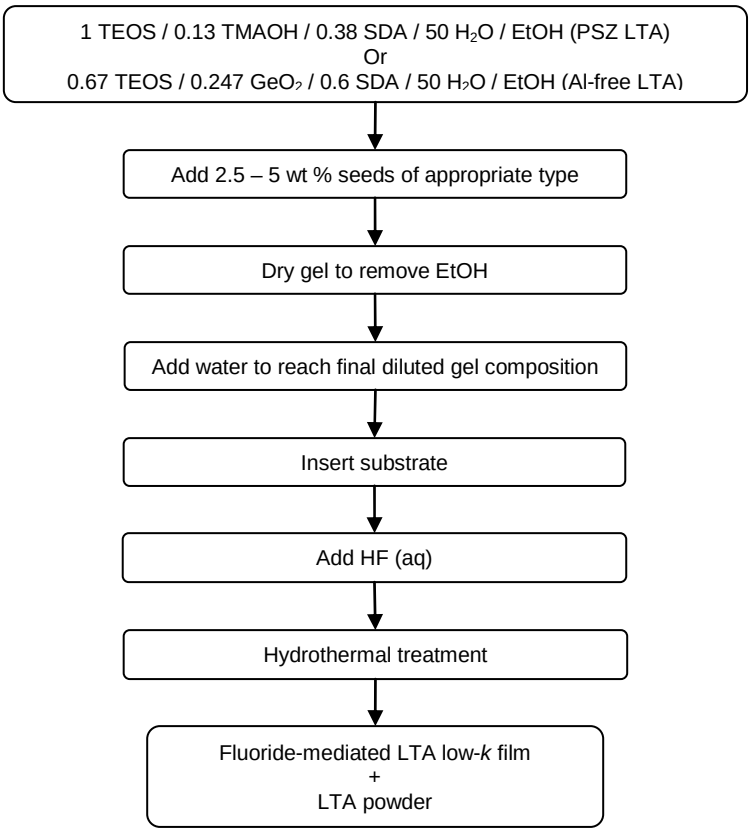

Figure 3.1 Schematic of the synthesis process of fluoride-mediated zeolite films by the seeding / diluting modification to in situ crystallization

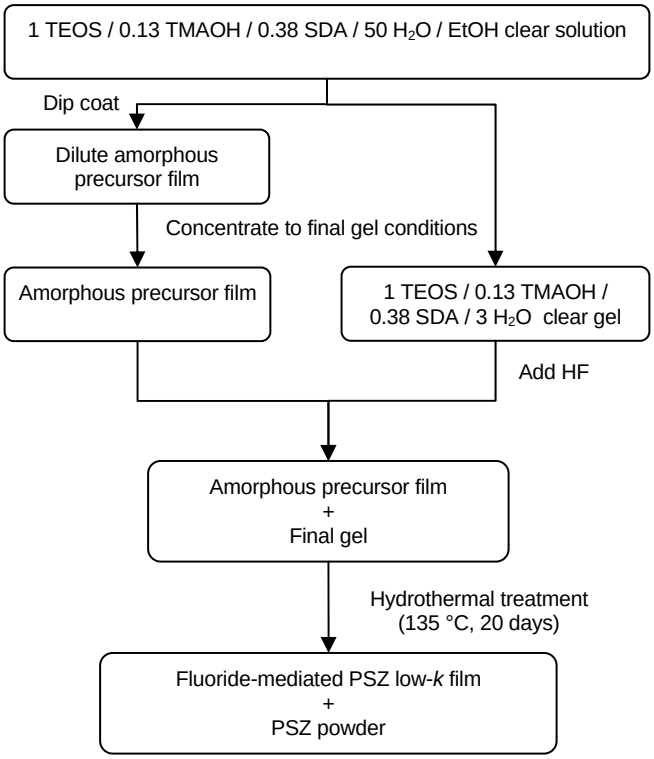

Figure 3.2 Schematic of the synthesis process of fluoride-mediated, pure-silica zeolite LTA films by the vapor phase transport of fluoride

2. Results and Discussion

The key to a film deposition method applicable to fluoride-mediated zeolites is to accommodate the common aspects of their powder syntheses: (1) tetraethylorthosilicate (TEOS) is the liquid silica source that is hydrolyzed for several hours to produce the source of silica, (2) the hydrolysis of TEOS requires excess water that must be removed from the gel prior to crystallization, (3) the final gel is usually very concentrated and extremely dry, and (4) hydrofluoric acid is used as the mineralizing agent, and is added to the gel just prior to crystallization. Additionally, many zeolite gels may be seeded to encourage growth of zeolite crystals of a specific phase, a step that detatchs the nucleation and crystal growth mechanisms of zeolite formation, as discussed in Chapter 1. To overcome the limitations of a lack of bulk transport of the zeolite precursor gel to the substrate surface, we must take advantage of either the ability to seed the precursor gel, which promotes growth of a pure phase of LTA, or of the time when the zeolite gel is dilute. The seeding / diluting modification takes advantage of the first, while the vapor phase transport of fluoride modification takes advantage of the second.

2.2 Seeding and Diluting the Zeolite Precursor Gel

Shortly after the introduction by Corma et al. of the pure-silica ITQ-29 (LTA topology) in 2004, Bouiza et al. demonstrated that, although the synthesis of pure-silica LTA is often difficult to repeat because of the difficulties of a fluoride-mediated synthesis that uses not one, but two structure-directing agents, the zeolite synthesis for high silicon-to-aluminum ratios could be greatly simplified by the addition of pre-formed LTA seeds.[25]

For instance, the LTA synthesis described by Corma et al. often resulted in a mixed LTA / AST zeolite phase if any of the conditions in the synthesis were even slightly off the described procedure. The addition of LTA seeds allowed the synthesis of the pure LTA phase to proceed repeatably, even when the synthesis conditions were slightly incorrect. This approach intrigued us, because seeding the zeolite precursor gel prior to hydrothermal treatment could allow us to also dilute the gel to conditions under which ITQ-29 does not typically form. Dilution of the gel would then solve the transport and adhesion limitation problems. Therefore, we modified the standard in situ crystallization protocols to include seeding the zeolite precursor gel with previously-made ITQ-29 seeds, diluting the zeolite gel by adding excess distilled, de-ionized water, and subjecting the gel to hydrothermal treatment in the presence of a substrate. The experimental ranges for the seed amount are 2.5 - 20 wt % of the amount of silica present in the zeolite gel, and for the water-to-silica ratio are 10 - 200 (germanosilicate phase) and 2 - 50 (pure-silica zeolite phase), as shown in Figures 3.3 and 3.4, below. Using this method over a wide range of synthesis conditions demonstrated that while the modifications to the in situ crystallization protocols did result in the formation and growth of the desired ITQ-29 composition in the bulk zeolite gel and powder, even at high dilutions (which was gratifying, as it increases the flexibility of the conditions under which ITQ-29 could form), it did not produce films of any quality on the substrate.

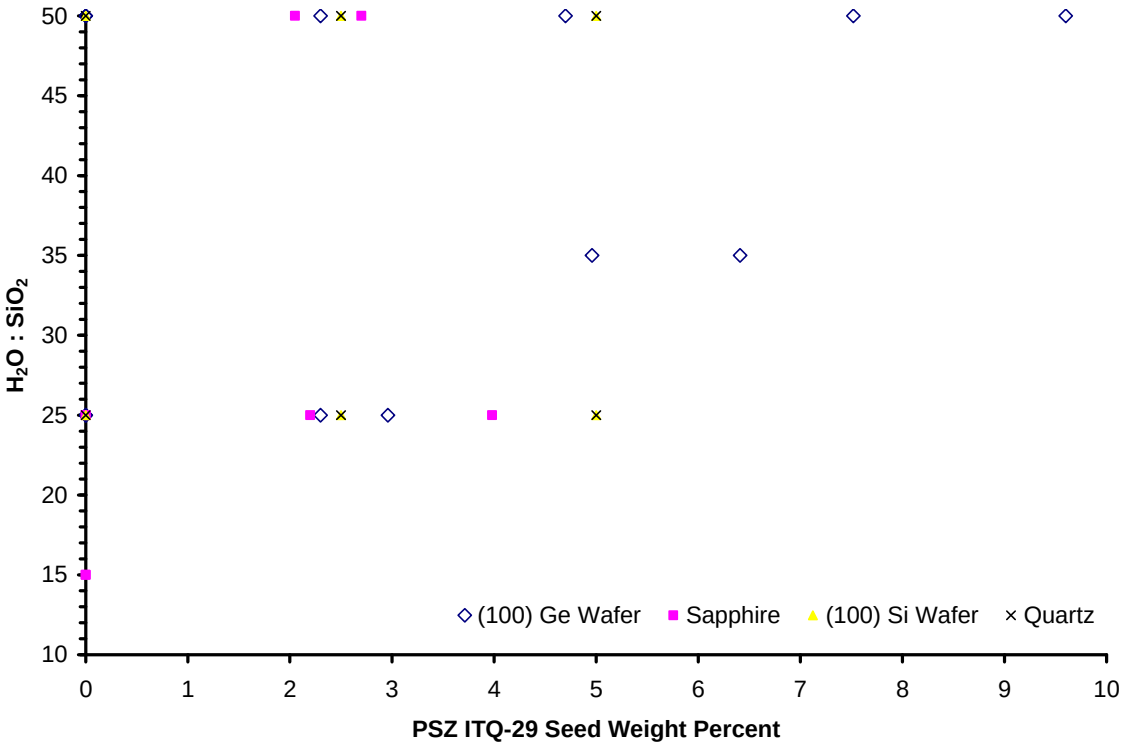

Figure 3.3 PSZ ITQ-29 (LTA) film synthesis attempts using various substrates, seed amounts, and dilutions

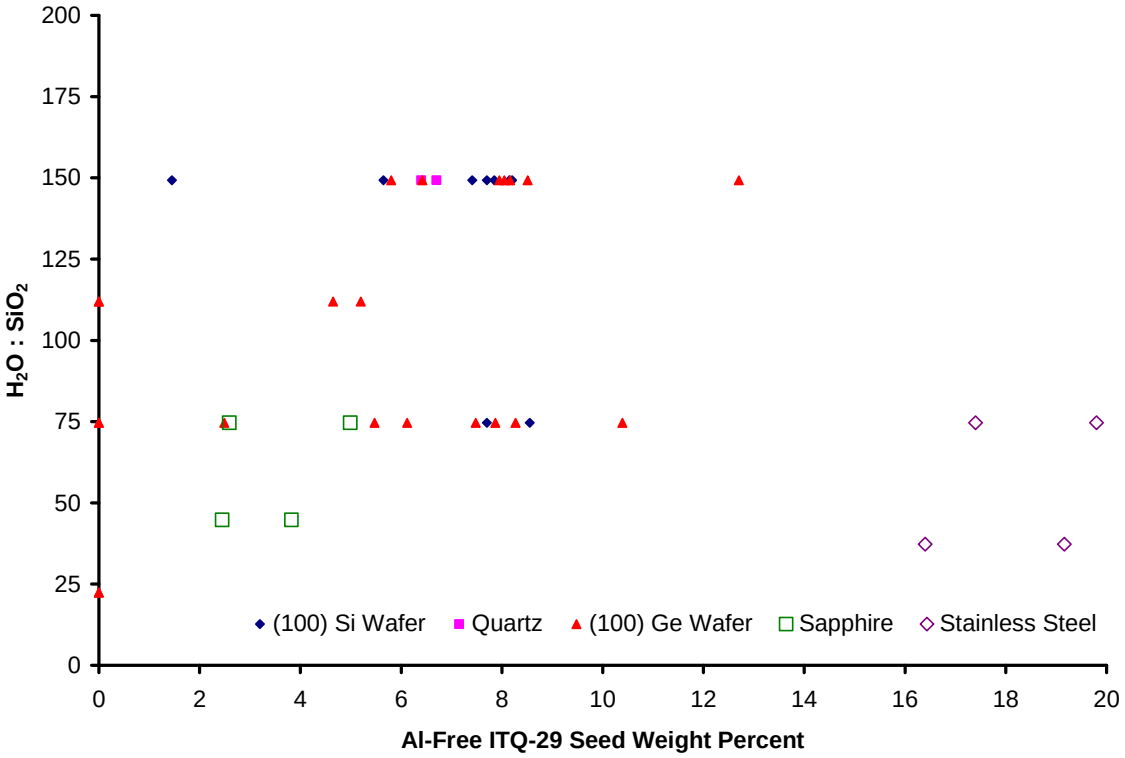

Figure 3.4 Al-free ITQ-29 (LTA) film synthesis attempts using various substrates, seed amounts, and dilutions

Low dilution and high seed amounts generally resulted in more favorable conditions for the development of ITQ-29 crystals in the bulk zeolite gel, but did not promote transport of nucleated zeolite crystals from the bulk gel to the support, nor did they promote nucleation on the surface of the substrate. The supports inspected for their viability as substrates included (100) Si, (100) Ge, sapphire (Al_2O_3 in a corundum topology, without impurities), stainless steel, and quartz. Additionally, the dilution of the zeolite precursor gel resulted in a slurry when the aqueous hydrofluoric acid was added, instead of the hoped-for clear solution. The presence of the hydrofluoric acid in the diluted bulk zeolite precursor gel also presented problems during crystallization, as the acid readily attacked the surface of the substrate, leading to leaching of the substrate into the bulk, and destroying the substrate itself. For instance, the (100) Si wafers, which had one polished side, frequently were blackened, pocked, and very brittle after hydrothermal treatment in the gel. The substrate itself also presented challenges to ITQ-29 formation, whether in the bulk or on the surface, because material from the substrate leaches very easily into the bulk gel, which adversely affected the gel composition, especially in the case of the stainless steel substrate. The presence of aluminum in the ITQ-29 syntheses, even in small amounts, and with seeds present, significantly reduced the ability of the ITQ-29 material to form. These results demonstrated that, although seeding and diluting the zeolite precursor gel increased the range of acceptable conditions for the synthesis ITQ-29 beyond what has been reported in literature, the modification did not fully address the problems associated with the fluoride-mediated, thin film syntheses.

2.3 Vapor Phase Transport of Fluoride

Traditionally, VPTM has been used to create membranes of aluminosilicate zeolites on porous alumina substrates by first covering the support by submersion in a parent gel containing alumina, silica, water, and the mineralizing agent, and then crystallizing the covered substrate hydrothermally in the presence of SDA and water in the vapor phase (the remaining parent gel not used for coating is not crystallized).[26] This process has been used to produce non-fluoride-mediated, pure-silica zeolite films of ZSM-48 (*MRE), for example. More recently, Matsukata and co-workers have extended this approach by incorporating the silica source in the vapor phase, rather than the SDA and solvent.[27] The traditional VPTM is not directly suited to fluoride-mediated zeolite film formation for the reasons mentioned previously regarding the unsuitability of standard *in situ* and spin-on techniques, but it does have some aspects that may be modified to fluoride syntheses. Traditional VPTM syntheses require a clear solution *containing the mineralizing agent* into which the substrate may be submerged, resulting in a loosely adhered coating. The only time a clear solution is present during a fluoride-mediated zeolite synthesis is during the hydrolysis of TEOS – prior to the addition of the mineralizing agent. After hydrolyzing, the water is evaporated from the gel, thus beginning the concentration of the gel to the required water content. We, therefore, modified the VPTM to take advantage of the time the gel is actually dilute - *prior to evaporation and addition of the mineralizing agent*. We deposited the amorphous precursor film by dipcoating of the dilute solution right after hydrolysis, before the precursor concentration (Figure 3.5).

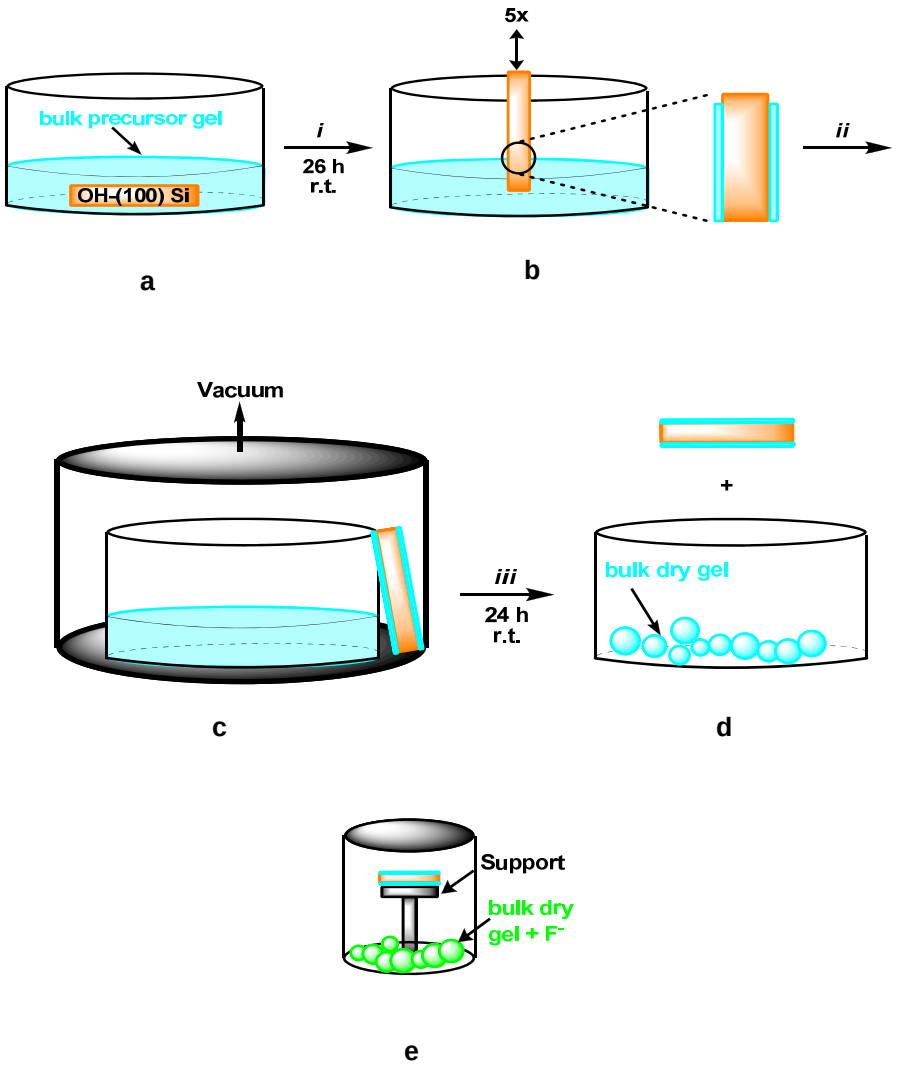

Figure 3.5 (a) Substrate submerged in ITQ-29 precursor gel of appropriate molar composition, (*i*) Stir to hydrolize the TEOS; (b) Substrate subjected to dip-coating, (*ii*) Dip-coat substrates, 5x, in the hydrolyzed gel to create amorphous precursor film; (c) Coated substrate and bulk precursor gel placed inside vacuum desiccator, (*iii*) Evaporate ethanol produced during hydrolysis and excess H_2O; (d) Amorphous precursor film and solid (dry) gel; (e) Introduce dry gel into Teflon®-lined Parr Autoclave after addition of HF (aq) to dry gel, introduce coated substrate (no HF present in amorphous film) into autoclave on elevated Teflon® platform, and crystallize via VPTM

Our new methodology for the synthesis of pure-silica zeolite films involves the dip-coating of the prepared substrate in a hydrolized parent gel *prior to evaporation and addition of the mineralizing agent,* and an ethanol/water evaporation step that is conducted in a low-temperature oven or at room temperature to adhere an amorphous film of that gel to the substrate. This low-temperature process prevents crack formation during evaporation of the excess solvent, a common problem with the coating process in the VPTM.[26] To prevent the amorphous films from flaking off the substrate, the native oxide layer present on the substrate is replaced with silanols via successive HF / piranha dips prior to dip-coating the substrate. This increases the hydrophilicity of the substrate and improves adhesion between the substrate and the amorphous precursor film. Dip-coating at this point also allows the final film thickness to be modified based on the number of coats; similarly, spin-coating could also be used to ensure repeatable, tunable film thicknesses. Note that dip-coating results in a substrate coated on both sides, and a final film on both sides of the substrate. After dip-coating and evaporating excess solvent, a solution of HF (aq) is then added to the dry bulk gel (not the dip-coated precursor film), which is mixed, and then introduced into a Teflon®-lined, Parr Autoclave. The coated substrate is placed on an elevated, Teflon® platform inside the autoclave to prevent contact with the fluoride-containing bulk gel. Crystallization of the film and bulk gel proceeds using temperatures reported in the literature from synthesis of powdered samples.

It should be noted that crystallizing the bulk gel with the coated substrate leads to a low process economy; however, we found that we could crystallize up to five films at once

(limited by the space in the Teflon liner) using one synthesis gel. It should also be possible to crystallize the substrate coating using only the aqueous solution of hydrofluoric acid in the linter, if the appropriate ratio of acid to gel coating is used. However, we did not investigate this, and instead used the presence of the bulk gel as a mediation tool for obtaining the correct ration of reagents. Note that, unlike the traditional VPTM, neither the solvent or the SDA is introduced purposefully to the amorphous precursor film via the vapor phase. Instead, we take advantage of the volatile nature (in the form of HF gas) of the mineralizing agent (F^-), and its transport via the vapor phase. It is possible that some amount of the other reagents in the bulk transfer via the vapor phase, but without the transport of the fluoride, the films would not crystallize. The vapor phase transport of the mineralizing agent prevents etching of substrate surfaces from direct contact with the aqueous hydrofluoric acid. Presumably, at long crystallization times, the F^- is present in three phases: the bulk gel, the vapor, and the supported gel. As the F^- transport through the supported gel, it is also consumed during crystallization, leading to a lower concentration reaching the substrate surface than the original concentration of F^- in the bulk gel, which reduces the possibility of damaging the substrate. Also, unlike the traditional VPTM, the bulk gel is crystallized in the same reactor as the amorphous substrate; this allows the dry bulk gel to correctly mediate the amount of F^- that reaches the precursor film through the vapor phase. Using these protocols, well-adhered, continuous thin films of both the silicate, and the germanosilicate compositions of ITQ-29 (LTA) were prepared, on (100) Si, quartz, and glass substrates. These syntheses consistently (~ 95% of synthesis trials) yielded high-quality films with similar characteristics. Interestingly, these results suggest that the

mechanism of film formation for this method is the crystallization of an amorphous gel coating on the surface of the support, as suggested by Myatt et al. and Kita et al.[28,29] Post-synthesis, the ITQ-29 films were calcined and mechanically polished to create thin films in the range of 0.5 – 2 μm thick for further characterization.

XRD patterns (Figure 3.6) show that the as-synthesized ITQ-29 films have pure LTA structure that is not affected by calcination and polishing. Micrographs, obtained via Field Emission Scanning Electron Microscopy (FE SEM), of a typical pure-silica ITQ-29 film show that the films are polycrystalline, intergrown, and continuous (Figure 3.7a), and are composed of cubic LTA crystals, (typical habit) ranging in size from less than 1 μm to 20 μm. Note that the films do not show evidence of cracking. Improper calcination (i.e., calcination at ramp rates faster than 1 °C / minute) result in cracked films due to the difference in thermal expansion of the substrate vs. the film itself. The ITQ-29 films on glass were calcined once to evaluate the effects of calcination. Interestingly, the film did not crack, but rather bent as the substrate melted. Additionally, films that were not calcined for an appropriate length of time under air still exhibited the presence of the structure-directing agents in the pore system; for particularly thick films, this resulted in a grey coloration to the film. A thin section (Figure 3.7b) of the film indicates that the thickness can be increased up to ~ 115 μm, although thinner films are generally obtained by using fewer dip-coats during synthesis. A relatively smooth surface (Figure 3.7c) with an average thickness of 1.7 μm (Fig. 3.7d) results from mechanically polishing the film. Interestingly, the LTA film syntheses tend to produce very regular crystals of its typical habit with the cubic face roughly normal to the substrate. This

suggests that zeolite crystal growth is more favorable in the direction that results in a high surface area contact with the substrate. Also interesting is that while the films could be produced with ease on quartz, glass, and (100) Si, we were unable to produce films on stainless steel or (111) Ge. The former was due to leaching of aluminum from the substrate during the film synthesis, which inhibits the growth of pure-silica zeolite LTA for the compositional regime discussed here, while the latter was due to a lattice mismatch between the substrate and the film, which prevented good adhesion to the substrate via typical bonding. The end results of this method are polycrystalline, intergrown, and continuous films on silicon-based substrates that can be polished to smooth surfaces.

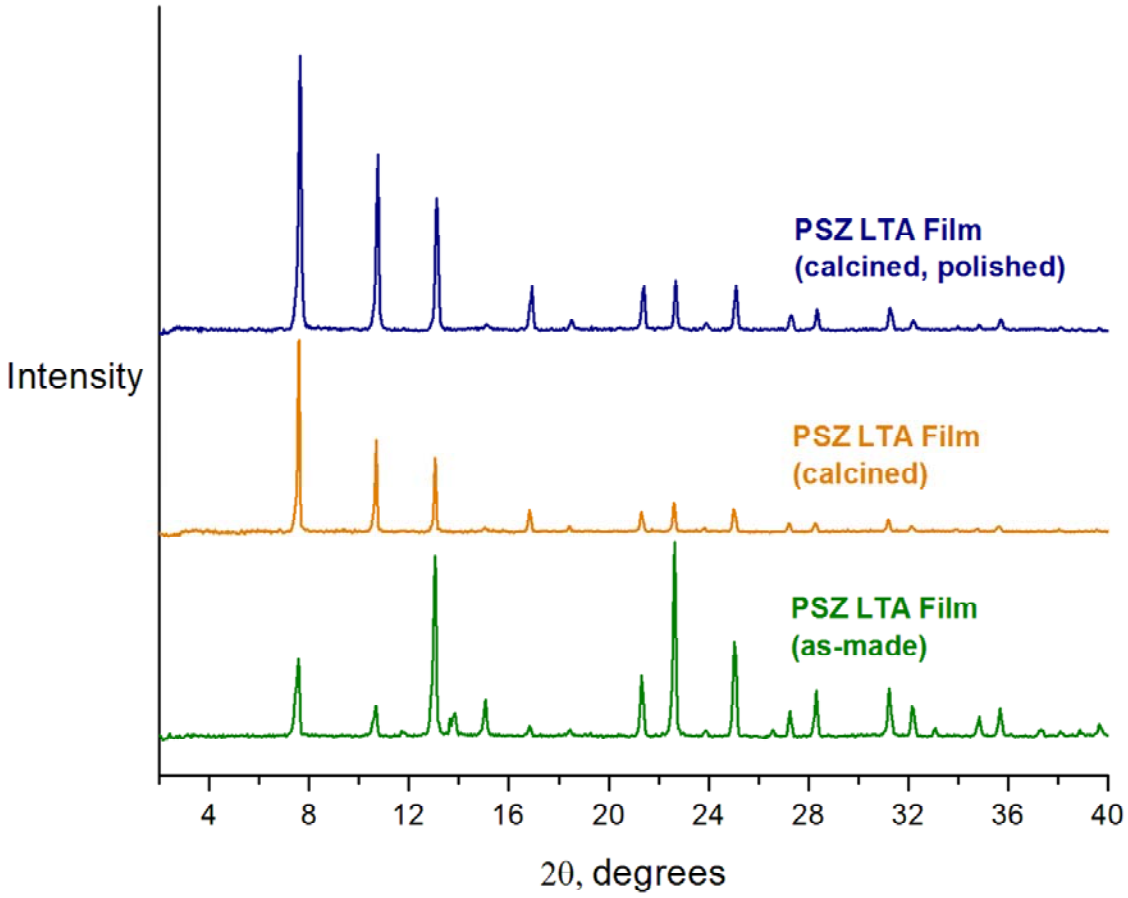

Figure 3.6 X-ray diffraction patterns of as-made, calcined and polished PSZ LTA film samples on OH-(100) Si demonstrates phase crystallization of the precursor film using the VPTM of fluoride

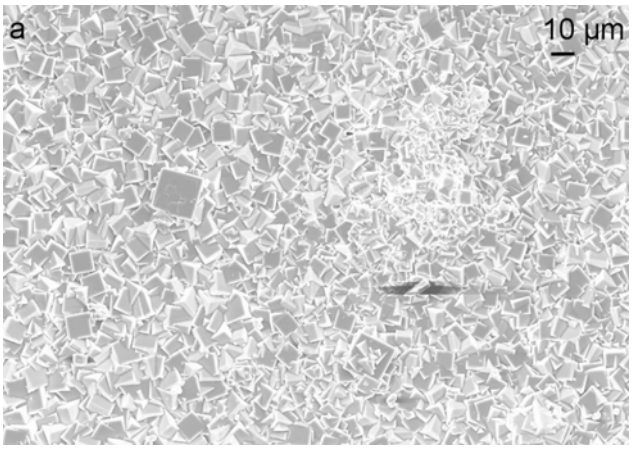
a
10 µm

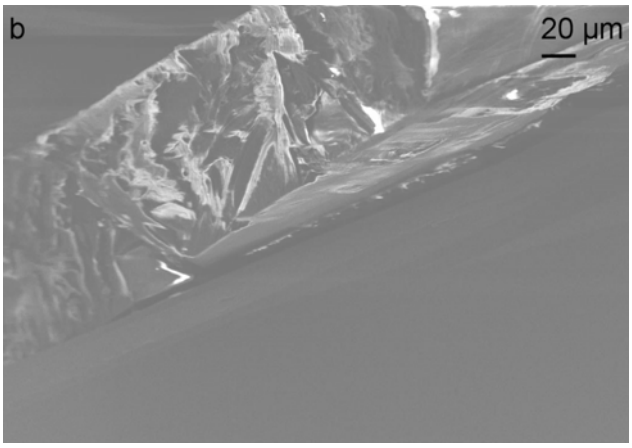
b
20 µm

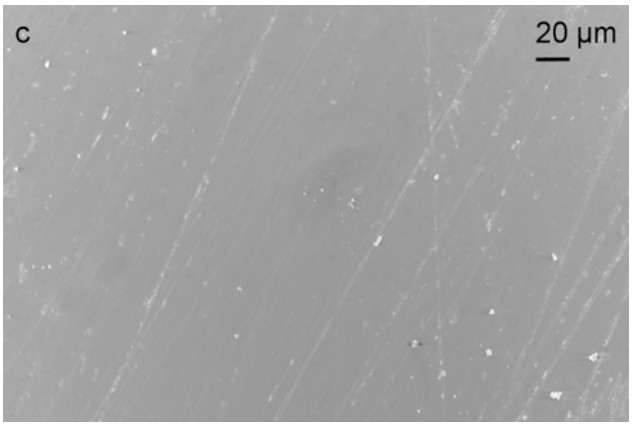
c
20 µm

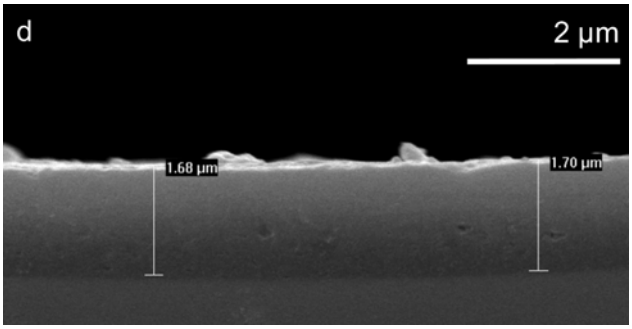

Figure 3.7 FE SEM micrographs of (a) surface of calcined PSZ LTA film; (b) a thin section of calcined PSZ LTA film showing ~ 115 µm thick film; (c) surface of calcined PSZ LTA film after mechanical polishing; (d) a thin section of calcined PSZ LTA film after polishing showing ~ 1.7 µm thick film

Energy Dispersive X-ray Spectroscopy (EDS, Table 3.1) was used to show that the calcined, pure-silica LTA films are indeed pure-silica (66.65 atomic % O and 33.21 atomic % Si, with other elements (for example, carbon, tungsten, and vanadium, likely due to contaminants in the FE SEM) present in trace quantities), and that the SDA has been fully removed from the pores.

Table 3.1 Energy dispersive spectrometry (EDS) data of the amorphous precursor film supported on OH-(100) Si demonstrates that the film is pure-silica, with the carbon content appearing due to the TMAOH and SDA in the precursor gel. EDS data for the calcined sample indicates that the carbon content has been completely removed.

	Amorphous Precursor Film			Calcined Film	
	Si	**O**	**C**	**Si**	**O**
Weight %	28.42	33.52	38.07	46.58	53.25
Weight % σ	1.56	1.96	3.14	0.53	0.58
Atomic %	16.12	33.38	50.50	33.21	66.65

The average mechanical properties of the ITQ-29 films on low-resistivity (100) silicon wafers were evaluated (Figure 3.8). A mean elastic modulus of E = 49 GPa (σ = 18) was obtained for the samples via nanoindentation tests, which surpasses the minimum modulus (E > 6 GPa) required for survival in the chemical and mechanical polishing process during integrated circuit fabrication. The reasons for the wide range in the modulus obtained from these nanoindentation measurements are currently unknown, but it is likely due to a combination of factors, including (1) the polycrystallinity of the film, whose grain boundaries may affect the compression tests, (2) the varying orientation of the crystals, since the mechanical properties of the crystals may be different for different orientations, and (3) the presence of some small crystals remaining on the surface after polishing, which will behave differently than a crystal fully imbedded in the film.

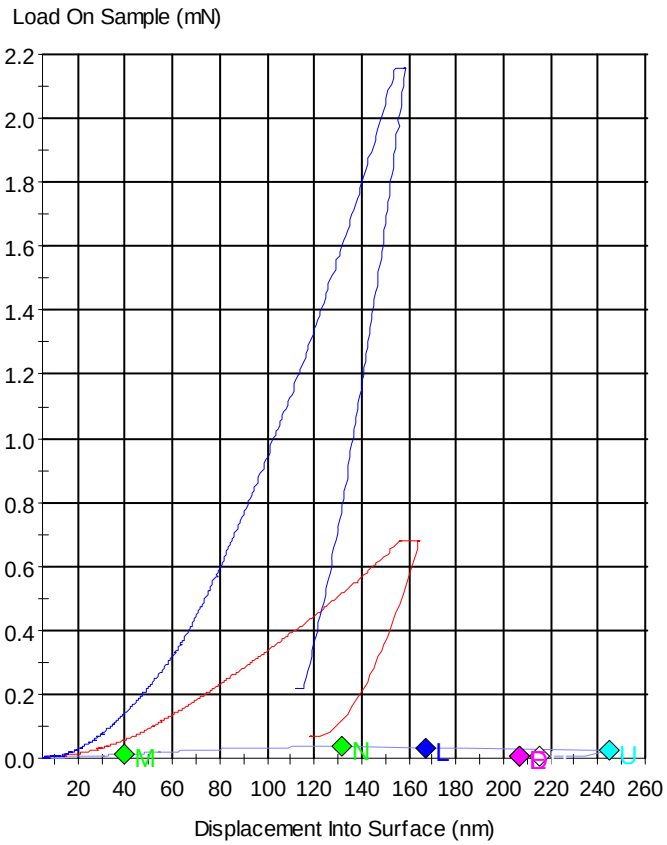

Figure 3.8 Load / displacement curves for the PSZ ITQ-29 films on (100) Si wafers indicate that different elastic moduli are obtained at different indentation sites

3. Conclusions

We have examined two signficant modifications to standard in situ film crystallization techniques: a seeding / diluting modification, and a vapor phase transport of the fluoride ion modification on the film synthesis of the ITQ-29 (LTA) zeolite. While the seeding / diluting modification did not yield ITQ-29 films, it did show that the acceptable composition range for producing ITQ-29 could be increased by the presence of pre-formed ITQ-29 seeds. This modification was particularly stymied by the degradation of the substrate due to direct contact with hydrofluoric acid in the synthesis. The second modification, which used the vapor phase transport method, eliminated the problems of contact with the hydrofluoric acid by transporting the fluoride via the vapor phase. Therefore, we developed a new and general film deposition method that takes advantage of the vapor phase transport of the fluoride mineralizing agent. Specifically, we made a simple but significant modification of the Vapor Phase Transport Method (VPTM, for generating aluminosilicate membranes) by taking advantage of the volatility of the mineralizing agent and transporting it (not the solvent or SDA as in the traditional VPTM) via the vapor phase.[30,31] Using this method, we obtained well-adhered, continuous, and polycrystalline films of the pure-silica and germanosilica zeolites with LTA topology for the first time. This was a facile, reproducible, and general scheme for the production of fluoride-mediated, pure-silica zeolite films. The synthesis scheme may extend the current library of pure-silica zeolite films to include a wider range of topologies not obtainable via other synthetic methodologies. These materials could be beneficial to low-*k* dielectric applications, as well as catalytic and sensor applications.

Lastly, this method could result in other approaches to applications, such as ink-jet printing and patterning of films.

4. Experimental

4.1 Synthesis of Structure-Directing Agent (4-methyl-2,3,6,7-tetrahydro-1H,5H-pyrido [3.2.1-ij] quinolinium hydroxide)

10 g of julolidine (97%, Aldrich) was dissolved in 100 mL of $CHCl_3$ (EMD). 24.5 g of CH_3I (99%, Aldrich) was then added and the resulting mixture was stirred at room temperature under Ar for three days. The addition of CH_3I, followed by stirring for three days, was repeated twice more. The solution was then quenched with 50 mL of double de-ionized (DDI) H_2O, and stirred for 30 min. The solvent was removed using a rotovap and the solids obtained were washed with ether and dried again using a rotovap. The crude product was recrystallized from 100 mL dichloromethane (EMD) at its boiling point and 50 mL of cold hexane (EMD). Pale yellow crystals of 4-methyl-2,3,6,7-tetrahydro-1H,5H-pyrido [3.2.1-ij] quinolinium iodide were obtained after vacuum drying the resulting solid; ^{13}C-NMR of the product (300MHz, D_2O, δ): 18.2, 25.8, 53.5, 65.9, 131.2, 132.0, 132.5, 141.0. The product (5.54 g, 17.6 mmol) was ion-exchanged from its iodide form to its hydroxide form by dissolution in 150 mL of DDI H_2O and stirring with 25.1 g of Bio-Rad AG1-X8 anion exchange resin for 24 h. The solution was then filtered and concentrated to 0.1 - 0.3 M concentration of the hydroxide form using a rotovap. The conversion from iodide to hydroxide was 95.2% based on titration of the resultant solution.

4.2 Synthesis of ITQ-29 (LTA) Films and Powder Via Seeding / Diluting

ITQ-29 (LTA) can be made with a germanosilicate, as well as a purely siliceous, composition. We attempted to synthesize films of each composition on a variety of substrates (low-resistivity (0.008 – 0.02 Ω cm), (100) silicon wafers (University Wafers), quartz wafers (University Wafers), glass microslides (Corning), sapphire wafers (University Wafers), and stainless steel. The pure-silica or germanosilicate precursor gel was prepared in a Teflon® jar by hydrolyzing tetraethylorthosilicate (TEOS, 98%, Aldrich) in an aqueous solution of SDA A and either tetramethylammonium hydroxide (TMAOH, 25%, Aldrich) for the pure-silica form or germanium (IV) oxide (GeO_2, Alfa Aesar) for the germanosilicate form. The precursor gel of molar composition 1.0 TEOS / 0.13 TMAOH / 0.38 SDA / 50 H_2O / 0 – 5 wt % seeds (pure-silica gel) or 0.67 TEOS / 0.247 GeO_2 / 0.6 SDA / 50 H_2O / 0-5 wt % seeds (germanosilicate gel), on a 1.000 g TEOS basis, was stirred for 26 h at room temperature to ensure complete hydrolysis of TEOS. A Teflon® cap with two small holes drilled in it was screwed onto the jar containing the bulk precursor gel. The enclosed bulk precursor gel was placed inside a vacuum desiccator, and the ethanol and excess H_2O present in the bulk precursor gel and precursor film were evaporated. Evacuation for 48 h at room temperature yielded a solid (dry) bulk gel of molar composition 1.0 SiO_2 / 0.13 TMAOH / 0.38 SDA / 2.0 H_2O / 0 – 5 wt % seeds (for the pure-silica form) or .67 TEOS / 0.247 GeO_2 / 0.6 SDA / 7.0 H_2O / 0 - 5 wt % seeds(for the germanosilicate form). The gel was then diluted to the final water concentration, an aqueous solution of hydrofluoric acid (48%, Mallinckrodt) was added to the jar in molar ratio 0.50 HF / 1.0 SiO_2 (pure-silica form) or 0.60 HF / 0.67 SiO_2 (germanosilicate form), and the sample was stirred with a Teflon® spatula. The dry bulk

gel, followed by a 4 cm x 2 cm substrate cleaned of organics via an HF etch, was introduced into a Teflon®-lined Parr Autoclave. The crystallization was carried out at 135 °C (pure-silica form) or at 150 °C (germanosilicate form) for 7 – 20 days. The reactor was removed from the oven and cooled. The bulk solids and the substrate were washed with 100 mL each of acetone (EMD) and DDI H_2O. The crystalline material was placed in an evaporating dish and dried for 24 h in a 100 °C oven. The organic SDA was removed from the powder samples by calcination in air at 700 °C for 5 h using a ramp rate of 2 °C / min, with pauses at 350 °C and 580 °C for 3 h each.

4.3 Synthesis of ITQ-29 (LTA) Films and Powder Via Vapor Phase Transport of Fluoride

ITQ-29 (LTA) can be made with a germanosilicate, as well as a purely siliceous, composition. We synthesized films of each composition on a variety of substrates (low-resistivity (0.008 – 0.02 Ω cm), (100) silicon wafers (University Wafers), quartz wafers (University Wafers), and glass microslides (Corning). These substrates were modified to present Si-OH terminal groups on their surface by soaking in a pirahna-type etch solution, i.e., 10 mL H_2SO_4 (97%, J.T. Baker) : 40 mL H_2O_2 (30%, EMD) : 2 drops of HF (48%, Mallinckrodt), for 2 min, followed by 15 min in DDI H_2O [29]. The pure-silica or germanosilicate precursor gel was prepared in a Teflon® jar by hydrolyzing tetraethylorthosilicate (TEOS, 98%, Aldrich) in an aqueous solution of SDA A and either tetramethylammonium hydroxide (TMAOH, 25%, Aldrich) for the pure-silica form or germanium (IV) oxide (GeO_2, Alfa Aesar) for the germanosilicate form. A 4 cm x 2 cm, previously modified substrate was then submerged in the gel. The precursor gel of molar

composition 1.0 TEOS / 0.13 TMAOH / 0.38 SDA / 50 H_2O (pure-silica gel) or 0.67 TEOS / 0.247 GeO_2 / 0.6 SDA / 50 H_2O (germanosilicate gel), on a 1.000 g TEOS basis, was stirred for 26 h at room temperature to ensure complete hydrolysis of TEOS. The submerged substrate was thereafter removed from the gel, and subjected to dip-coating up to five times in the hydrolyzed gel, with 30 min of drying on a Teflon® substrate holder at room temperature between coats. This created an amorphous precursor film on the substrate. A Teflon® cap with two small holes drilled in it was screwed onto the jar containing the bulk precursor gel. The coated substrate, in its holder, and the enclosed bulk precursor gel were each placed inside a vacuum desiccator, and the ethanol and excess H_2O present in the bulk precursor gel and precursor film were evaporated. Evacuation for 48 h at room temperature yielded an amorphous precursor film and a solid (dry) bulk gel of molar composition 1.0 SiO_2 / 0.13 TMAOH / 0.38 SDA / 2.0 H_2O (for the pure-silica form) or .67 TEOS / 0.247 GeO_2 / 0.6 SDA / 7.0 H_2O (for the germanosilicate form). If, after drying, too much H_2O had been removed, DDI H_2O was added to the jar to obtain the correct total gel mass. An aqueous solution of hydrofluoric acid (48%, Mallinckrodt) was added to the jar in molar ratio 0.50 HF / 1.0 SiO_2 (pure-silica form) or 0.60 HF / 0.67 SiO_2 (germanosilicate form) and the sample was stirred with a Teflon® spatula. The dry bulk gel, followed by the coated substrate on an elevated Teflon® platform, was introduced into a Teflon®-lined Parr Autoclave. The crystallization of the bulk gel and the precursor films for 20 days was carried out at 135 °C (pure-silica form) or at 150 °C (germanosilicate form). The reactor was removed from the oven and cooled. The bulk solids and the film were washed with 100 mL each of acetone (EMD) and DDI H_2O. The crystalline material was placed in an evaporating

dish and dried for 24 h in a 100 °C oven. The organic SDA was removed from the powder and film samples by calcination in air at 700 °C for 5 h using a ramp rate of 1 °C / min, with pauses at 350 °C and 580 °C for 3 h each.[17]

4.4 Characterization

The chemicals synthesized to produce the zeolite precursor gels were characterized using a combination of liquid-state ^{1}H and ^{13}C NMR with a Varian Mercury 300 MHz spectrometer. The as-made and calcined zeolite samples were evaluated using powder X-ray diffraction (XRD) on a Scintag XDS 2000 diffractometer operated at -40 kV and 40 mA using Cu K_{α} radiation (λ = 1.54056 Å) and a solid-state Ge detector in the 2θ range of 2-40 at a step size of 0.5 ° / min. TGA was performed on a NETZSH STA 449C analyzer in air using an aluminum sample pan at a rate of 5 °C / min. All FE SEM was done on a LEO 1550 VP FE SEM at an electron high tension (EHT) of 10 kV using samples that were coated, using a metal sputtering coater, with 5 nm of Pt to minimize the effects of charging. EDS measurements were carried out using an Oxford INCA Energy 300 EDS system. Elastic modulus and hardness measurements for the pure-silica zeolite LTA films on (100) Si were obtained via nanoindentation with an Agilent Corp. Nanoindenter G200 using a Berkovich diamond punch, a strain rate of 0.050, an indentation depth of 150 nm, and a Poisson ratio of 0.329, obtained via averaging data from Hazen et al. on the compressibility of zeolite LTA.[12,32,33,34,35] The calcined films were mechanically polished using a Buehler EComet 3000 Polisher equipped with 0.05 μm Al_2O_3 polishing suspension and a 3 μm abrasive lapping film.

5. References

[1] Davis, M. E. Ordered porous materials for emerging applications. *Nature* **417**, 813-821 (2002).

[2] Caro, J. & Noack, M. Zeolite membranes - Recent developments and progress. *Microporous Mesoporous Mat.* **115**, 215-233 (2008).

[3] McLeary, E. E., Jansen, J. C. & Kapteijn, F. Zeolite based films, membranes and membrane reactors: Progress and prospects. *Microporous Mesoporous Mat.* **90**, 198 (2006).

[4] Bein, T. Synthesis and applications of molecular sieve layers and membranes. *Chem. Mater.* **8**, 1636-1653 (1996).

[5] Mintova, S. & Bein, T. Nanosized zeolite films for vapor-sensing applications. *Microporous Mesoporous Mat.* **50**, 159-166 (2001).

[6] Yan, Y. G. & Bein, T. Molecular Recognition Through Intercalation Chemistry - Immobilization Of Organoclays On Piezoelectric Devices. *Chem. Mater.* **5**, 905-907 (1993).

[7] Yan, Y. G. & Bein, T. Molecular Recognition On Acoustic-Wave Devices - Sorption In Chemically Anchored Zeolite Monolayers. *J. Phys. Chem.* **96**, 9387-9393 (1992).

[8] Bein, T. *et al.* Microporous Assemblies For Chemical Recognition - Zeolite Layers And Sol-Gel-Derived Glass-Films On Sensors. *Abstr. Pap. Am. Chem. Soc.* **204**, 161-COLL (1992).

[9] Salomon, M. A., Coronas, J., Menendez, M. & Santamaria, J. Synthesis of MTBE in zeolite membrane reactors. *Appl. Catal. A-Gen.* **200**, 201-210 (2000).

[10] *International Technology Roadmap for Semiconductors* (2007).

[11] Maex, K. *et al.* Low dielectric constant materials for microelectronics. *J. Appl. Phys.* **93**, 8793-8841 (2003).

[12] Li, Z. J. *et al.* Mechanical and dielectric properties of pure-silica-zeolite low-k materials. *Angew. Chem.-Int. Edit.* **45**, 6329-6332 (2006).

[13] Morgen, M. *et al.* Low dielectric constant materials for ULSI interconnects. *Annu. Rev. Mater. Sci.* **30**, 645-680 (2000).

[14] Yan, Y., Wang, Z. & Wang, H. *Silica Zeolite Low-K Dielectric Thin Films*. U.S. Patent #6573131 (2003).

[15] Wang, Z. B., Wang, H. T., Mitra, A., Huang, L. M. & Yan, Y. S. Pure-silica zeolite low-k dielectric thin films. *Adv. Mater.* **13**, 746-749 (2001).

[16] Corma, A., Rey, F., Rius, J., Sabater, M. J. & Valencia, S. Supramolecular self-assembled molecules as organic directing agent for synthesis of zeolites. *Nature* **431**, 287-290 (2004).

[17] Tiscornia, I. *et al.* Preparation of ITQ-29 (Al-free zeolite a) membranes. *Microporous Mesoporous Mat.* **110**, 303-309 (2008).

[18] Liu, Y., Sun, M. W., Lew, C. M., Wang, J. L. & Yan, Y. S. MEL-type pure-silica zeolite nanocrystals prepared by an evaporation-assisted two-stage synthesis method as ultra-low-k materials. *Adv. Funct. Mater.* **18**, 1732-1738 (2008).

[19] Mitra, A. *et al.* Synthesis and evaluation of pure-silica-zeolite BEA as low dielectric constant material for microprocessors. *Ind. Eng. Chem. Res.* **43**, 2946-2949 (2004).

[20] Hu, L. L., Wang, J. L., Li, Z. J., Li, S. & Yan, Y. S. Interfacial adhesion of nanoporous zeolite thin films. *J. Mater. Res.* **21**, 505-511 (2006).

[21] Cho, Y. Pure Silica Zeolite Films Prepared by a Vapor Phase Transport Method. *Japanese Journal of Applied Physics, Parts 1 & 2* **47**, 8360-8363 (2008).

[22] Chen, Y. L. *et al.* Synthesis and characterization of pure-silica-zeolite Beta low-k thin films. *Microporous Mesoporous Mat.* **123**, 45-49, doi:10.1016/j.micromeso.2009.03.022 (2009).

[23] Zones, S. I. *et al.* The fluoride-based route to all-silica molecular sieves; a strategy for synthesis of new materials based upon close-packing of guest-host products. *Comptes Rendus Chimie* **8**, 267-282 (2005).

[24] Corma, A. & Davis, M. E. Issues in the synthesis of crystalline molecular sieves: Towards the crystallization of low framework-density structures. *ChemPhysChem* **5**, 304-313 (2004).

[25] Bouizi, Y., Paillaud, J. L., Simon, L. & Valtchev, V. Seeded synthesis of very high silica zeolite A. *Chem. Mater.* **19**, 652-654 (2007).

[26] Matsukata, M. & Kikuchi, E. Zeolitic membranes: Synthesis, properties, and prospects. *Bull. Chem. Soc. Jpn.* **70**, 2341-2356 (1997).

[27] Mitra, A., Ichikawa, S., Kikuchi, E. & Matsukata, M. Hydrovapothermal conversion of tetraethoxysilane vapor to polycrystalline zeolite layer by in situ gelation. *Chem. Commun.*, 900-901 (2004).

[28] Myatt, G. J., Budd, P. M., Price, C. & Carr, S. W. Synthesis of a Zeolite NaA Membrane. *J. Mater. Chem.* **2**, 1103-1104 (1992).

[29] Kita, H., Horii, K., Ohtoshi, Y., Tanaka, K. & Okamoto, K. I. Synthesis of a Zeolite NaA Membrane for Pervaporation of Water-Organic Liquid-Mixtures. *J. Mater. Sci. Lett.* **14**, 206-208 (1995).

[30] Kim, M. H., Li, H. X. & Davis, M. E. Synthesis of zeolites by water-organic vapor-phase transport. *Microporous Mater.* **1**, 191-200 (1993).

[31] Brinker, C. J. Evaporation-induced self-assembly: Functional nanostructures made easy. *MRS Bull.* **29**, 631-640 (2004).

[32] Johnson, M., Li, Z. J., Wang, J. L. & Yan, Y. S. Mechanical characterization of zeolite low dielectric constant thin films by nanoindentation. *Thin Solid Films* **515**, 3164-3170 (2007).

[33] Xiang, Y., Chen, X., Tsui, T. Y., Jang, J. I. & Vlassak, J. J. Mechanical properties of porous and fully dense low-kappa dielectric thin films measured by means of nanoindentation and the plane-strain bulge test technique. *J. Mater. Res.* **21**, 386-395 (2006).

[34] Hazen, R. M. Zeolite Molecular-Sieve 4a - Anomalous Compressibility And Volume Discontinuities At High-Pressure. *Science* **219**, 1065-1067 (1983).

[35] Hazen, R. M. & Finger, L. W. Compressibility Of Zeolite-4a Is Dependent On The Molecular-Size Of The Hydrostatic-Pressure Medium. *J. Appl. Phys.* **56**, 1838-1840 (1984).

Chapter 4: Investigation of Dielectric Properties of Fluoride-Mediated, Pure-Silica Zeolite Thin Films

Abstract

The fluoride-mediated synthesis of pure-silica zeolite thin films with the CHA, STT, ITW and -SVR topologies on surface-modified (100) Si wafers is reported. The films are prepared using the vapor phase transport of the fluoride mineralizing agent, a method used previously to make thin films of the pure-silica zeolite topology LTA. The CHA, STT, ITW, and -SVR films are polycrystalline, intergrown, continuous, and well-adhered to their substrates. The films are characterized by a combination of techniques, including X-ray diffraction and field emission scanning electron microscopy. The fluoride-mediated, pure-silica LTA, CHA, STT, ITW, and -SVR zeolite powders and films are investigated for low dielectric constant (low-*k*) material applications. This investigation demonstrates not only that these materials are appropriate for low-*k* applications, especially the LTA topology, which has the lowest intrinsic dielectric constant of all the pure-silica zeolites, but also shows interesting dielectric behavior with respect to porosity. All the zeolites investigated here, except STT, give *k*-values lower than predicted from their structures using the Bruggeman effective medium model, which has been commonly employed and found able to predict dielectric constants of amorphous silicas. This marks an inherent difference between zeolites and other porous silicas, and suggests the potential to tailor the dielectric properties based on not only porosity, but also pore architecture.

Reproduced in part with permission from H. K. Hunt, C. M. Lew, M. Sun, Y. Yan and M. E. Davis, Pure-Silica LTA, CHA, STT, ITW, and -SVR Thin Films and Powders for Low-k Applications, submitted to *Microporous Mesoporous Mat*. 2009.

1. Introduction

As feature sizes in integrated circuits continue to decrease, a corresponding increase in energy dissipation, resistance-capacitance delay, and cross-talk noise is expected to become a significant issue for microprocessors.[1,2] To combat this, the semiconductor industry must develop a replacement for the traditional dense silica dielectric material used to insulate the wiring between transistors. According to the International Technology Roadmap for Semiconductors 2007 Edition – Interconnect, an ultra-low dielectric material with an effective k between 2.3 and 2.6 (in comparison to $k \sim 4$ for dense silica) is needed to accommodate an integrated circuit with feature sizes of 14 nm or smaller by 2020.[1] Additionally, this new material must be capable of integration with current fabrication processes, and must withstand normal operation conditions. These requirements restrict the types of materials that may be useful for this application. For instance, to integrate with the interconnect fabrication processes, the dielectric material must have mechanical and chemical properties similar to silica, such as an elastic modulus greater than 6 GPa to survive chemical and mechanical polishing, a high fracture toughness to prevent cracking, thermal expansion coefficients similar to that of the metal interconnects to reduce failure during thermal cycling, and lastly, high chemical and thermal stability to avert dielectric degradation or decomposition.[3,4,5] It is for these reasons that the general approach to finding new low-k materials involves investigating both their electronic and physicochemical properties.

The familiar parallel-plate capacitor is shown in Figure 4.1, with a dielectric medium between the two plates. A dielectric material for capacitive applications is ideally

electrically non-conductive, but easily polarized, as this allows the medium to store energy through polarization when an electric field is applied. Polarization induces a net charge density on the plates of the capacitor, and therefore increases the charge storage capacity of a capacitor. Dielectric materials are also useful, as mentioned above, for insulating current-carrying conductors. The dielectric constant, also known as the relative permittivity, of a dielectric medium is a measure of the relative increase in the capacitance of a capacitor when the insulation between the two plates is changed to a dielectric medium from vacuum. The capacitance equation is then given by Equation 4.1, where C is the capacitance, ε is the permittivity, A is the plate area, and d is the separation between plates. The permittivity is defined as the relative permittivity (symbolized by either *k*, as used in the microelectronic industry, or ε_r, as used in the scientific community) multiplied by the permittivity of free space (ε_0), as shown in Equation 4.2.

$$C = \frac{\varepsilon A}{d} \qquad \textbf{4.1}$$

$$\varepsilon = \kappa \varepsilon_0 \qquad \textbf{4.2}$$

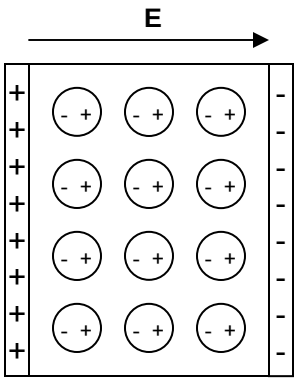

Figure 4.1 Cartoon of a parallel-plate capacitor with a dielectric medium polarized by an electric field, **E**

Typically, the intrinsic dielectric constant of a material is calculated from parallel-plate capacitance measurements and Equations 4.1 and 4.2, as shown in Figure 4.2a, obtained at a specific frequency (usually 1 MHz, as this is similar to operation conditions) using an LCR meter. This measurement is generally carried out under flowing, dry argon to prevent accumulation of water in the sample, which has been shown to increase the dielectric constant of materials with even a slight hydrophilicity. For additional prevention of water adsoption, the surface of the materials may be capped to prevent water adsorption; for instance, it is common to cap silicate materials using a vapor-phase silylation procedure.[6] Parallel-plate capacitance measurements are very straightforward, but have the disadvantage of requiring perfect parallelism via the preparation of high quality, thin films or sheet-like structures, in the metal-insulator-metal structures to obtain consistent and accurate capacitance measurements. An alternative method is time-domain reflectometry (TDR), in which it is coupled with a transmission line, as shown in Figure 4.2b. TDR is generally used to assess impedance variations along transmission lines such as cables, connectors, or circuit boards, and has been shown to be useful for studying small quantities of powders for both high- and low-*k* applications. This method

avoids the necessity of creating perfect thin films of materials, which often requires very expensive chemical or mechanical polishing equipment, and can be used to rapidly screen new materials.

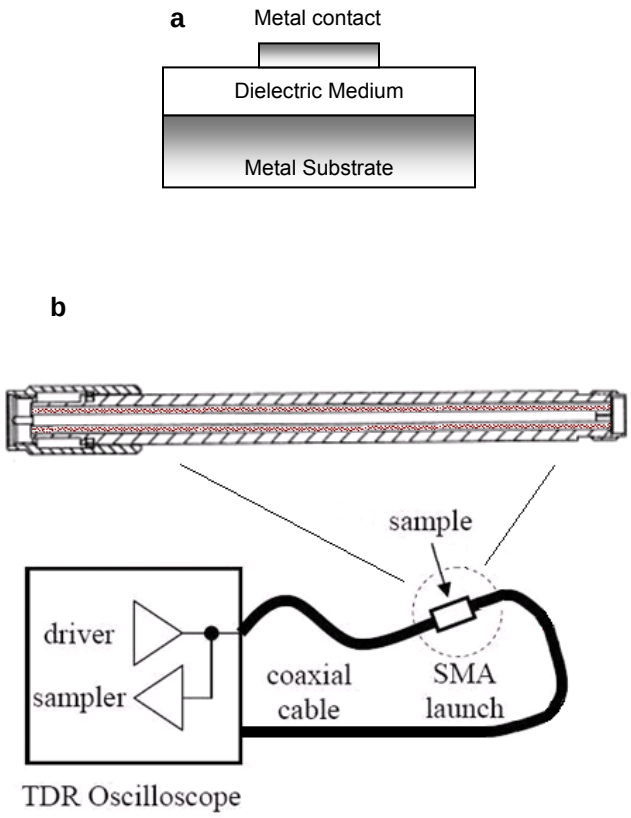

Figure 4.2 (a) Metal-insulator-metal structures used for parallel-plate capacitance measurements; (b) Schematic of a time-domain reflectometer (TDR) coupled with transmission line for dielectric measurements of powder samples (used with permission)[7]

A material's relative permittivity may also be predicted from the polarization properties of its constituent molecules. For instance, the phenomenological Debye equation, which describes the relationship between the dielectric constant (relative permittivity) of a material, and its characteristic properties (the density of molecules, and their response to an applied electric field, measured by their polarizability), is often used as a guideline for the selection of materials with appropriate electronic properties.[2] For instance, the dielectric constant of the material is increased if the molecules in the material have either a permanent dipole moment or an easily induced dipole moment. The ability of molecules to become polarized in an electric field, and thus gain a dipole moment, can be a result of the ease with which ionic polarization or electronic polarization (or frequently both) occurs. The former polarization phenomenon describes the compression or expansion of molecular bond lengths as their nuclei are shifted in response to an applied electric field, while the latter polarization phenomenon relates to the movement of the cloud of bound electrons around their nucleus under an applied electric field. Polar molecules may also undergo orientation polarization, which describes the movement or reorientation of entire molecules in response to the field. In materials not composed of single crystals, interfacial polarization may also play a role in determining polarization. This phenomenon occurs at the interface between two materials, such as grain boundaries, crystal defects, impurities, etc. The Debye equation, which relates these microscopic polarization phenomena to macroscopic relative permittivity, is given in Equation 4.3. N is the number density of molecules in the material, α_e is the electronic polarization of the molecules, α_i is the ionic polarization of the molecules, μ is the

orientation polarization of the molecules, k is the Boltzmann constant, and T is the temperature in Kelvin.

$$\frac{\kappa - 1}{\kappa + 1} = \frac{N}{3\varepsilon_0}\left(\alpha_e + \alpha_i + \frac{\mu^2}{3kT}\right) \qquad \textbf{4.3}$$

In cases where the material is composed of molecules without a permanent dipole, like pure silicas, the polarizability of the material then depends solely on the ease with which a dipole moment is induced, as well as the density of molecules in the material, and Equation 4.3 reduces to the well-known Clausius-Mossotti equation (Equation 4.4).

$$\frac{\kappa - 1}{\kappa + 1} = \frac{N}{3\varepsilon_0}\left(\alpha_e + \alpha_i\right) \qquad \textbf{4.4}$$

In general, the development of low-*k* materials focuses on reducing either the ionic and electronic polarizabilities. This is accomplished by modifying the material composition such that ionic bonds and electron density in the material are reduced, or by decreasing the density of the molecules in the material by introducing porosity into the material. The former approach uses either non-silica materials (such as non-polar organic polymers with fluoride or fluorocarbon substitution, and highly fluorinated carbonaceous compounds), or organosilicates (such as organic-inorganic silsesquioxane polymers, and fluorinated silicas).[8,9,10,11,12,13] In these materials, replacing an Si-O bond with Si-CH_3 or Si-F reduces the polarizability of the material, as does the insertion of C-C bonds. The leading approach to *k* reduction, however, is the introduction of porosity into pure-silica materials, organosilicates, or organic polymers.[14,15] This is due, in part, to the widespread use of porous silica-based materials in other industries, such as catalysis, separation, desiccation, etc., and in part to the well-understood methods of manufacturing porosity in

silica, such as sol-gel processes, surfactant-templating, and zeolite crystallization.[16] Using this approach, the electronic properties of the base material can be modified in relation to the amount of porosity introduced into the material.

Potential low-*k* materials, however, must also meet the processing requirements as mentioned above. Low-*k* materials based on organic polymers and organosilicates have very attractive electronic properties for low-*k* applications, but often suffer from poor chemical and thermal stability, as well as high coeffecients of thermal expansion when compared with metal interconnects.[3,5] Porous, pure-silica materials, on the other hand, have high chemical and thermal stability when compared with the aforementioned classes of materials, due to their chemical composition.[6,17,18] However, their mechanical properties frequently depend on how the porosity in the material is generated. For example, sol-gel processing or surfactant-templating often result in silica materials with poor mechanical strength due to their lack of crystallinity, and high hydrophilicity, due to a high number of silanol defects.[2,3,19] Materials with low mechanical stiffness, as determined by the elastic modulus, often have questionable ability to survive the chemical mechanical processing (CMP) necessary for integrated circuit fabrication. Hydrophilic materials adsorb water at ambient conditions, which significantly increases the effective *k* of the material (the dielectric constant of water ~ 80). These issues make many of the materials prepared by these porosity-inducing processes unsuitable for low-*k* applications, despite their excellent insulating properties.

Pure-silica zeolites (PSZ), in contrast, have all the aforementioned chemical and mechanical properties necessary to withstand CMP, due to their unique crystalline, microporous structures. This is especially true when fluoride is used as the mineralizing agent, as this generates materials with a low silanol defect density.[18] Additionally, the porosities of these zeolites are easily quantified based on their Framework Density (FD), which is the number of tetrahedrally coordinated atoms per 1000 $Å^3$, as compared to other types of porous silicas, leading to a quantitative expression of the relationship between zeolite porosity and the resulting dielectric constant. For instance, the LTA topology first produced in pure-silica form by Corma et al. in 2004 has the lowest framework density (FD = 14.2) among all available pure-silica zeolites, and therefore could have the lowest dielectric constant.[20,21] Finally, the abundance of zeolite topologies and hence porosities, allows for the investigation of the effects of not only porosity, but also the pore structure, on the *k*-value, as several pure-silica zeolites with framework densities in the range of interest for low-*k* materials (FD = 14.2 – 19) have similar framework densities, but very different pore structures. If pore structure does play a role in determining the dielectric constant of zeolites, then the ability to tune this parameter, in addition to porosity, could provide materials that are significant improvements over other types of porous silicas. For these reasons, pure-silica zeolites have been suggested as excellent candidates for low-*k* materials.[22]

Of the 19 known pure-silica zeolites, the intrinsic dielectric constant of only five (MFI, (FD = 18.4, $k = 2.7$ via *in situ* crystallization), MEL (FD = 17.4, $k = 1.9$ via spin-coating), *MRE (FD = 19.8, $k = 2.7$ via traditional vapor phase transport), BEA* (FD = 15.3, $k =$

2.3 via *in situ* crystallization, and 2.07 via secondary growth), and LTA (FD = 14.2, k = 1.69 via *in situ* crystallization) have been studied as low-*k* materials via thin film techniques.[4,23,24,25,26,27] This was caused by both limitations in the traditional methodology required to produce pure-silica zeolite thin films with low silanol defect density, and the necessity of obtaining perfect parallel-plate structures from which the *k*-value of the film may be determined.[6,27,28,29] Recently, we presented new techniques for both the dielectric characterization of pure-silica zeolite powders, which permits us to screen the dielectric properties of pure-silica zeolites without the necessity of creating parallel-plate structures from thin films,[7] and the synthesis of fluoride-mediated, pure-silica zeolite thin films, which allows us to expand the library of pure-silica topologies available as films.[30] The former technique used Time Domain Reflectometry (TDR), in conjunction with a transmission line, as shown in Figure 4.2b, to evaluate the *k*-value for pure-silica zeolite powders. TDR can measure the dielectric constant of powder samples in a large frequency range very rapidly with only a small amount (~ 300 mg) of sample, and is believed to be applicable to high-*k* materials, as well as low-*k* materials. Simultaneously, we developed a Vapor Phase Transport of Fluoride (VPTF) method to generate thin films of fluoride-mediated pure-silica zeolites; this method was demonstrated by producing thin films of LTA on a variety of substrates.[30] These techniques enable us to investigate several new, pure-silica zeolites in the porosity range of interest for low-*k* materials and to compare them with known materials. Here, we present the thin film synthesis of pure-silica zeolites CHA (FD = 15.1), STT (FD = 17.0), ITW (FD = 17.7), and –SVR (FD = 17.2) using the VPTF, and the results of an

investigation of the electronic properties of the fluoride-mediated, pure-silica LTA, CHA, STT, ITW, and -SVR materials as they relate to their porosity and pore structure.[31,32,33,34]

Five pure-silica zeolite materials are investigated in this report: LTA, CHA, ITW, STT, and -SVR. The unit cell structures of the five materials are shown in Figure 4.3a-e. These five materials are chosen because each is a material potentially useful in low-*k* applications, due to their relatively low framework density, and in other applications, such as catalysis, separation, membrane reactors, chemical sensors, etc., applications. For instance, PSZ LTA (FD = 14.2) has the lowest framework density of all the pure-silica zeolites, and not only should have the lowest dielectric constant, but it should also be useful as a material for a high-flux membrane due to its open framework.[35] PSZ CHA (FD = 15.1) has been suggested for the adsorption and separation of organics, as well as for the storage of hydrogen and methane.[31] Similarly, PSZ ITW (FD = 17.7) has shown an ability to selectively adsorb propene from a propane / propene mixture, and therefore may be used as an adsorbent for pressure swing adsorbers.[32,36] PSZ STT (FD = 17.0) is a frequent result of PSZ CHA syntheses crystallized over long times due to the non-selectivity of the structure-directing agent, N,N,N-trimethyladamantammonium hydroxide, and is unique in that it has two types of pore channels, one defined by nine-member rings, and the other defined by seven-member rings.[34] Lastly, PSZ -SVR (FD = 17.2), may have intriguing possibilities for gas separation, due to its three-dimensional 10-member ring pore system and periodic Si vacancy, and has shown to be a good catalyst when made as a high-silica zeolite.[33] Some of the applications described above may require zeolites in planar (thin film or membrane) form. Films and membranes are

often synthesized through the use of colloidal zeolite suspensions and nanoparticles, but these methods are generally unsuited for the synthesis of these pure-silica zeolites, as they are made via the fluoride route. Therefore, we are interested in demonstrating that these zeolites can be synthesized into thin films as well as powders, and then investigating their dielectric properties to determine if not only porosity, but also pore structure, influence their *k*-value.

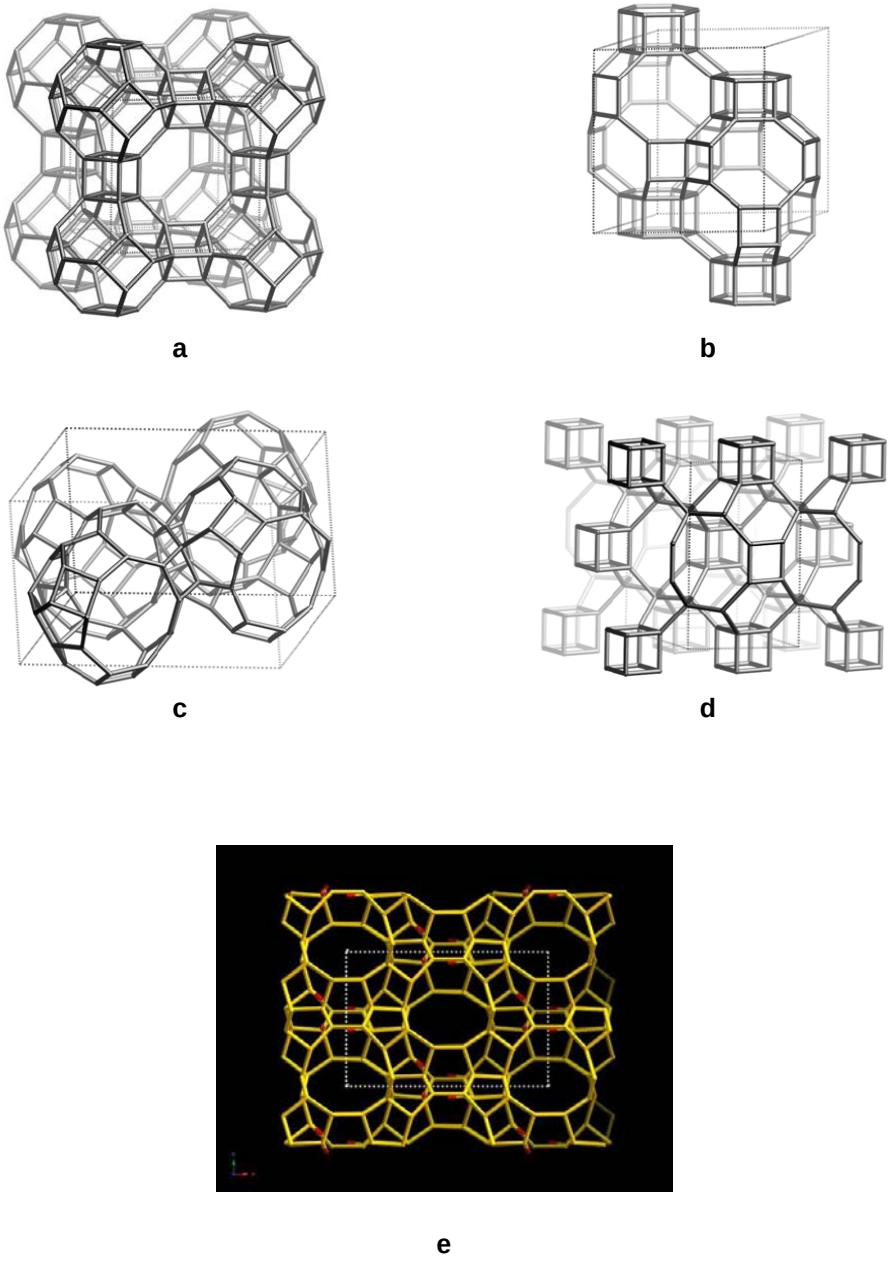

Figure 4.3 (a) LTA framework, viewed along the [001] axis; (b) CHA framework, viewed normal to the [001] axis; (c) STT framework, viewed normal to the [100] axis; (d) ITW framework, viewed along the [100] axis;[37] (e) -SVR framework, viewed along the [001] axis (courtesy of A. Burton, Chevron)

2. Results and Discussion

Using the vapor phase transport of the fluoride mineralizing agent, we created pure-silica zeolite films of each of the CHA, STT, ITW, and -SVR topologies on surface-modified (100) Si wafers (films of PSZ LTA were discussed in Chapter 3). XRD analysis showed that the calcined, and polished films have the correct structures (Figure 4.4), and that the films remained intact after polishing. FE SEM micrographs (Figure 4.5) of the calcined pure-silica films demonstrated that the films were polycrystalline, intergrown, and crack-free; these films were composed of small crystals on the order of a few microns to tens of microns in length. Micrographs of pure-silica CHA (Figure 4.5a), for instance, show 10-20 μm crystals with approximately square facets that are completely intergrown, while the pure-silica ITW crystals (Figure 4.5e) are frequently quite small (< 1 μm), and form intergrown, sphere-like aggregates that are themselves intergrown with neighboring aggregates. Interestingly, while the LTA film syntheses discussed in Chapter 3 tend to produce very regular crystals of its typical habit, the four film types generated here are composed of less regular crystals. The pure-silica STT films (Figure 4.5b) were synthesized using the same gel composition, SDA, and crystallization temperature as the previously reported films of PSZ CHA, whose structure has three-dimensional channels, as opposed to the two-dimensional structure of STT; for the STT films, however, the crystallization time was longer. For intermediate crystallization times (40 – 60 h), films composed of PSZ CHA and STT intergrowths could be formed (Figure 4.5c), although longer times would complete the phase transformation to STT. Mechanical polishing of the calcined PSZ STT and -SVR films (Figure 4.5d and Figure 4.5g, respectively), yielded films of 1.5 – 2.0 microns thickness (Figure 4.5h).

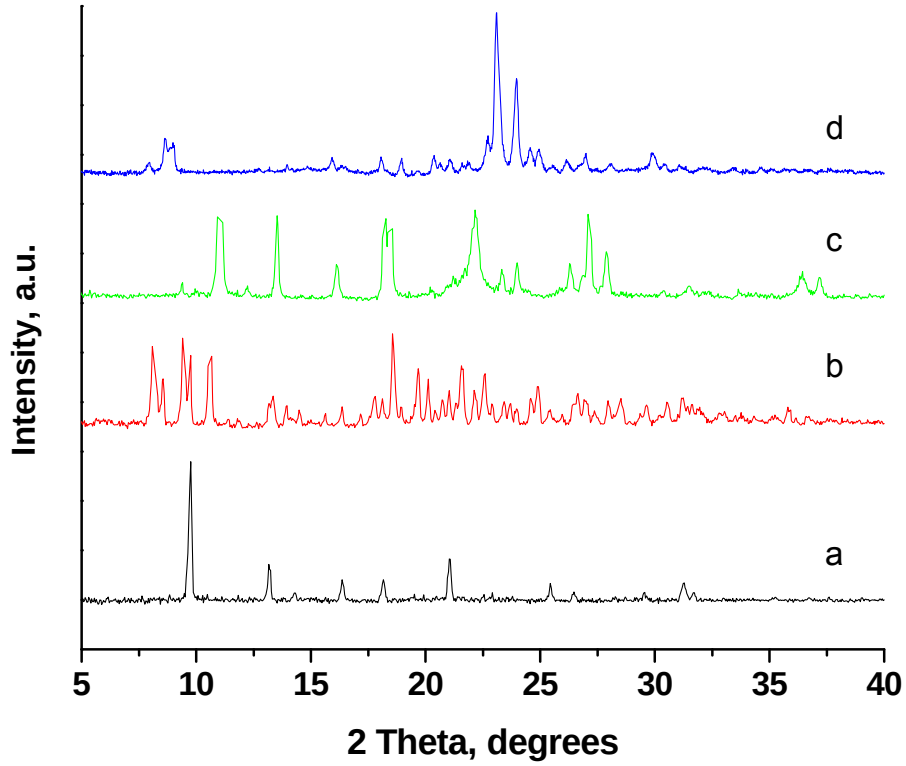

Figure 4.4 X-ray diffraction patterns of calcined and polished (a) PSZ CHA films on (100) Si; (b) PSZ STT films on (100) Si; (c) PSZ ITW films on (100) Si; (d) PSZ -SVR films on (100) Si

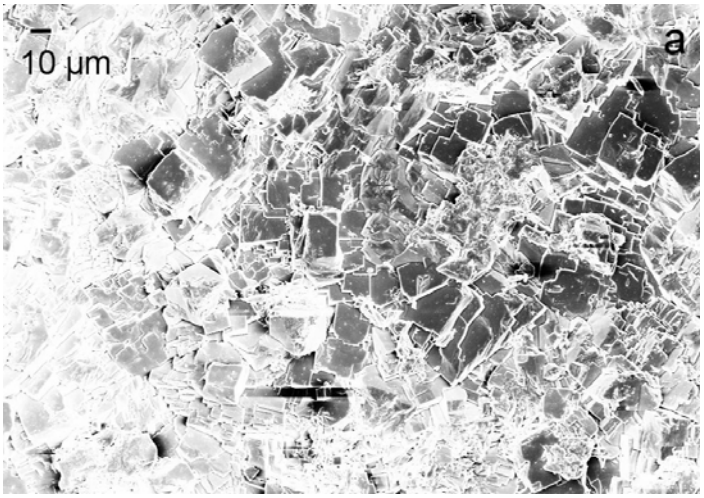
10 µm
a

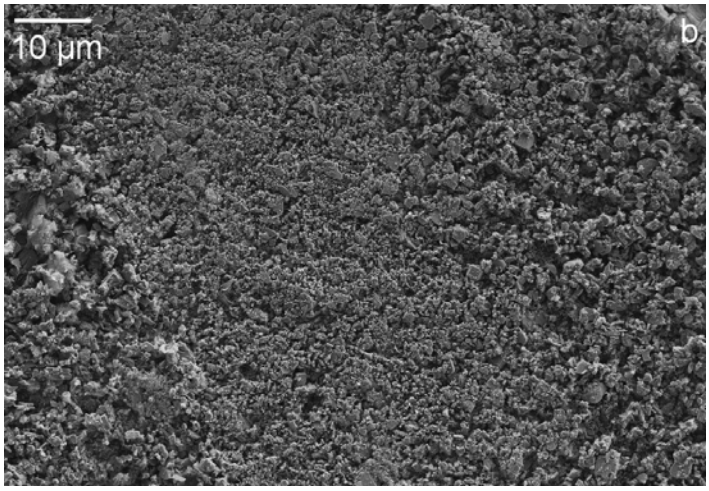
10 µm
b

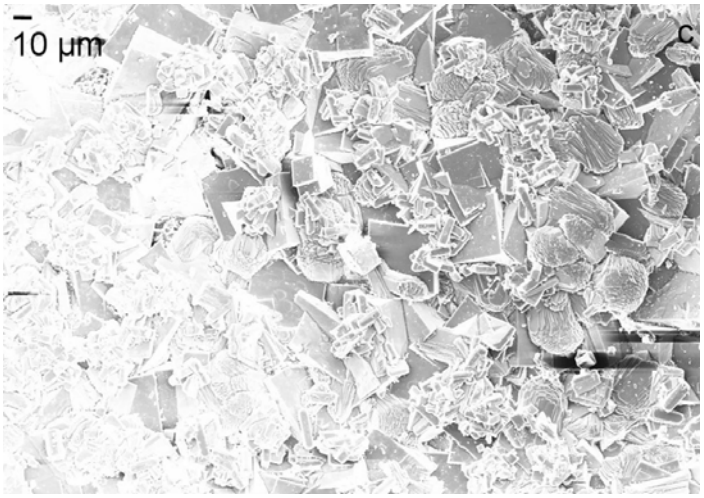
10 µm
c

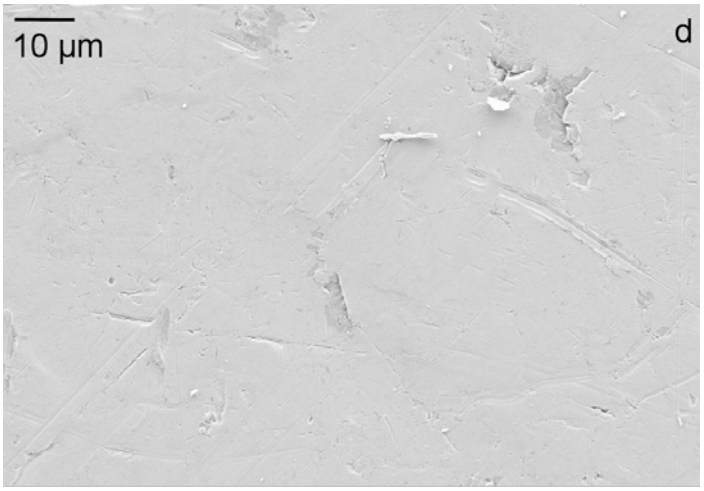
10 µm
d

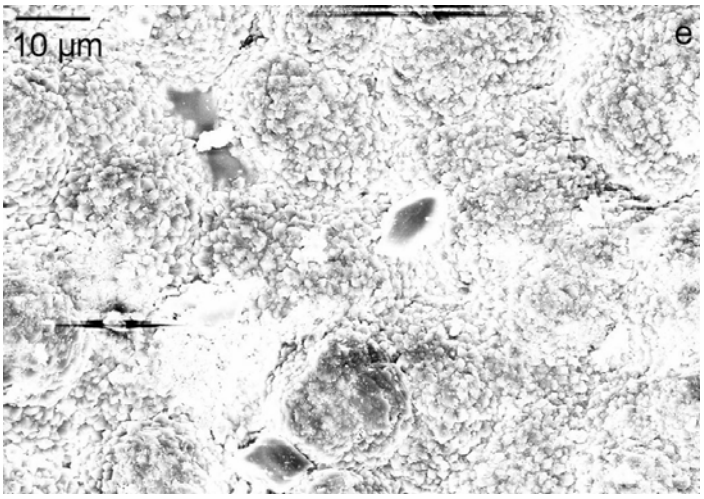
10 µm
e

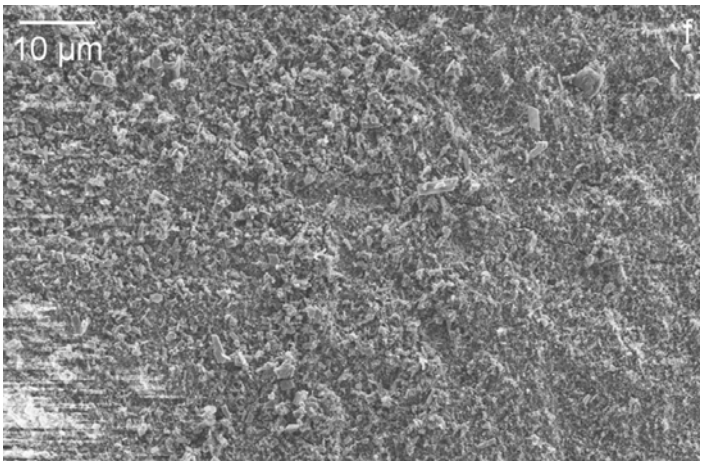
10 µm
f

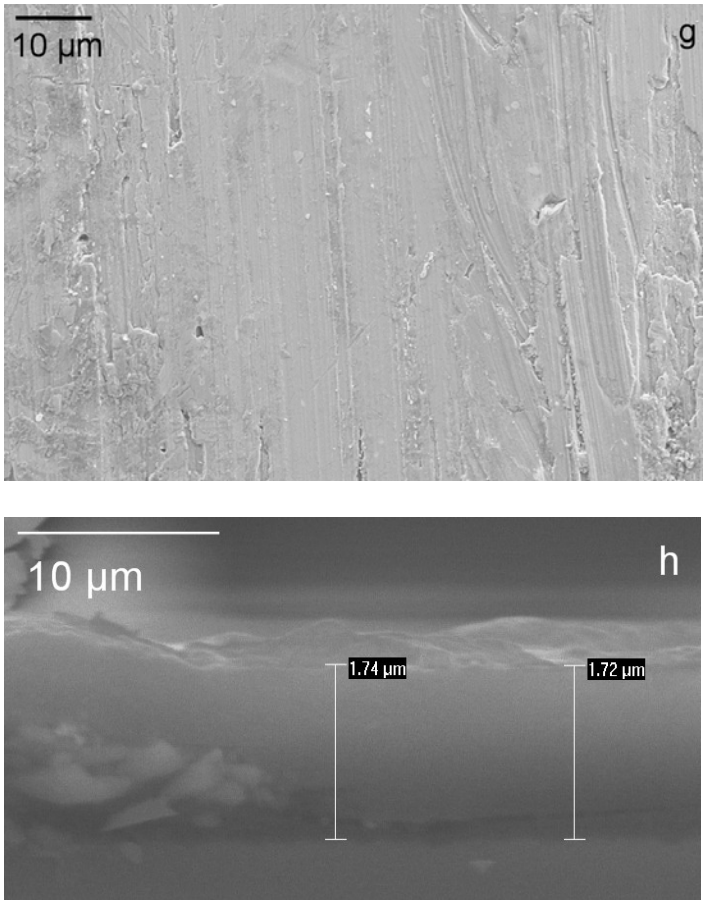

Figure 4.5 FE SEM micrographs of (a) surface of calcined PSZ CHA film; (b) surface of calcined PSZ STT film; (c) surface of PSZ CHA / STT intergrowth; (d) calcined, polished PSZ STT film; (e) surface of calcined PSZ ITW film; (f) surface of calcined PSZ -SVR film; (g) surface of calcined, polished PSZ -SVR film; (h) thin section of a typical PSZ STT film after mechanical polishing, showing ~ 1.7 µm thick film with variable height

The dielectric properties of the five pure-silica materials were investigated to determine their relevance for low-*k* applications. Initially, we attempted to measure the *k*-value using thin film, metal-insulator-metal, parallel-plate capacitance measurements using an LCR meter, as described earlier.[6] However, the results of these measurements were inconsistent, due to the variable thickness of the films, which led to metal-insulator-metal structures that were not perfectly parallel. This was caused by the limitations of the mechanical polishing equipment available rather than the materials themselves; we could not polish the samples with the precision necessary to create perfectly parallel structures. This was demonstrated via the capacitance measurements on the PSZ LTA thin films, which yielded a *k*-value of $k = 1.69$ ($\sigma = 0.18$). Here, an increase in film thickness of 20 nm over a 5 μm length of film (shown in Chapter 3) resulted in a standard deviation in the *k*-value measurements of 0.18. The theoretical *k*-value of PSZ LTA obtained from GULP (general utility lattice program) calculations at infinite frequency is 1.55. [7,38] Considering the range of errors inherent in the film measurements, the *k*-values obtained on the films in this study are in good agreement with those obtained from calculations. Comparison of the *k*-values from PSZ LTA films to PSZ *MRE ($k = 2.7$), PSZ BEA* ($k = 2.3$ and 2.07), and MFI ($k = 2.7$), that are obtained via *in situ* techniques that result in polycrystalline, intergrown, films whose porosity is solely due to the internal zeolite structure, shows a 37%, 26%, 18%, and 37% decrease in *k*, respectively (Figure 4.6). The *k*-value of the PSZ LTA film is the lowest obtained for any *in situ* synthesized polycrystalline PSZ film.

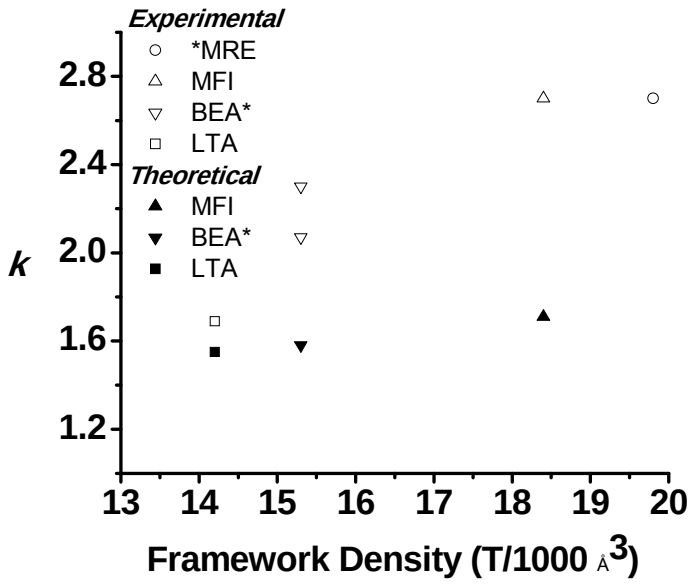

Figure 4.6 *k*-values obtained for PSZ thin film of *MRE, MFI, BEA*, and LTA topologies made by *in situ* (MFI and BEA*) and vapor phase transport methods (*MRE and LTA)

In order to avoid the problems mentioned earlier with parallel-plate capacitance measurements, and to evaluate the intrinsic *k*-values of the new film topologies, we instead utilized the Time-Domain Reflectometry method to analyze the dielectric properties of the powder generated during these film syntheses.[7] Using this method, we measured the dielectric constant of PSZ CHA, ITW, STT, and -SVR powder samples (Table 1; the dielectric constant of PSZ LTA powder was measured in a previous report[7]). For these measurements, the Bruggeman effective medium approximation, given by Equation 4.5, was used to calculate the dielectric constant of the zeolite crystals from the effective dielectric constant of the powder plus the air in the transmission line [7].

$$f_1 \frac{\kappa_1 - \kappa_e}{\kappa_1 + 2\kappa_e} + f_2 \frac{\kappa_2 - \kappa_e}{\kappa_2 + 2\kappa_e} = 0 \qquad \textbf{4.5}$$

In Equation 4.5, f_i symbolizes the volume fraction of components *i*, k_i the dielectric constant of component *i*, and k_e the effective (measured) dielectric constant of the mixture. The volume fraction of the components can be calculated from the mass of the loaded powder, the powder density, and the transmission line volume. In this case, we use k_1 as the dielectric constant of air, 1.0005, and k_2 as the dielectric constant of the measured powder material. The dielectric constant of the zeolites were obtained at a frequency of 2 GHz (shown in Table 4.1), from data of the effective dielectric constant determined over a range of frequencies, as shown in Figures 4.5 – 4.8. The *k*-value of PSZ LTA measured via Time Domain Reflectometry is in good agreement with the *k*-value measured via parallel-plate capacitance.[38]

Table 4.1 Dielectric constant (k) of various pure-silica zeolite powders measured at 2 GHz.

Sample	FD_{Si}	Channel Type	Smallest Ring Size	Largest Ring Size	Symmetry	*k* at 2 GHz
MFI[a]	18.4	3D	4	10	Orthorhombic	2.13
ITW	17.7	2D	4	8	Monoclinic	2.58
FER[a]	17.6	2D	5	10	Orthorhombic	2.01
-SVR	17.2	3D	4	10	Monoclinic	2.56
STT	17.0	2D	4	9	Monoclinic	3.22
CHA	15.1	3D	4	8	Rhombohedral	2.40
LTA[a]	14.2	3D	4	8	Cubic	1.62

[a] Dielectric constants reported in prior work [7]

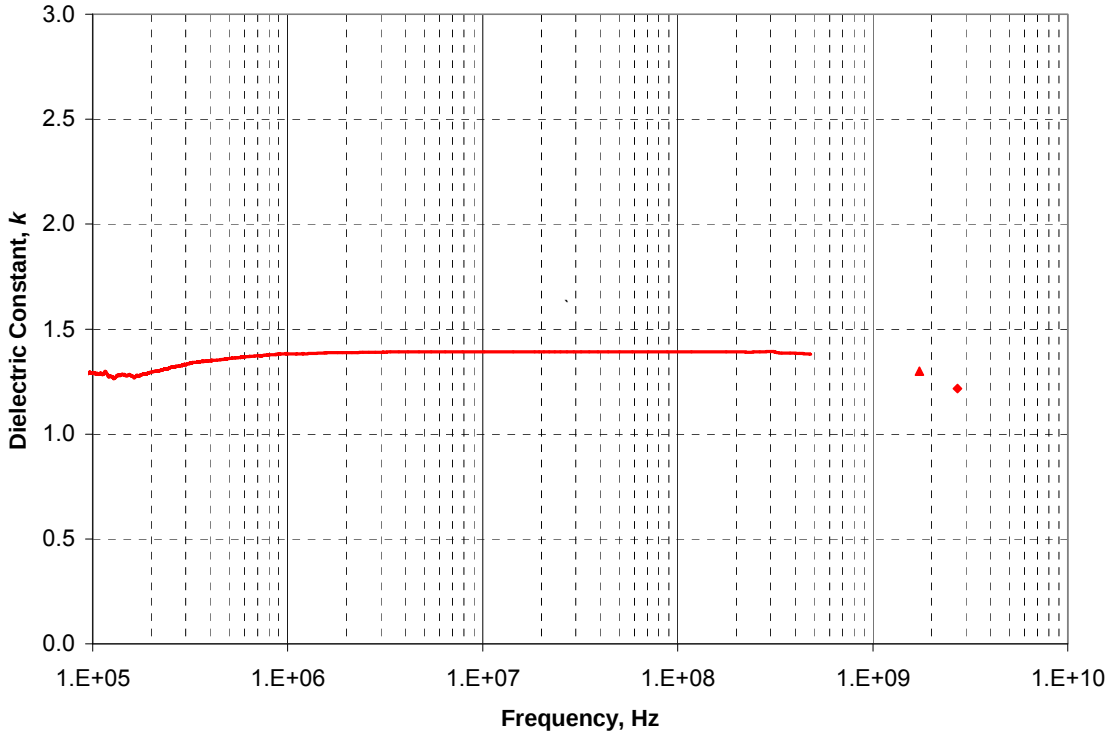

Figure 4.7 Effective dielectric constant of pure-silica CHA measured over a range of frequencies

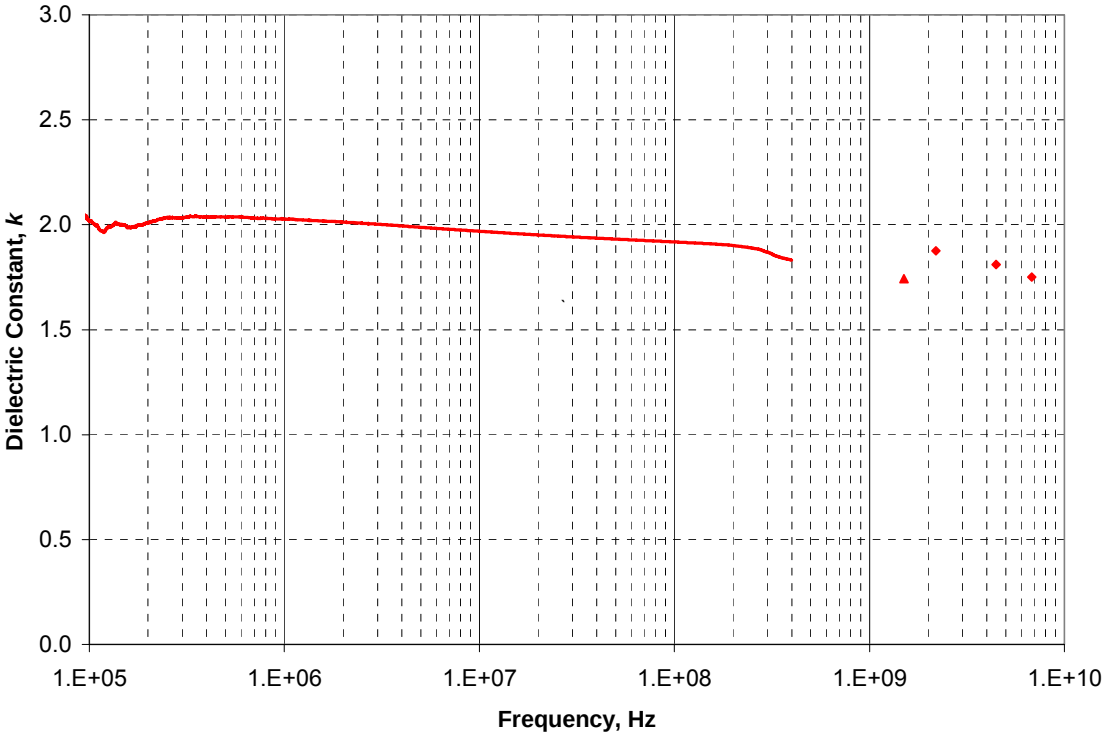

Figure 4.8 Effective dielectric constant of pure-silica STT measured over a range of frequencies

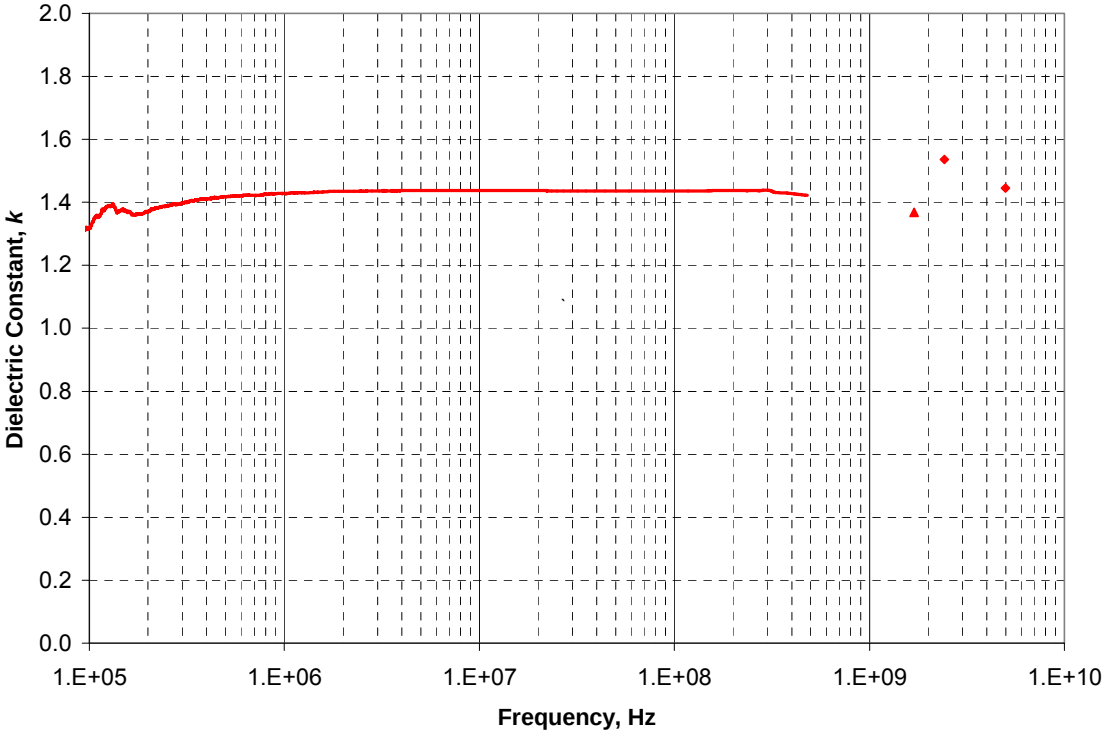

Figure 4.9 Effective dielectric constant of pure-silica ITW measured over a range of frequencies

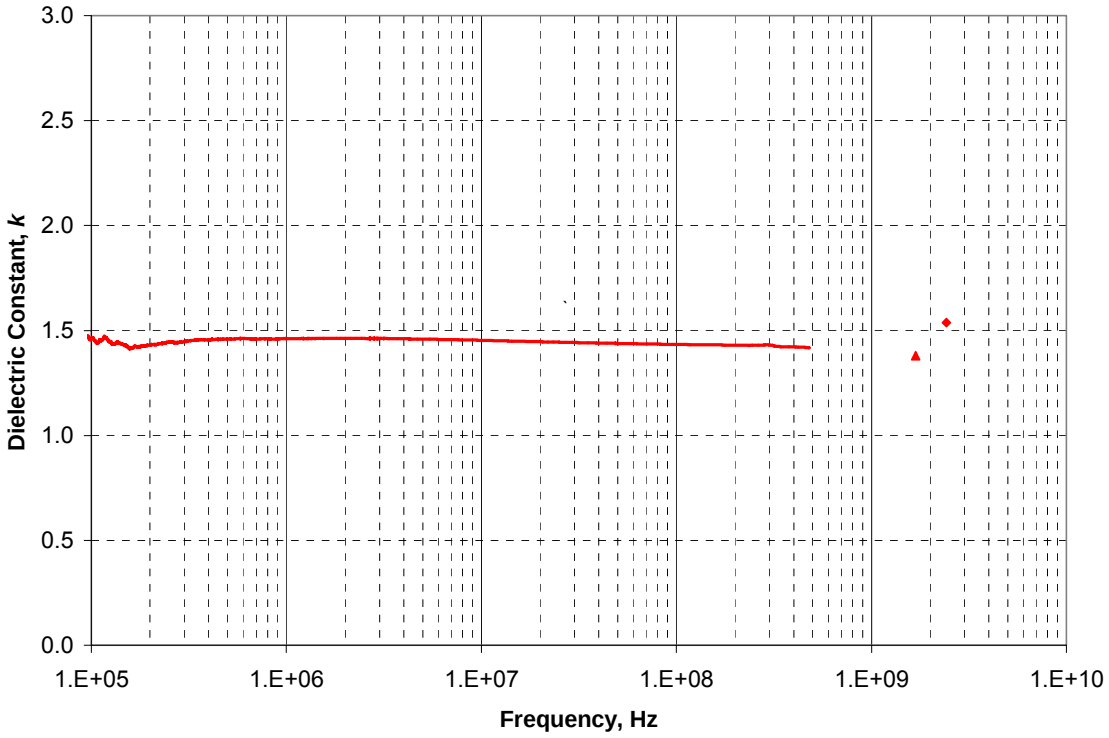

Figure 4.10 Effective dielectric constant of pure-silica -SVR measured over a range of frequencies

The *k*-values of these four PSZ topologies, along with the dielectric constants of PSZ LTA, FER, and MFI (all measured using TDR), are shown in Figure 4.11.[7] In the case of the PSZ ITW powder samples, we were unable to completely remove the organic SDA from the crystals, even with up to five cycles of calcination in air, resulting in very pale grey samples. The occlusion of organic molecules may result in a higher dielectric constant, because the internal void space of the sample is not fully open. The results of thermogravimetric analysis on the calcined, and prepared for TDR, powder samples demonstrate that the samples prepared as described each retain or adsorb while in storage very low amounts of water (< 1.0 % mass loss due to water adsorption up to 200 °C, and < 3.0 % mass loss overall up to 1000 °C). Figure 4.11 also shows the line that represents

the Bruggeman effective medium correlation, which has been used as a guideline for the dielectric constant of solid materials (including zeolites). The Bruggeman correlation assumes that the intrinsic *k*-value of a material is the weighted average of the *k* from air in pores of the material, and the *k* from dense silica, as determined by the volume fraction of each. This implies that the measured *k* should be dependent entirely on the porosity of the zeolites; however, as Figure 4.11 shows, this is not the case. All the zeolites shown here fall below the line for the Bruggeman correlation, except for STT, which falls on the line, suggesting that their dielectric constants depend on pore structure in addition to the porosity. This is further shown by the ITW / FER / -SVR / STT series, whose framework densities all fall in the range 17.0 – 17.7. The smallest ring size for each of these materials is 4 for ITW, -SVR, and STT, while FER has a 5-ring as the smallest. Both the FER, and -SVR have 10-rings as their largest rings, although FER has only two-dimensional channels, as compared to the three-dimensional channels of -SVR. Interestingly, direct comparison between the *k*-values of the FER and ITW materials' *k*-values suggests that not only does a lower FD reduce the *k*-value of a sample, but so does the greater largest ring size in the FER material. Additionally, although the FD of -SVR is lower than that of FER, and has three-dimensional channels, its *k*-value is higher. However, in comparison to the *k*-value of STT, -SVR is lower. Like FER, STT has two-dimensional channels, but different ring sizes (4-rings at the smallest, and 9-rings at the largest). The differences in pore connectivity between STT and -SVR are likely the cause of the differences between their respective *k*-values. Further evaluations of the *k*-values from a symmetry perspective suggest that zeolites with a higher symmetry have a lower dielectric constant, as shown in Table 4.1, primarily because higher symmetry

lattice arrangements of molecules lead to lower polarizability. The three zeolites with monoclinic symmetry (ITW, -SVR, and STT) all show higher *k*-values than the other materials. This may explain the distinct differences between the *k*-values of FER and ITW, for instance, whose pore architecture is similar in terms of framework density, and close in smallest and largest ring sizes, but different in terms of lattice symmetry. The comparatively high *k*-value of STT may then be a result of a combination of factors, including a high framework density, a two-dimensional pore channel system, and low symmetry. Additionally, the data shown in Figure 4.8 suggest that the STT sample may have had slight water adsorption, due to the slightly negative slope of the dielectric constant over the range of frequencies; materials with water adsorption generally show very steep declines in the dielectric constant as the frequency is increased. Perhaps most interesting is the nonlinear, although generally negative, dependence of *k*-values on FD. This indicates that, although porosity is the main factor in inducing a lower dielectric constant in porous silica, as compared to bulk silica, the structure of the porosity, as indicated by the ring size, micropore volume, and lattice symmetry, also plays a role in determining the *k*-value.

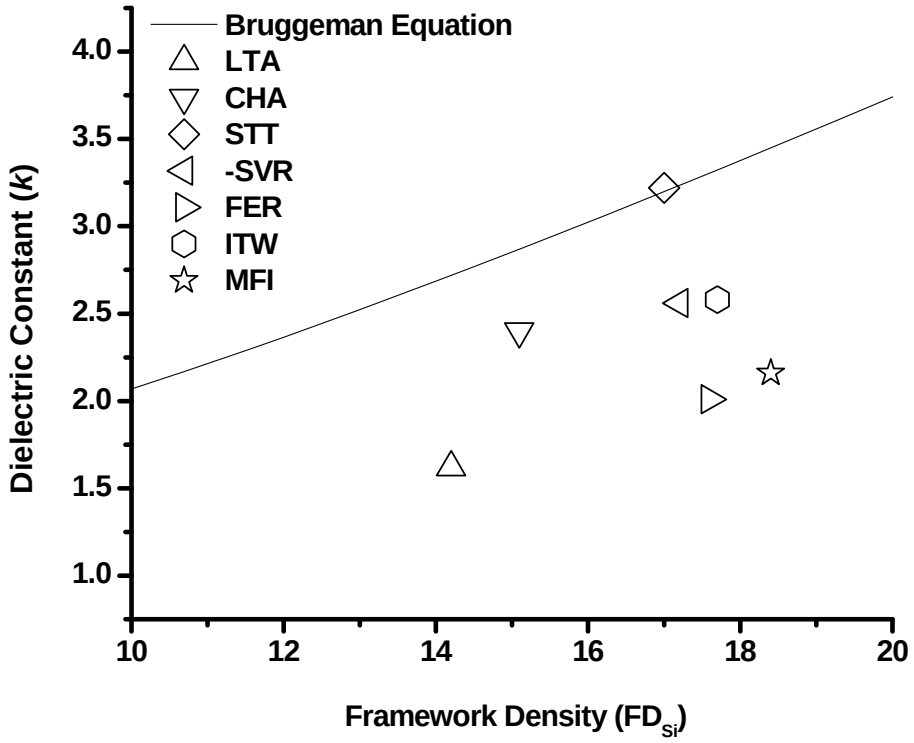

Figure 4.11 *k*-values obtained for fluoride-mediated, PSZ powders of MFI, ITW, FER, -SVR, STT, CHA, and LTA topologies via TDR

3. Conclusions

Application of the vapor phase transport of fluoride method to the pure-silica zeolite systems CHA, ITW, STT, and -SVR yielded thin films on surface-modified, (100) Si wafers. These films were continuous, polycrystalline, intergrown, and well-adhered to their substrates. The pure-silica ITQ-29 (LTA) films synthesized in Chapter 3 using this method were demonstrated to have a *k*-value of 1.69 via parallel-plate capacitance measurements, which is the lowest value experimentally obtained on any zeolite film. The pure-silica zeolite powders crystallized in conjunction with the film syntheses of these materials were examined via Time Domain Reflectometry at high frequencies to determine their dielectric properties, and compared to *k*-values of other pure-silica zeolites measured using this technique to evaluate if the reduction in their relative permittivity is solely the result of the introduction of porosity, or if other factors, such as pore structure, affect their *k*-value. These data demonstrate that the dielectric properties of zeolites are primarily a result of their porosities, but are also affected by their pore structures. Generally, materials with low framework density *and* high symmetry have low relative permittivities. Using this general relationship between the dielectric constant, and the porosity / pore structure of the zeolite, it is possible to tune the final values of the dielectric properties of the materials. For instance, the dielectric constant of these materials may be further reduced by the incorporation of porogens into the initial gel that is dip-coated onto the substrate; after crystallization and calcination, the continuous film will have a lower effective dielectric constant due to the presence of additional porosity. These properties make pure-silica zeolites excellent candidates for low-*k* materials.

4. Experimental

4.1 Synthesis of Structure-Directing Agent A (1,2,3-trimethylimidazolium hydroxide)

9.6 g of 1,2-dimethylimidazole (98%, Aldrich) was dissolved in 100 mL ethyl acetate (EMD). 20 g of CH_3I (99%, Aldrich) was added and the reaction mixture was stirred at room temperature under Ar for three days. The addition of CH_3I, followed by stirring for three days, was repeated once. The solution immediately produces white precipitate; this was collected via centrifugation. The solids so collected were washed copiously with diethyl ether (J. T. Baker), centrifuged again, decanted from the supernatant, and dried using a rotovap. The crude product was recrystallized from chloroform (EMD) at its boiling point and cold diethyl ether. White crystals of 1,2,3-trimethylimidazolium iodide were obtained after vacuum drying the resulting solid. The product (23.0 g, 96.6 mmol) was ion-exchanged from its iodide form to its hydroxide form by dissolution in 700 mL of DDI H_2O and stirring with 75 g of Bio-Rad AG1-X8 anion exchange resin for 24 h. The solution was then filtered and concentrated to 1 – 1.2 M concentration of the hydroxide form using a rotovap. The conversion from iodide to hydroxide was 85% based on titration of the resultant solution.

4.2 Synthesis of Structure-Directing Agent B (N,N,N-trimethyl-1-adamantylammonium hydroxide)

25 g of 1-adamantylamine (97%, Aldrich) was dissolved in 200 mL methanol (EMD). 33 g of potassium bicarbonate (99.7%, Aldrich) was added to the solution, which was then placed under an Ar atmosphere in an ice bath. 77.4 g of CH_3I was added to the solution,

and the reaction mixture was stirred for 3 days, slowly coming to room temperature. The solution was evaporated using a rotovap, and the product was extracted from the resulting solids with a large excess of chloroform. The solution was filtered to remove the potassium bicarbonate byproducts, and the solids were again washed with chloroform. The filtrate was dryed with magnesium sulfate (99%, Aldrich) until it no longer clumped in the solvent. The solution was filtered again to remove the magnesium sulfate. The solution was evaporated using a rotovap, the solids were washed with diethyl ether, and the solution was evaporated again using a rotovap. The crude product was recrystallized from a minimum of hot methanol at its boiling point. White crystals of N,N,N-trimethyl-1-adamantylammonium iodide were obtained after vacuum drying the resulting solid. The product (7.3 g, 22.7 mmol) was ion-exchanged from its iodide form to its hydroxide form by dissolution in 150 mL of DDI H_2O and stirring with 20 g of Bio-Rad AG1-X8 anion exchange resin for 24 h. The solution was then filtered and concentrated to 0.75 M concentration of the hydroxide form using a rotovap. The conversion from iodide to hydroxide was 95% based on titration of the resultant solution.

4.3 Synthesis of Structure-Directing Agent C (Hexamethylene-1,6-bis-(N-methyl-N-pyrrolidinium) hydroxide)

4.1 g of N-methylpyrrolidine (97%, Aldrich) was dissolved in 50 mL acetone (Fisher). 4.9 g of 1,6-dibromohexane (98%, Acros Organics) was added to the solution, and the resulting solution was stirred for three days. The solids produced were collected via centrifugation, washed with diethyl ether, centrifuged again, decanted from the supernatant, and dried using a rotovap. Crystals of hexamethylene-1,6-bis-(N-methyl-N-

pyrrolidinium) bromide were obtained after vacuum drying the resulting solid. The product (3.7 g, 8.9 mmol) was ion-exchanged from its iodide form to its hydroxide form by dissolution in 20 mL of DDI H_2O and stirring with 10 g of Bio-Rad AG1-X8 anion exchange resin for 24 h. The solution was then filtered and concentrated to 0.23 wt % concentration of the hydroxide form using a rotovap. The conversion from iodide to hydroxide was 90% based on titration of the resultant solution.

4.4 Surface Modification of the Substrates

The low-resistivity (0.008 – 0.02 Ω cm), (100) silicon wafers (University Wafers) were modified to present Si-OH terminal groups on their surface by soaking in a pirahna-type etch solution, i.e., 10 mL H_2SO_4 (97%, J.T. Baker) : 40 mL H_2O_2 (30%, EMD) : 2 drops of HF (48%, Mallinckrodt), for 2 min, followed by 15 min in DDI H_2O.

4.5 Synthesis of Fluoride-Mediated, Pure-Silica Zeolite Films and Powder

Pure-silica precursor gels of ITW, CHA, STT, and -SVR were prepared in a Teflon® jar by hydrolyzing tetraethylorthosilicate (TEOS, 98%, Aldrich) in an aqueous solution of SDA (see Table 4.2 for gel compositions and reaction conditions). A 4 cm x 2 cm, previously modified substrate was then submerged in the gel. The precursor gel was stirred for 48 h, while covered with parafilm, at room temperature to ensure complete hydrolysis of TEOS. The submerged substrate was thereafter removed from the gel, and subjected to dip-coating up to five times in the hydrolyzed gel, with 30 min of drying on a Teflon® substrate holder at room temperature between coats. A Teflon® cap with two small holes drilled in it was screwed onto the jar containing the bulk precursor gel. The

coated substrate, in its holder, and the enclosed bulk precursor gel were each placed inside a vacuum desiccator, and the ethanol and excess H_2O present in the bulk precursor gel and precursor film were evaporated. Evacuation for 48 h at room temperature yielded an amorphous precursor film and a solid (dry) bulk gel of molar composition of the appropriate final gel. If, after drying, too much H_2O had been removed, DDI H_2O was added to the jar to obtain the correct total gel mass. An aqueous solution of hydrofluoric acid (48%, Mallinckrodt) was added to the jar in molar ratio 0.50 HF / 1.0 SiO_2, and the sample was stirred with a Teflon® spatula. The dry bulk gel, followed by the coated substrate on an elevated Teflon® platform, was introduced into a Teflon®-lined Parr Autoclave. The crystallization of the bulk gel and the precursor films was carried out at conditions listed in Table 4.2. The reactor was removed from the oven and cooled. The bulk solids and the film were washed with 100 mL each of acetone (EMD) and DDI H_2O. The crystalline material was placed in an evaporating dish and dried for 24 hours in a 100 °C oven. The organic SDA was removed from the powder and film samples by calcination in air to the temperature given in Table 4.2 using a ramp rate of 1 °C / min, with pauses at 350 °C and 580 °C (for calcination temperatures over 580 °C) for 3 h each. The calcined films were mechanically polished using a Buehler EComet 3000 Polisher equipped with 0.05 μm Al_2O_3 polishing suspension and a 3 μm abrasive lapping film. To minimize water adsorption in the powder samples, after the powder was calcined, it was placed in a sealed vial and evacuated to 2 x 10^{-5} Torr overnight at 140 °C. The vial was then backfilled with dry argon and stored inside two Ziploc bags, each containing several grams of desiccant.

Table 4.2 Synthesis conditions for zeolite films and powders

Sample	Final Gel Composition	Crystallization Temperature	Crystallization Time	Calcination Temperature	Calcination Time @ T
ITW	1.0 TEOS / 0.5 SDA A / 0.5 HF / 3.0 H_2O	150 °C	10 days	650 °C	10 h
CHA	1.0 TEOS / 0.5 SDA B / 0.5 HF / 3.0 H_2O	150 °C (60 rpm)	40 h	580 °C	10 h
STT	1.0 TEOS / 0.5 SDA B / 0.5 HF / 3.0 H_2O	150 °C	3 – 10 days	580 °C	10 h
-SVR	1.0 TEOS / 0.5 SDA C / 0.5 HF / 3.0 H_2O	150 °C	20 days	595 °C	5 h

4.6 Characterization

The as-made and calcined zeolite powder and film samples were evaluated using X-ray diffraction (XRD). XRD was carried out on a Scintag XDS 2000 diffractometer operated at 40 kV and 40mA using Cu K_α radiation (λ = 1.54056 Å) and a solid-state Ge detector in the 2θ range of 2-55 at a step size of 0.5 ° / min. Thermogravimetric analysis (TGA) was performed on the calcined powder samples using a NETZSH STA 449C analyzer in air using an aluminum sample pan. All FE SEM was done on a LEO 1550 VP FE SEM at an electron high tension (EHT) of 10 kV using samples that were coated, using a metal sputtering coater, with 5 nm of Pt to minimize the effects of charging. EDS measurements were carried out using an Oxford INCA Energy 300 EDS system. The dielectric constants of the powder samples were obtained using time-domain reflectometry (TDR) carried out with a Tektronix TDS8200 equivalent time sampling oscilloscope and an Agilent E5071B vector network analyzer with a frequency range of 200 kHz – 8.5 GHz, coupled with a 50 Ω coaxial transmission (air) line from Maury

Microwave Corporation.[7] The dielectric constant of the calcined, polished, pure-silica LTA films on low-resistivity (100) Si was calculated from parallel-plate capacitance measurements obtained at a frequency of 1 MHz using an LCR meter under flowing dry argon to prevent accumulation of water in the sample, which has been shown to increase the dielectric constant value. For additional prevention of water adsoption, the surface of the pure-silica LTA films was capped using a vapor-phase silylation procedure described elsewhere to prevent water adsorption.[6] The capacitance measurements on the PSZ LTA films were carried out on metal-insulator-metal structures created by depositing, on the film, aluminum dots of diameter 1.62 mm, and on the backside of the silicon substrate, an aluminum layer. Four to five Al dots were usually deposited on each film sample, and their average *k* reported.

5. References

[1] *International Technology Roadmap for Semiconductors.* (2007).

[2] Maex, K. *et al.* Low dielectric constant materials for microelectronics. *J. Appl. Phys.* **93**, 8793-8841 (2003).

[3] Li, Z. J. *et al.* Mechanical and dielectric properties of pure-silica-zeolite low-k materials. *Angew. Chem.-Int. Edit.* **45**, 6329-6332 (2006).

[4] Lew, C. M. *et al.* Hydrofluoric-Acid-Resistant and Hydrophobic Pure-Silica-Zeolite MEL Low-Dielectric-Constant Films. *Langmuir* **25**, 5039-5044 (2009).

[5] Xiang, Y., Chen, X., Tsui, T. Y., Jang, J. I. & Vlassak, J. J. Mechanical properties of porous and fully dense low-kappa dielectric thin films measured by means of nanoindentation and the plane-strain bulge test technique. *J. Mater. Res.* **21**, 386-395 (2006).

[6] Wang, Z. B., Wang, H. T., Mitra, A., Huang, L. M. & Yan, Y. S. Pure-silica zeolite low-k dielectric thin films. *Adv. Mater.* **13**, 746-749 (2001).

[7] Sun, M. *et al.* Dielectric constant measurement of zeolite powders by time-domain reflectometry. *Microporous Mesoporous Mat.* **123**, 10 (2009).

[8] Lee, B. D. *et al.* Ultralow-k nanoporous organosilicate dielectric films imprinted with dendritic spheres. *Nat. Mater.* **4**, 147-U126 (2005).

[9] Chen-Yang, Y. W., Chen, C. W., Wu, Y. Z. & Chen, Y. C. High-performance circuit boards based on mesoporous silica filled PTFE composite materials. *Electrochemical And Solid State Letters* **8**, F1-F4 (2005).

[10] Loboda, M. J. New solutions for intermetal dielectrics using trimethylsilane-based PECVD processes. *Microelectron. Eng.* **50**, 15-23 (2000).

[11] Vitale, S. A. & Sawin, H. H. Etching of organosilicate glass low-k dielectric films in halogen plasmas. *J. Vac. Sci. Technol. A-Vac. Surf. Films* **20**, 651-660 (2002).

[12] Larlus, O. *et al.* Silicalite-1/polymer films with low-k dielectric constants. *Appl. Surf. Sci.* **226**, 155 (2004).

[13] Lin, Y. B., Tsui, T. Y. & Vlassak, J. J. Octamethylcyclotetrasiloxane-based, low-permittivity organosilicate coatings - Composition, structure, and polarizability. *J. Electrochem. Soc.* **153**, F144-F152 (2006).

[14] Long, T. M. & Swager, T. M. Molecular design of free volume as a route to low-kappa dielectric materials. *J. Am. Chem. Soc.* **125**, 14113-14119 (2003).

[15] Baklanov, M. R. & Maex, K. Porous low dielectric constant materials for microelectronics. *Philos. Trans. R. Soc. A-Math. Phys. Eng. Sci.* **364**, 201-215 (2006).

[16] Davis, M. E. Ordered porous materials for emerging applications. *Nature* **417**, 813-821 (2002).

[17] Yan, Y. & Wang, H. in *Encyclopedia of Nanoscience and Nanotechnology.* Vol. X, (H. S. Nalwa, ed.) 1-19 (American Scientific Publishers, 2003).

[18] Yan, Y., Wang, Z. & Wang, H. *Silica Zeolite Low-K Dielectric Thin Films.* U.S. Patent #6573131 (2003).

[19] Morgen, M. *et al.* Low dielectric constant materials for ULSI interconnects. *Annu. Rev. Mater. Sci.* **30**, 645-680 (2000).

[20] Corma, A., Rey, F., Rius, J., Sabater, M. J. & Valencia, S. Supramolecular self-assembled molecules as organic directing agent for synthesis of zeolites. *Nature* **431**, 287-290 (2004).

[21] Tiscornia, I. *et al.* Preparation of ITQ-29 (Al-free zeolite a) membranes. *Microporous Mesoporous Mat.* **110**, 303-309 (2008).

[22] Davis, M. E. *Zeolite Films for Low k Applications*. U.S. Patent # 7,109,130 B2.

[23] Chen, Y. L. *et al.* Synthesis and characterization of pure-silica-zeolite Beta low-k thin films. *Microporous Mesoporous Mat.* **123**, 45-49, doi:10.1016/j.micromeso.2009.03.022 (2009).

[24] Cho, Y. Pure Silica Zeolite Films Prepared by a Vapor Phase Transport Method. *Japanese Journal of Applied Physics. Parts 1 & 2* **47**, 8360-8363 (2008).

[25] Lew, C. M. *et al.* Pure-Silica-Zeolite MFI and MEL Low-Dielectric-Constant Films with Fluoro-Organic Functionalization. *Adv. Funct. Mater.* **18**, 3454-3460 (2008).

[26] Li, Z. J., Lew, C. M., Li, S., Medina, D. I. & Yan, Y. S. Pure-silica-zeolite MEL low-k films from nanoparticle suspensions. *J. Phys. Chem. B* **109**, 8652-8658 (2005).

[27] Liu, Y., Sun, M. W., Lew, C. M., Wang, J. L. & Yan, Y. S. MEL-type pure-silica zeolite nanocrystals prepared by an evaporation-assisted two-stage synthesis method as ultra-low-k materials. *Adv. Funct. Mater.* **18**, 1732-1738 (2008).

[28] Mitra, A. *et al.* Synthesis and evaluation of pure-silica-zeolite BEA as low dielectric constant material for microprocessors. *Ind. Eng. Chem. Res.* **43**, 2946-2949 (2004).

[29] Hu, L. L., Wang, J. L., Li, Z. J., Li, S. & Yan, Y. S. Interfacial adhesion of nanoporous zeolite thin films. *J. Mater. Res.* **21**, 505-511 (2006).

[30] Hunt, H. K., Lew, C. M., Sun, M., Yan, Y. & Davis, M. E. Pure-Silica Zeolite Thin Films by Vapor Phase Transport of Fluoride for Low-*k* Applications. *Microporous Mesoporous Mat.* (In Press).

[31] Diaz-Cabanas, M. J., Barrett, P. A. & Camblor, M. A. Synthesis and structure of pure SiO2 chabazite: the SiO2 polymorph with the lowest framework density. *Chem. Commun.*, 1881-1882 (1998).

[32] Yang, X. B., Camblor, M. A., Lee, Y., Liu, H. M. & Olson, D. H. Synthesis and crystal structure of As-synthesized and calcined pure silica zeolite ITQ-12. *J. Am. Chem. Soc.* **126**, 10403-10409 (2004).

[33] Baerlocher, C. *et al.* Ordered silicon vacancies in the framework structure of the zeolite catalyst SSZ-74. *Nat. Mater.* **7**, 631-635 (2008).

[34] Camblor, M. A. *et al.* A synthesis, MAS NMR, synchrotron X-ray powder diffraction, and computational study of zeolite SSZ-23. *Chem. Mater.* **11**, 2878-2885 (1999).

[35] Caro, J. & Noack, M. Zeolite membranes - Recent developments and progress. *Microporous Mesoporous Mat.* **115**, 215-233 (2008).

[36] Barrett, P. A. *et al.* ITQ-12: a new microporous silica polymorph potentially useful for light hydrocarbon separations. *Chem. Commun.*, 2114-2115 (2003).

[37] *Database of Zeolite Structures*. http://www.iza-structure.org/databases/ (2009).

[38] Sun, M. *et al.* Dielectric Constant Measurement of Zeolite Powders by Time Domain Reflectometry. *Microporous Mesoporous Mat.* (2009).

Part II:

Removal of Structure-Directing Agents from Molecular Sieves Via the Use of Photolabile Structure-Directing Agents

Chapter 5: Introduction to Part II of Thesis

1. Introduction

The unique chemical and structural properties of zeolites, such as their compositional variety, uniform pore spaces, structural symmetry, high surface areas, the ability to sieve molecules based on size- and shape-selectivity, etc., result in the use of zeolites in a wide array of applications.[1] Additionally, the potential to tailor many of these properties by modifying the zeolite synthesis conditions can yield materials that are exceptionally well-suited to their applications. These applications generally require full access to the internal surface area of the prepared materials, which necessitates the removal of any organics occluded during the synthetic process, such as structure-directing agents (SDAs) and pore filling agents, to open the pore space. There are four methods to clear the pore space of the organic materials: high-temperature calcination, ultra-violet (UV) irradiation / ozonolysis, extraction, and acid-cleavage / recombination.[2,3,4,5] The first three of these methods result in the destruction of the occluded organics, while the last method uses the chemical nature of the structure-directing agent to recover the original occluded organic after removal.

High-temperature calcination, which destroys the structure-directing agent via thermal decomposition at temperatures above 200 °C and more commonly between 500 – 700 °C, is the most frequently used method to remove occluded organics from inside the zeolite pore space. This is primarily due to the ease with which organic removal can be accomplished using a high temperature oven connected to gas sources such as air, nitrogen, or oxygen. However, it has several disadvantages. First, because this method

removes the organic through combustion, it generates various CO_2, NO_x, etc., greenhouse gas species that must be removed from the effluent for environmental reasons. Second, for applications that require the use of zeolite nanoparticles of uniform size, calcination may cause aggregation of zeolite nanoparticle colloids due to Si-O-Si bridging, rendering the colloids unusable.[6] Third, calcination may result in the collapse of the zeolite framework due to thermal stresses or dehydration if the calcination temperature is too high. Fourth, in non-traditional applications that require zeolites in planar form, calcination can lead to crack formation, buckling, and/or delamination in zeolite thin films or membranes due to thermal stresses (typically caused by differences in the coefficients of thermal expansion between the planar zeolite and the substrate) within the film and at the film / substrate interface (Figure 5.1).[7] Fifth, calcination is a nondiscriminatory process through which all organic molecules are removed; this is a problem for new classes of zeolite-like materials, such as organic-inorganic hybrids with zeolite structures, which may contain organic molecules in the framework itself.[8,9] These disadvantages result in higher processing costs and unwieldy procedures to synthesize, for instance, zeolite films with minimal defects, and nanoparticles with minimal aggregation. For example, current methods for reducing aggregation during template removal include the use of organic or polymeric matrices to physically bar aggregation[10], the surface functionalization of colloidal particles to minimize interactions[11], and acid extraction of structure-directing agents from surface-modified zeolite nanoparticles.[12] To minimize crack formation in zeolite films, calcination studies are carried out for each film topology, thickness, substrate, etc.[13] Moreover, many films and membranes may be part of devices incompatible with high-temperature calcination procedures, thus

disallowing “fixes” of this sort. For these types of applications, calcination may present a pyrrhic victory in terms of material costs and processing problems.

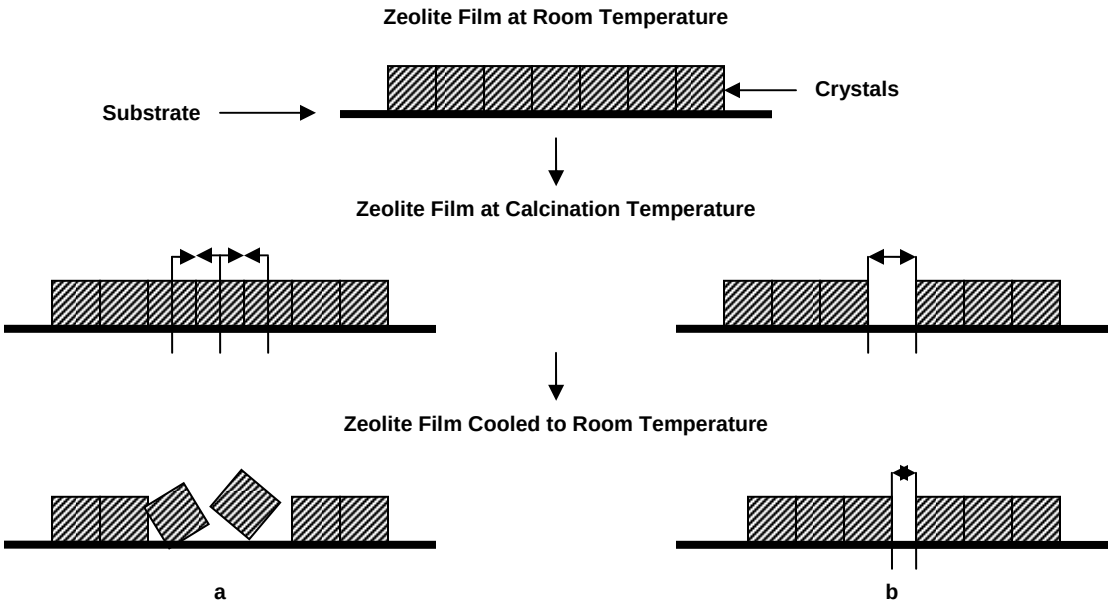

Figure 5.1 Schematic representation of the results of thermal stresses on zeolite films during calcination: (a) cracking at film / substrate interface if film is not well-adhered to substrate, (b) cracking within film if film is well-adhered to substrate

In an effort to address some of the problems with calcination, a solvent extraction approach was developed as a structure-directing agent removal technique wherein the occluded organic is washed out of the zeolite pore space with a solvent.[5] Although rarely used because it requires small structure-directing agents that can fit through the small pores and cages of the zeolite framework in order to exit the structure during extraction, it

can be beneficial in applications where high temperatures would adversely affect the physicochemical properties of the final material. Because of this, it is frequently used to remove templating agents for mesoporous (non-zeolite) materials. In general, the ease with which an occluded organic molecule can be removed from the pore space correlates well with its decomposition temperature during Thermogravimetric Analysis (TGA).[5] For instance, the fraction of a structure-directing agent that can be removed, if the molecule is small in comparison to the zeolite's micropore size, via extraction has been shown to depend on the fraction of the molecule that is combusted below 400 °C. The fraction that combusts above this temperature may be strongly bound to the zeolite framework and solvent extraction of this portion of the molecule can damage the framework. Additionally, if the interaction between the organic molecule and the inorganic framework is too strong, the extraction technique does not work; for many zeolites, the interaction is quite large (-181 ± 21 kJ per mole SDA), rendering the technique unusable except in specific cases.[14]

UV irradiation / ozonolysis is a non-thermal, photochemical "calcination" approach that recently has been used as a replacement for calcination for applications that require planar zeolites. This approach was designed to eliminate the film defects caused by thermal stresses generated during calcination.[3,15] It has the additional benefit that it can be used in conjunction with masking techniques to generate spatial patterns over thin films, where some of the zeolite film has been photochemically treated to open the pore space, and other areas have not (Figure 2). However, this method also results in the destruction of the organic molecules through the proposed mechanism of photo-induced

chemical reactions, in which short-wave UV radiation generates ozone and atomic oxygen that attack the organic species. Additionally, the method could potentially damage the inorganic framework, as the method generates activated species such as ions, free radicals, and excited organic molecules.[15]

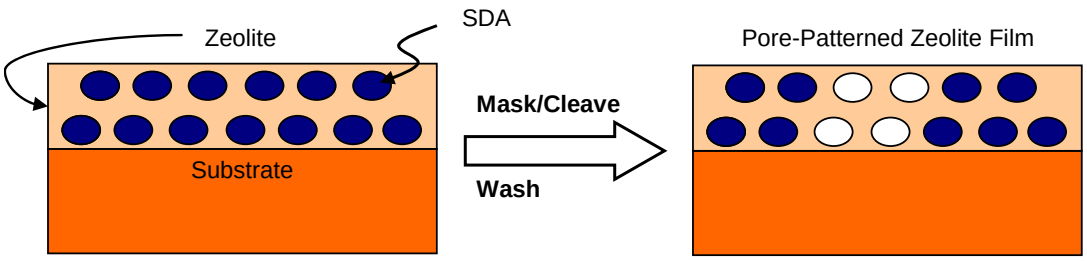

Figure 5.2 Schematic of zeolite film patterning using UV / ozonolysis photochemical "calcination" treatment to remove occluded organics

The three previously mentioned organic-removal techniques all result in the destruction of the structure-directing agent or other occluded organics. Recently, the use of larger, more complex and frequently more expensive structure-directing agents has increased due to industrial interest in creating new zeolite framework types with larger pores or nontraditional framework components.[16,2] Novel structure-directing agents often provide the best means to develop these new types of materials, as the structure-directing agents can act as direct templates around which the zeolite pores form, such as in the zeolite ZSM-18 (structure code MEI)[17], or as guides to the development of a given pore structure, without actually templating the zeolite.[18] Frequently, one structure-directing agent, like tetraethylammonium hydroxide, can synthesize several zeolite topologies through the use of differing synthesis conditions, such as reaction mixture composition,

reaction / zeolite crystallization time, reaction temperature, etc. Additionally, slight changes in the size and shape of a structure-directing agent can greatly influence the resulting crystalline product.[19] For these reasons, investigations of various structure-directing agents are often of primary importance when attempting to crystallize a new zeolite structure. However, when novel structure-directing agents can account for up to 25% of the total cost of industrial zeolite syntheses, techniques that destroy the organics to open the pore space become cost-prohibitive.[1,20] For this reason, removal techniques that can result in a partially or wholly reusable structure-directing agent are desirable.

The fourth and final method to eliminate occluded organics addresses the issue of structure-directing agent expense by removing the organics via a combustion-free methodology: acid cleavage / recycling. In this case, the zeolite is formed using a structure-directing agent that is a member of a class of quaternary ammonium cation-containing acid-cleavable ketal compounds.[2,21] These compounds can be cleaved into much smaller ketone- and diol-containing fragments (Figure 5.3), which can then be removed from the pore space and recombined into the original molecule for further zeolite syntheses, as shown in Figure 5.4. Figure 5.5 shows the organic molecules that

[1] For example, a typical SDA is tetrapropylammonium bromide (98%), which can be purchased in bulk for about 1/10 of the cost cited in the Fluka catalogue ($0.227 / g), or $0.028 / g. Generally, the SDA : SiO_2 molar ratio in synthesis is < 0.2, so for every pound of silica used, the SDA costs approximately $0.912. The SDA tends to be the most expensive chemical and its cost must be balanced against the average processing costs of $10-12 per pound of zeolite per day. Fairly inexpensive organic molecules like tetrapropylammonium bromide (98%), then, are approximately 7% of the overall cost of zeolite synthesis industrially.

have been used to date with this method, which has been shown to synthesize ZSM-5 (structure code MFI), ZSM-12 (structure code MTW), MOR, and VPI-8 (structure code VET).[21]

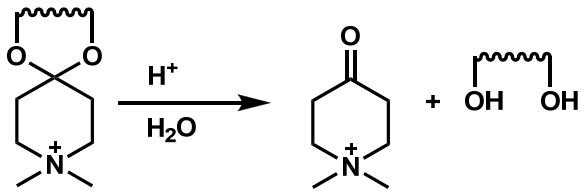

Figure 5.3 Cleavage reaction of ketal-containing structure-directing agent into smaller fragments[21]

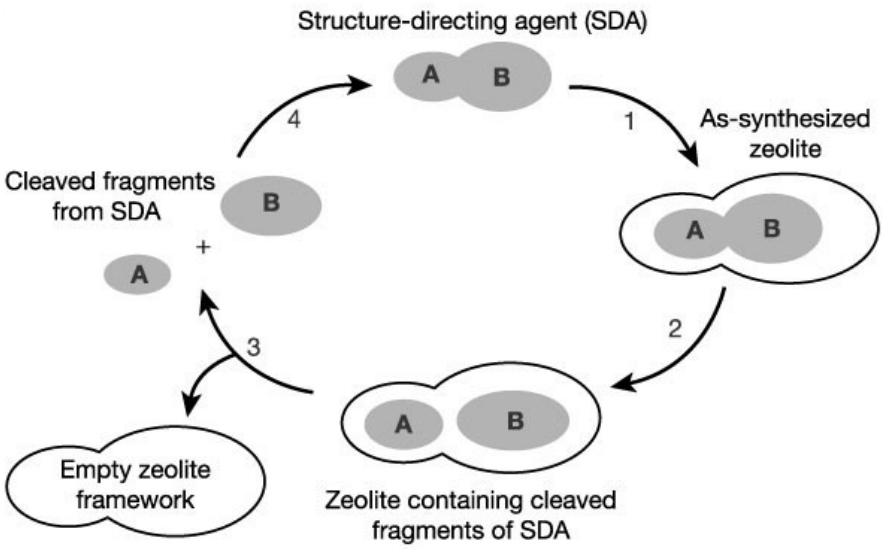

Figure 5.4 Recyclable structure-directing agent route – (1) zeolite synthesis; (2) cleavage of the organic molecules inside the zeolite pores; (3) removal of the cleaved fragments; (4) recombination of the fragments into the original SDA molecule[2]

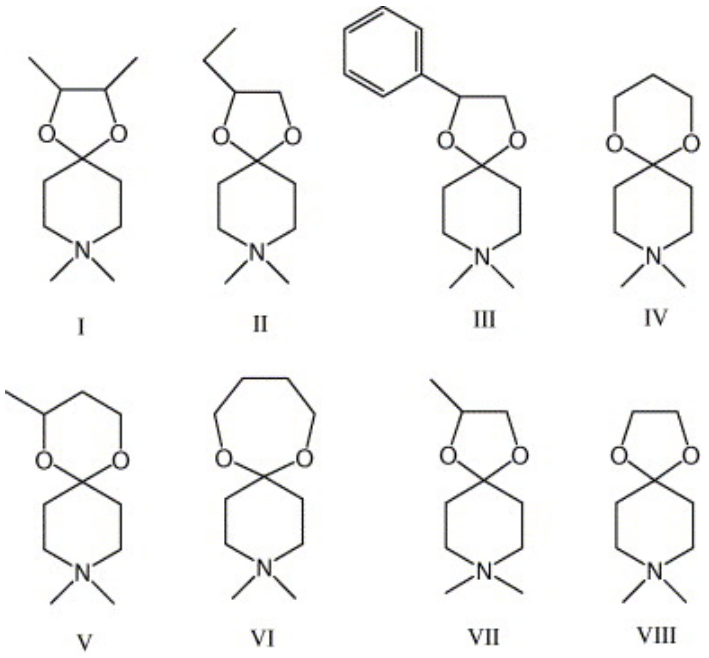

Figure 5.5 Various acid-cleavable ketal structure-directing agents [21]

Since this method allows for the removal and reuse of the structure-directing agent, it can be used as a low-cost zeolite preparation method. However, it may not be suitable for nanoparticle suspensions, thin films, or for many zeolite phases in general due to the nature of the extraction process – i.e., the presence of acid and water may change the suspension properties and can cause hydrolysis of unstable zeolite phases due to their siliceous nature. Hydrolysis is frequently a problem that occurs during high-temperature calcination of zeolites, because generation of water vapor during structure-directing agent destruction can lead to leaching of elements like Fe, Ga, and Zn (used in de-NO_x catalysts, chemical sensors, etc.) from the framework.[22] This places constraints upon the acid-cleavable, recyclable method of structure-directing agent removal.

While each of the aforementioned structure-directing agent removal techniques has advantages, each is limited by cost, effectiveness, or potential compatibility with end-use requirements. Although the recycling of structure-directing agents has addressed the reduction of zeolite cost, and the use of UV / ozonolysis photochemical "calcination" has reduced the problems associated with high-temperature calcination for thin films and nanoparticle suspensions, a method that can address both sets of problems simultaneously in a way that is compatible with more recent technologies that use zeolites in planar form would be beneficial. Given the recent attention to the development of these types of nontraditional zeolite applications, it is apparent that a structure-directing agent removal technique that is compatible with various planar zeolite fabrication processes, has a low cost, and is environmentally sustainable must be developed.

2. Photolabile Structure-Directing Agents

A pore-opening technique to remove occluded organics via a combination of recyclable structure-directing agents and a photochemical treatment wherein the original structure-directing agent is not completely destroyed could be developed using potentially recyclable, photolabile structure-directing agents. The proposed method is similar to the recyclable, acid-cleavable SDA method mentioned earlier and shown in Figure 5.3, in that the original structure-directing agent is cleaved post-zeolite synthesis; however, it differs in two major aspects. First, the organic molecule designed for zeolite synthesis is photoactive at a given wavelength of light; and second, the cleavage step inside the pores is carried out by photolysis. The cleaved molecule may then be washed out the pores

using a simple extraction process. The cleavage products may then be recombined, or, if photocleavage results in one unstable cleavage product (as is common), the stable cleavage product may be photoprotected again for reuse as a structure-directing agent. UV cleavage neatly avoids the problems calcination presents in various systems, as well as the issues with the use of acid in the acid cleavage / recycling methodology.

The photolabile structure-directing agent method is particularly advantageous for the development of nanostructured, planar zeolite materials because, like UV / ozonolysis, it can be used in conjunction with micropatterning techniques. For instance, recyclable, photolabile structure-directing agents, in conjunction with physical masks to generate electronic features through filled and unfilled pore space, may provide an interesting method with which to synthesize pure-silica zeolitic thin films of various topologies by *in-situ* crystallization techniques that are suitable for extension into the semiconductor development process, and could avoid the problems associated with thin films and high temperature calcination. This could be useful for the development of pure-silica zeolite thin films for low-*k* materials. Micropatterning could also be used to selectively functionalize certain areas of a zeolite film for catalysis applications by eliminating organics in some regions whilst leaving the pore space filled in others. Lastly, micropatterning could also lead zeolites to be more readily used as media for the organization of semiconductor quantum dots, as nanoreactors, and as storage for nonlinear molecules, such as proteins.[23]

The development of a photolabile structure-directing agent (P-SDA) route to zeolite synthesis requires three items to demonstrate its feasibility. First, an organic molecule must be created that is capable of acting in a structure-directing role. Therefore, the molecule must be stable at common zeolite synthesis conditions (basic pH, 100 – 200 °C temperatures) and able to crystallize a zeolite. The molecule's ability to do this hinges on the ability of the P-SDA to interact with the hydrophobically hydrated silica whilst retaining enough hydrophilicity to remain in the reaction solution, a condition frequently satisfied by the presence of quaternary ammonium ions in the SDA.[24] Second, the molecule must be photolytically active, which requires the development of potential photolabile structure-directing agents using photochemical protecting groups common in organic chemistry research, in conjunction with small molecules that have shown potential as structure-directing agents for a variety of zeolites. Third and finally, these photolabile molecules must then be capable of cleavage inside the framework of the zeolites they have crystallized to yield organic-free zeolites, implying that the zeolite they become trapped within must have large enough pore structures with low enough inorganic-organic interactions to prevent steric hindrance of cleavage. These three conditions for proof of feasibility impose strict requirements on both the type of organic molecule that can be used, as well as the choice of zeolite synthetic chemistry, and guide the selection of potential photolabile structure-directing agents.

3. Photochemical Protecting Groups in Organic Synthesis

Protecting groups are widely used during the organic synthesis of polyfunctional molecules. In order to generate an array of functionalities on the same molecule, or

substrate, individual functional groups must be blocked or protected in order to attach the next group without destroying the pre-existing groups. To do this, each functional group is directly converted into a derivative group, which is easily regenerated into the original group, and which is stable under the synthetic conditions of further steps. Typically, removal of the protecting group is affected via treatment or a combination of treatments with acids, bases, catalytic reduction, etc. In cases where the deprotection treatment is too harsh to guarantee survival of the substrate, blocking groups that respond to photochemical treatment can be used to avoid more rigorous regeneration conditions. These groups are light-sensitive chromophores, relatively stable to a variety of chemical reagents, responsive to wavelengths of light that will not damage the substrate, and able to regenerate the original functionality in good yield. Generally, protecting groups whose excited state lifetimes are short are preferred, as this can minimize the quenching processes that reduce overall cleavage yield. Based on these qualifications, several families of photoprotecting groups have been created. This section provides a brief overview of these families and the functional groups they protect.[25,26,27]

3.1 2-Nitrobenzyl Family

The 2-nitrobenzyl group (Figure 5.6), when a carbon-hydrogen bond is *ortho* to the nitro group, undergoes a light-induced intramolecular rearrangement where the nitro group (NO_2) is reduced to a nitroso group (NO) and an oxygen is inserted into the carbon-hydrogen bond at the 2-position. The nitroso-containing molecule that results from the hydrogen-abstraction mechanism (Figure 5.7) is relatively unstable, can decompose quickly under irradiation conditions, and cannot be used again to protect another

molecule. However, this is a particularly useful group that can be used to generate a variety of photochemical protecting groups. For instance, the plain 2-nitrobenzyl group can protect (a) carboxylic acid functionalities in aromatic and aliphatic acids, (b) imidazole functionalities in histidine-type molecules, and (c) phenolic hydroxyl functionalities in tyrosine-like molecules. By adding an oxycarbonyl group to become the 2-nitrobenzyloxycarbonyl, it can protect amino functionalities by generating urethanes in molecules like tryptophan. If instead an ethylene glycol function is added to the group, the photoprotecting molecule becomes 2-nitrophenylethyleneglycol, which can protect the carbonyl functionalities of aldehydes and ketones. The 2-nitrobenzyl family is one of the most common photochemical protecting groups used in organic chemistry, due to the array of functionalities it can protect, and the relative stability of the groups to both acidic and basic conditions. A note should be made, however, that the 2-nitrophenylethyleneglycol group forms acetals and ketal bonds with aldehydes and ketones, respectively, which are acid-cleavable under strong acid conditions.

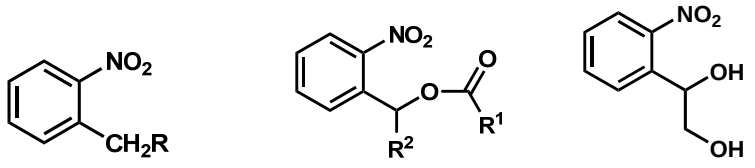

a b c

Figure 5.6 Examples of the 2-nitrobenzyl family of photochemical protecting groups: (a) 2-nitrobenzyl group, (b) 2-nitrobenzyloxycarbonyl, and (c) 2-nitrophenylethyleneglycol

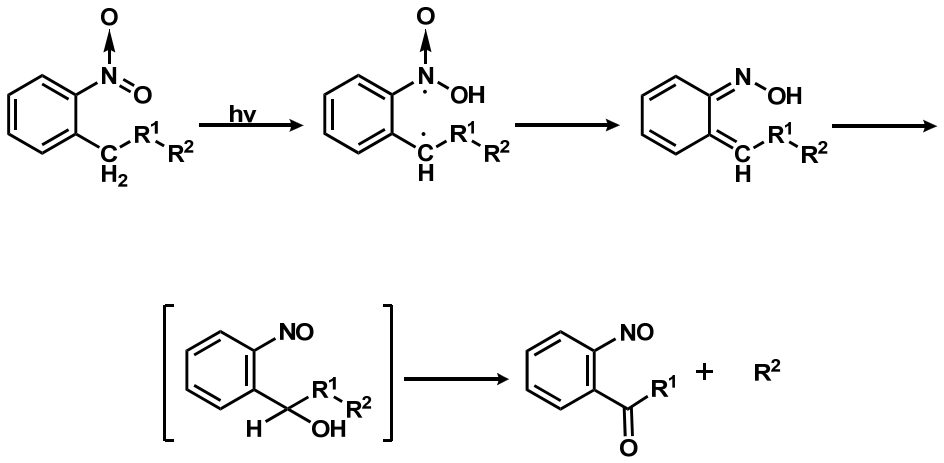

Figure 5.7 Schematic of the 2-nitrobenzyl group cleavage mechanism via hydrogen abstraction

3.2 Benzyloxycarbonyl Family

The benzyloxycarbonyl family of photochemical protecting groups (Figure 5.8) makes use of the different reactivity of its excited state with respect to its ground state to undergo light-induced cleavage that exactly regenerates the original functionality and partially regenerates the photochemical protecting group to the phenylmethanol molecule. Unlike the 2-nitrobenzyl family, which undergoes structural rearrangement to a new, unstable molecule, phenyl methanol can be regenerated into benzyloxycarbonyl using phosgene ($COCl_2$) chemistry. Generally, this molecule is used to protect amino functionalities via the formation of urethanes. The reactivity of this family may also be modified by the proper selection of moieties attached to the aromatic portion of the molecule. A typical example of this is the formation of the 3,5-dimethoxybenzyloxycarbonyl group, which has enhanced reactivity towards amino functionalities when compared with the benzyloxycarbonyl group itself, and is typically

used during peptide synthesis. The primary disadvantage of this photochemical protecting family is the formation of side-products of the original photochemical protecting group during photolytic removal via *N*- and *C*-alkylation. Additionally, the use of substituents on the aromatic portion of the photochemical protecting group to enhance photolytic cleavage generates bulky molecules that may be unsuitable for use in zeolite applications.

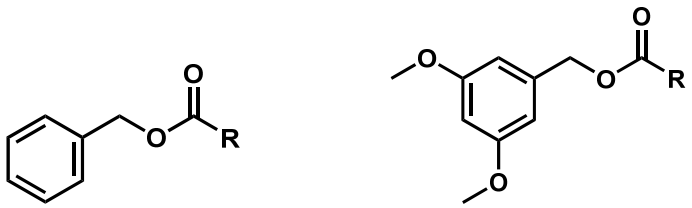

a b

Figure 5.8 Examples of the benzyloxycarbonyl family of photochemical protecting group: (a) benzyloxycarbonyl group, and (b) 3,5-dimethoxybenzyloxycarbonyl

3.3 3-Nitrophenyl Family

The 3-nitrophenyl family (Figure 5.9), like the benzyloxycarbonyl family, undergoes light-induced cleavage due to differences in ground state and excited state energies, again resulting in the regeneration of both the original photochemical protecting group and the functional group on the substrate. It is often used due to its stability in aqueous solutions over a wide pH range. Two typical examples of this family are the 3-nitrophenyloxy group, which protects pyrophosphate diester functionalities, and 3-nitrophenyloxycarbonyl, which protects amino functionalities.

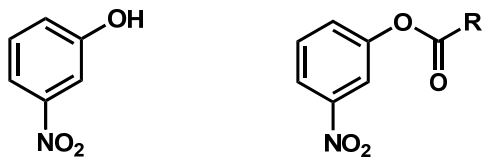

a b

Figure 5.9 Examples of the 3-nitrophenyl photochemical protecting group: (a) 3-nitrophenylhydroxide, and (b) 3-nitrophenyloxycarbonyl

3.4 Phenacyl Family

The phenacyl photochemical protecting group (Figure 5.10) is unusual in that it is the interaction between electrons in the carbonyl group and the phenyl ring that gives the phenacyl group low-lying excited states and makes light-induced cleavage possible. Like the benzyloxycarbonyl family, this photochemical protecting group's reactivity may be modified by placing substituents on the aromatic portion of the molecule. This family is primarily used to protect carboxylic functionalities.

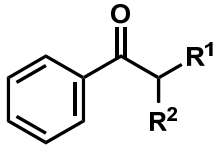

Figure 5.10 The phenacyl photochemical protecting group family

The selection of a particular family of photochemical protecting group depends on the type of functionality that must be protected, and conditions under which they must be stable. For common aluminosilicate zeolite syntheses, this requires stability in basic to

extremely basic conditions (pH > 10), and thermal stability up to 200 °C. Other types of zeolite syntheses, such as fluoride-mediated syntheses and aluminophosphate syntheses, require stability at neutral (pH between 6 and 8) and acidic (pH < 4) conditions, respectively. The photochemical protecting groups discussed here can generally withstand these conditions, although the groups that form esters with the substrate, such as the phenacyl, 3-nitrophenyl, and benzyloxycarbonyl families, are unlikely to survive the zeolite synthesis. Thermal stability of the photochemical protecting group may be evaluated using Thermogravimetric Analysis; generally rigid molecules can withstand higher temperatures, and for these purposes all the photochemical protecting groups mentioned here could be applicable. Additionally, the synthesis of the photochemical protecting group must be reasonable; for instance, many of the reactions that generate the oxycarbonyl functionality to create the photochemical protecting group require the use of phosgene gas, which is inappropriate for laboratory-scale use. Lastly, the cleavage mechanism of the photochemical protecting group must be appropriate for the particular zeolite within which it becomes occluded. Cleavage that requires rotational freedom might not occur if the photoprotected molecule is tightly constrained inside the zeolite pore space.

4. Photofunctional Zeolites

The study of photochemistry inside zeolites is often aimed at discovering the effects of adsorption or constraint on the photochemical and photophysical properties of photoactive molecules, since the behavior of constrained molecules is very different from that of gas or liquid-phase molecules. Typical aluminosilicate, silicate, and

aluminophosphate zeolites are inert to photochemistry (except for situations where photoactive elements are inserted into the inorganic framework), and therefore can be used as micro-reactors to investigate host-guest interactions and their role in photochemistry of the occluded molecules.[28]

The effects of zeolite constraint on the behavior of photoactive molecules are primarily the result of the chemical environment and pore architecture.[28] The silica to alumina ratio of aluminosilicate zeolites can affect the wavelength at which the molecule absorbs; for instance, a decrease in the ratio frequently causes shifts in the molecule's absorption spectra to longer wavelengths. This implies that when attempting to cleave a photoactive molecule inside a zeolite framework, the use of a UV lamp with a relatively broad band (for instance, UV-A or UV-B radiation) would be more likely to achieve cleavage than the use of a very specific wavelength lamp. The presence of charge-balancing cations can also affect the electrostatic fields and vacant space that is usable by the photoactive molecule. For instance, the polarity of the zeolite cavities can be increased by using lighter charge-balancing atoms, such as Li^+ and Na^+, causing interactions between the framework and any aromatic portions of the photoactive molecule, leading to some distortion in the symmetry of the molecule and potentially poor cleavage. Heavier charge-balancing cations, on the other hand, can enhance the generation of excited triplet states in some molecules, thus improving the cleavability of the occluded organic. The acidity of the surface hydroxyl groups and the basicity of the lattice oxygen can also affect the behavior of the photoactive molecule. Lastly, and perhaps most importantly, the cavity size or pore space can impose steric hindrance on the molecule, and potentially

reduce cleavability. These factors imply that even if a photoactive molecule is capable of acting in a structure-directing role, it may be difficult to cleave if it is tightly constrained or bound within the zeolite it helps to form.

5. Development of a Photolabile Structure-Directing Agent

The ability of a molecule to act in a structure-directing role is determined in large part by its hydrophobicity. An intermediate hydrophobicity, represented by a C / N+ ratio of 12 – 13, gives the molecule the ability to transfer between an organic phase and the aqueous phase in the zeolite precursor gel; molecules within this range tend to direction the formation of zeolites. In general, the Liebau rules that describe conditions at which organic guest molecules best form clathrasils can be used as guidelines for the selection of molecules appropriate for use as structure-directing agents.[29] First, there must be sufficient room in a cage or pore for the organic guest. Second, the organic guest must be stable under synthetic conditions. Third, the organic guest should fit within the inner surface of the inorganic framework with as many van der Waals interactions as possible, but with the least deformation of the guest molecule. Fourth, the guest molecule should have only weak tendencies to form complexes with the solvent. Fifth, more rigid molecules will tend to form clathrasils more easily than flexible molecules. And sixth, a guest molecule's tendency to form clathrasils will increase with the basicity or polarizability of a guest molecule.

In order to develop a photolabile structure-directing agent that reasonably fits within the criteria mentioned previously for photoactivity, cleavability, and structure-direction, the

2-nitrobenzyl family of photochemical protecting groups was chosen, to "protect" portions of two smaller molecules that have been shown to aid in the synthesis of zeolites: 1,1-dimethyl-4-oxopiperidinium- and imidazole / imidazolium-based molecules.[21,30,31] The first molecule was created using the 2-nitrophenylethylglycol group, to form the photolabile equivalent (Figure 5.11) of molecule III in Figure 5.5, 8,8-dimethyl-2-(2-nitrophenyl)-1,4-dioxa-8-azoniaspiro[4.5]decane hydroxide (P-SDA 1) by protection of the carbonyl functionality. The second molecule was created using the 2-nitrobenzyl group to form the photolabile compound 1-(2-nitrobenzyl)-1H-imidazole (Figure 5.12, P-SDA 2) by protection of the imidazole functionality. The benefits of the selection of both this family of photochemical protecting group and the small molecule substrates are (a) the chemistry of these molecules follows a well-understood pattern (although P-SDA 1 has not previously been synthesized), (b) examples exist in the literature of the use of the substrate molecules themselves or very similar molecules as structure-directing agents, (c) the molecules are stable within the thermal range of zeolite syntheses, and (d) each molecule has a different stability to pH (P-SDA 1 is very stable under basic conditions, while P-SDA 2 is stable under acidic to basic conditions). The primary disadvantage of these molecules is their inability to be completely regenerated upon cleavage, as the light-induced cleavage mechanism of the 2-nitrobenzyl family renders the photochemical protecting group unstable via the reduction of the nitro group to a nitroso group. However, the molecule is partially recyclable given that the original small molecule substrate is still intact and may be protected again. A choice of another family of photochemical protecting groups, like the benzyloxycarbonyl group, could avoid this disadvantage and render the structure-directing agent wholly recyclable

following treatment with phosgene (a safety hazard), but the types of linkages the protecting group forms are unlikely to survive zeolite synthesis.

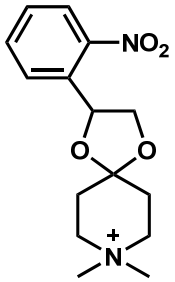

Figure 5.11 P-SDA 1, 8,8-dimethyl-2-(2-nitrophenyl)-1,4-dioxa-8-azoniaspiro[4.5]decane

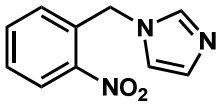

Figure 5.12 P-SDA 2**,** 1-(2-nitrobenzyl)-1H-imidazole

Part II of this thesis discusses the development of a new route to zeolite crystallization and occluded organic removal via the use of photolabile structure-directing agents. Chapters 6 and 7 detail the experimental work done to demonstrate the feasibility of this new method using P-SDA 1 and P-SDA 2, respectively. If this method is effective, it could make currently expensive zeolite syntheses commercially feasible, decrease the

process’ detrimental environmental side effects, and lastly, increase the facility of further processing steps used in various industries.

6. References

[1] Bein, T. Synthesis and applications of molecular sieve layers and membranes. *Chem. Mater.* **8**, 1636-1653 (1996).

[2] Lee, H., Zones, S. I. & Davis, M. E. A combustion-free methodology for synthesizing zeolites and zeolite-like materials. *Nature* **425**, 385-388 (2003).

[3] Parikh, A. N. *et al.* Non-thermal calcination by ultraviolet irradiation in the synthesis of microporous materials. *Microporous Mesoporous Mat.* **76**, 17-22 (2004).

[4] Szostak, R. *Molecular Sieves: Principles of Synthesis and Identification*. 2nd ed., (Blackie Academic & Professional, 1998).

[5] Jones, C. W., Tsuji, K., Takewaki, T., Beck, L. W. & Davis, M. E. Tailoring molecular sieve properties during SDA removal via solvent extraction. *Microporous Mesoporous Mat.* **48**, 57-64 (2001).

[6] Tosheva, L. & Valtchev, V. P. Nanozeolites: Synthesis, crystallization mechanism, and applications. *Chem. Mater.* **17**, 2494-2513 (2005).

[7] Dong, J. H., Lin, Y. S., Hu, M. Z. C., Peascoe, R. A. & Payzant, E. A. Template-removal-associated microstructural development of porous-ceramic-supported MFI zeolite membranes. *Microporous Mesoporous Mat.* **34**, 241-253 (2000).

[8] Yamamoto, K., Sakata, Y., Nohara, Y., Takahashi, Y. & Tatsumi, T. Organic-inorganic hybrid zeolites containing organic frameworks. *Science* **300**, 470-472 (2003).

[9] Yamarnoto, K. & Tatsumi, T. ZOL: A new type of organic-inorganic hybrid zeolites containing organic framework. *Chem. Mater.* **20**, 972-980 (2008).

[10] Wang, H. T., Wang, Z. B. & Yan, Y. S. Colloidal suspensions of template-removed zeolite nanocrystals. *Phys. Chem. Chem. Phys.* **2**, 2333-2334 (2000).

[11] Smaihi, M., Gavilan, E., Durand, J. O. & Valtchev, V. P. Colloidal functionalized calcined zeolite nanocrystals. *J. Mater. Chem.* **14**, 1347-1351 (2004).

[12] Gautier, B. & Smaihi, M. Template extraction from surface-functionalised zeolite beta nanoparticles. *New J. Chem.* **28**, 457-461 (2004).

[13] Geus, E. R. & Vanbekkum, H. Calcination Of Large Mfi-Type Single-Crystals .2. Crack Formation And Thermomechanical Properties In View Of The Preparation Of Zeolite Membranes. *Zeolites* **15**, 333-341 (1995).

[14] Piccione, P. M., Yang, S. Y., Navrotsky, A. & Davis, M. E. Thermodynamics of pure-silica molecular sieve synthesis. *J. Phys. Chem. B* **106**, 3629-3638 (2002).

[15] Li, Q. H., Amweg, M. L., Yee, C. K., Navrotsky, A. & Parikh, A. N. Photochemical template removal and spatial patterning of zeolite MFI thin films using UV/ozone treatment. *Microporous Mesoporous Mat.* **87**, 45-51 (2005).

[16] Blasco, T. *et al.* Preferential location of Ge in the double four-membered ring units of ITQ-7 zeolite. *J. Phys. Chem. B* **106**, 2634-2642 (2002).

[17] Lobo, R. F., Zones, S. I. & Davis, M. E. Structure-Direction In Zeolite Synthesis. *J. Inclusion Phenom.* **21**, 47-78 (1995).

[18] Corma, A., Rey, F., Rius, J., Sabater, M. J. & Valencia, S. Supramolecular self-assembled molecules as organic directing agent for synthesis of zeolites. *Nature* **431**, 287-290 (2004).

[19] Zones, S. I., Burton, A. W., Lee, G. S. & Olmstead, M. M. A study of piperidinium structure-directing agents in the synthesis of silica molecular sieves under fluoride-based conditions. *J. Am. Chem. Soc.* **129**, 9066-9079 (2007).

[20] Zones, S. I. Personal Communication. (Richmond, 2006).

[21] Lee, H., Zones, S. I. & Davis, M. E. Synthesis of molecular sieves using ketal structure-directing agents and their degradation inside the pore space. *Microporous Mesoporous Mat.* **88**, 266-274 (2006).

[22] Deruiter, R., Pamin, K., Kentgens, A. P. M., Jansen, J. C. & Vanbekkum, H. Synthesis Of Molecular-Sieve [B]-Bea And Modification Of The Boron Site. *Zeolites* **13**, 611-621 (1993).

[23] Sun, W. Q., Lam, K. F., Wong, L. W. & Yeung, K. L. Zeolite micropattern for biological applications. *Chem. Commun.*, 4911-4912 (2005).

[24] Davis, M. E. in *Zeolites: A Refined Tool for Designing Catalytic Sites Studies in Surface Science and Catalysis* (L. Bonneviot & S. Kaliaguine, eds.) (Elsevier Science, 1995).

[25] Pillai, V. N. R. Photoremovable Protecting Groups in Organic Synthesis. *Synthesis* **1980**, 1-27 (1980).

[26] Hoffmann, N. Photochemical Reactions as Key Steps in Organic Synthesis. *Chem. Rev.* (2008).

[27] Greene, T. W. *Protective Groups in Organic Synthesis*. (John Wiley & Sons, Inc., 1981).

[28] Yamashita, H. & Anpo, M. in *Photofunctional Zeolites: Synthesis, Characterization, Photocatalytic Reactions, Light Harvesting* (Masakazu Anpo, ed.) (Nova Science Publishers, 2000).

[29] Liebau, F. *Zeolites* **3** (1983).

[30] Lee, H., Zones, S. I. & Davis, M. E. Zeolite synthesis using degradable structure-directing agents and pore-filling agents. *J. Phys. Chem. B* **109**, 2187-2191 (2005).

[31] Zones, S. I. & Burton, A. W. Diquaternary structure-directing agents built upon charged imidazolium ring centers and their use in synthesis of one-dimensional pore zeolites. *J. Mater. Chem.* **15**, 4215-4223, doi:10.1039/b500927h (2005).

Chapter 6: Photolabile structure-directing agents for zeolite synthesis

Abstract

The synthesis, photocleavage, and structure-directing ability of the photolabile molecule 8,8-dimethyl-2-(2-nitrophenyl)-1,4-dioxa-8-azoniaspiro[4.5]decane hydroxide (P-SDA 1) is presented and discussed. The organic molecule is synthesized via ketalization procedures, followed by amine quaternization and ion exchange to the final hydroxide form, generating P-SDA 1 in approximately 50% overall yield. Photolytic cleavage of the molecule proceeds via long-wave UV radiation with a Hg arc lamp to generate the unstable 2-nitrosophenylcarbonyl derivative of the 2-nitrophenylethylene glycol photochemical protecting group and 1,1-dimethyl-4-oxopiperidium hydroxide. Cleavage of the photolytic P-SDA 1 is demonstrated in a homogeneous solution of acetonitrile, and intercalated into a dealuminated zeolite FAU, an open-framework zeolite. Attempts to synthesize silicate and aluminosilicate zeolites through procedures similar to those used to prepare various compositions of the BEA* and MFI zeolite structures, using P-SDA 1 as the structure-directing agent, resulted in the formation of primarily amorphous and layered materials. One synthesis did yield crystalline material with the MFI zeolite topology; however, this synthetic result was not reproducible.

1. Introduction

As more zeolite phases are discovered through the use of novel and expensive organic structure-directing agents, and used in non-traditional applications like electronic devices and chemical sensors, the need for a low-cost alternative to the standard calcination process, which destroys the organic molecules, increases. Previous work by Lee et al.

demonstrated a combustion-free zeolite synthesis method that removes structure-directing agents (SDAs) from pores, by using various acid-cleavable ketal compounds that contain quaternary ammonium cations.[1,2] The acid-cleavable ketal compounds can be cleaved into smaller ketone- and diol-functionalized fragments, which can then be recombined into the original molecule for further zeolite syntheses. This method avoids problems commonly caused by high-temperature calcination, such as crack formation in zeolite thin films or membranes due to thermal stresses within the film and at the film / substrate interface.[3] However, this method may not be suitable for nanoparticle suspensions, thin films, or for many zeolite phases in general due to the nature of the extraction process – i.e., the presence of acid and water may change the suspension properties and can cause hydrolysis of unstable zeolite phases due to their siliceous nature, and like calcination, can cause aggregation of zeolite nanoparticle colloids due to Si-O-Si bridging.[4] Therefore, an alternative to calcination that is both simple and more compatible with end-use processing and fabrication steps for non-traditional zeolite applications would be valuable.

The use of UV radiation, as opposed to aqueous acid, to cleave the structure-directing agents would provide a simpler method of liberating the zeolite pores. Additionally, it could decrease the likelihood of film defect formation due to high temperature calcination in zeolite thin films and membranes, and could reduce aggregation in colloidal suspensions, thus avoiding complicated methods for reducing aggregation during template removal. These methods include the use of organic or polymeric matrices to physically bar aggregation[5], the surface functionalization of colloidal particles to

minimize interactions[6], and acid extraction of structure-directing agents from surface-modified zeolite nanoparticles.[7] Photolysis of the structure-directing agent could therefore be a useful strategy for a variety of applications developed using colloidal zeolite suspensions and zeolite nanoparticles, such as thin films and membranes (through spin / dip coating)[8], macroscopic, ordered zeolite structures (through macropatterning or macrotemplating)[9], micro-/mesoporous materials (through seeding)[10], medical diagnostics (through incorporation of Gd^{3+} ions for magnetic resonance imaging)[11], and chemical sensors[12], due to its relatively simple strategy compared with other techniques to minimize aggregation.

Towards this end, the development of partially recyclable, photo-cleavable structure-directing agents, is proposed, wherein the structure-directing agent is disassembled through photolysis within the zeolite pore space, removed, and then reassembled for the manufacture of additional zeolites – without the complete destruction of either the organic structure-directing agent or damage to the inorganic zeolite framework. The initial photolabile structure-directing agent to be developed is a derivative of 8,8-dimethyl-2-phenyl-1,4-dioxa-8-azoniaspiro[4,5]decane hydroxide, an acid-cleavable molecule that has been demonstrated to produce the zeolite known as mordenite (structure code MOR). This new molecule is a member of the 2-nitrobenzyl class of photochemical protecting groups commonly used in the organic synthesis of polyfunctional molecules (Figure 6.1b).[2,13] Here, its synthesis and photolysis is presented, and its feasibility as a structure-directing agent for common silicate and aluminosilicate zeolites is evaluated.

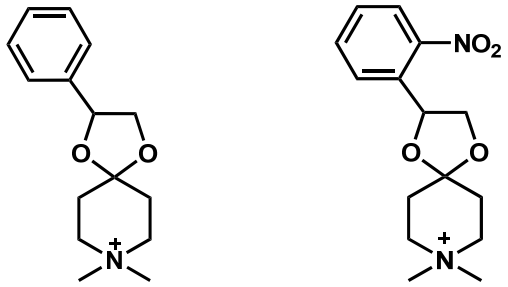

Figure 6.1 (a) Acid-cleavable structure-directing agent 8,8-dimethyl-2-phenyl-1,4-dioxa-8-azoniaspiro[4,5]decane hydroxide; (b) potential photolabile structure-directing agent, 8,8-dimethyl-2-(2-nitrophenyl)-1,4-dioxa-8-azoniaspiro[4.5]decane hydroxide

2. Results and Discussion

2.1 P-SDA 1 Synthesis

Although there are no reports in the literature of the synthesis of P-SDA 1, its preparation may be envisioned by the use of standard ketalization reaction techniques, followed by quaternization of the secondary amine, and finally, ion exchange of its iodide counter-ion to the hydroxide form (Figure 6.2).[14,15] Since the product molecule (P-SDA 1) may be cleaved by both acids as well as long-wave UV radiation, the initial ketalization reaction is run under an inert atmosphere in a covered apparatus, and is neutralized upon reaction completion by the addition of a small amount of a saturated solution of sodium bicarbonate in water while stirring the reaction mixture. Ketalization reactions of this type generally proceed to completion only if the water generated during the ring-formation is removed, hence a Dean-Stark apparatus is used during reflux. Although

standard literature procedures for ketalization reactions suggest that the diol be in excess of the ketone (to protect the ketone)[13], the diol in this case, 1-(2-nitrophenyl)ethane-1,2-diol (Aldrich), is very expensive[1] and is therefore used as the limiting reagent. The ketone (4-piperidone HCl•H_2O, Fluka) to diol molar ratio is at least 3:1. Crude ^1H nuclear magnetic resonance (NMR) spectroscopy data for this molecule before amine quaternization indicates peaks at 2.1, 3.1, 3.8, 4.6, 5.6, 7.6, 7.8, 8.1, and 8.3, in addition to low-intensity peaks due to the presence of small amounts of impurities at 1.0, 2.3, 3.4, 5.1, 7.5, and 7.7.

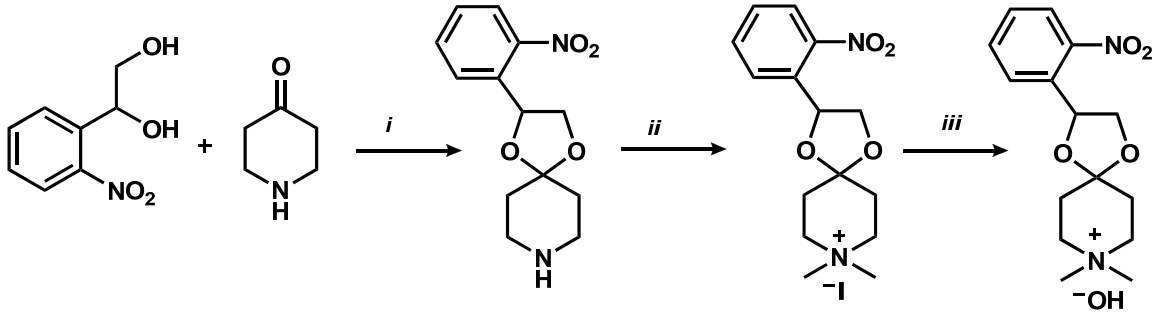

Figure 6.2 Proposed synthetic route for the preparation of P-SDA 1: (*i*) ketalization reaction; (*ii*) quaternization of the secondary amine; (*iii*) ion exchange of the quaternary amine counter-ion

To purify the ketal product, which is a reddish-colored resin, water / chloroform extraction was used to separate the excess ketone from the product ketal. Further

[1] approximately $325 for five grams

purification of the product by solid-liquid chromatography on a silica gel 60 column was attempted, but resulted in the breakdown of the molecule due to the slightly acidic nature of the silica gel. Purification by recrystallization was then attempted with a large variety of solvent systems, with varying degrees of success. A mixture of dichloromethane / hexanes appeared to yield the best results, although the product precipitated out of the solution as an oily substance, and not as a solid powder, as expected. Alternatively, repeated extraction from a water / chloroform solvent system resulted in adequate purification.

The amine quaternization reaction was tested in methanol for a variety of solution concentrations and molar equivalents of methyl iodide. The reaction was run under an inert atmosphere shielded from light sources, as previously discussed, and the methyl iodide to amine ratio was at least 5 : 1 to reduce the reaction time. Lower amounts of methyl iodide could be used, but this caused the reaction time to extend to several days to produce a quaternized product in over 40 % yield. Upon reaction completion, the product was recovered, and recrystallized from chloroform and ether. The ketal's iodide counter-ion was then ion-exchanged with the hydroxide ion, and the extent of conversion was determined by acid titration. The resulting photo-cleavable structure-directing agent was then characterized by ^{1}H NMR, as shown in Figure 6.3.

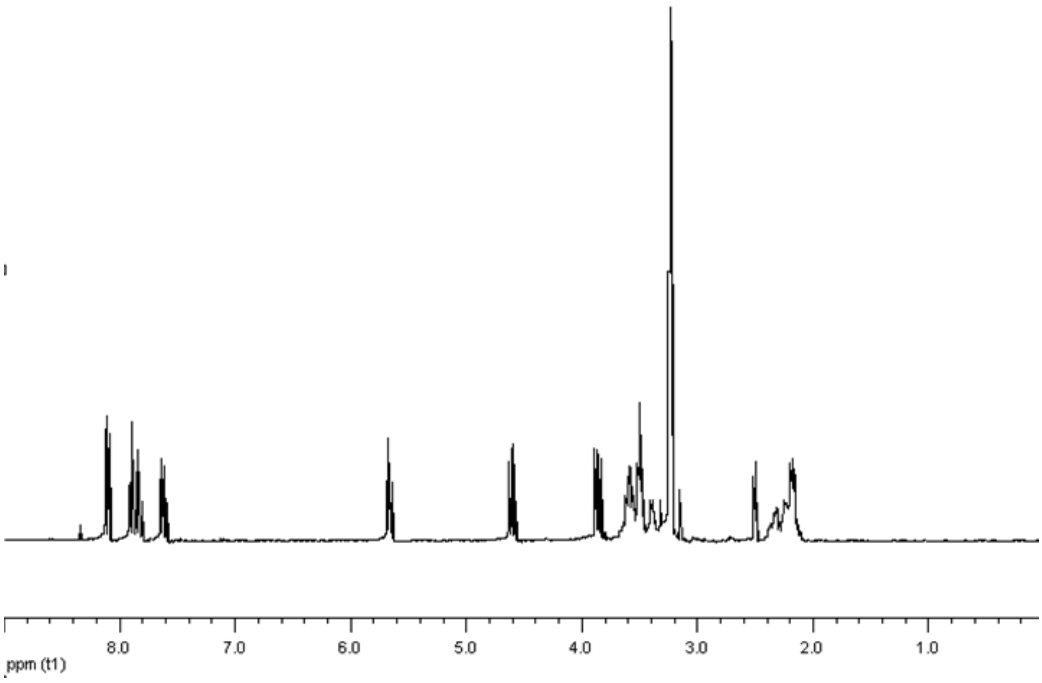

Figure 6.3 ^{1}H NMR spectrum of P-SDA 1 in its iodide salt form

The molecule was tested for thermal stability using thermogravimetric analysis (TGA) in its iodide salt form, which indicated that it experiences an initial mass loss of approximately 20% beginning at approximately 250 °C. This suggested that zeolite synthesis temperatures beyond this point will result in the breakdown of P-SDA 1 (Figure 6.4). Beyond 300 °C, another gradual mass loss occurred, but not all of P-SDA 1 was combusted off the sample pan at the end of the run; indeed, a small percent remained as black "coke" on the pan after the experiment finished. This type of coking can occur when aromatics are present in the sample. Also, the small endotherm at 200 °C is most likely a melting point for the sample. These data imply that the photolabile molecule is stable in the standard range of zeolite synthesis temperatures (although the stability of the molecule in caustic zeolite gels may differ from the given thermal stability).

Additionally, it was found that the iodide salt form of the ketal (the form obtained after step *ii* in Figure 6.2) is very stable to both air and visible light, whereas the photolabile molecule in its aqueous, ion-exchanged hydroxide form rapidly deteriorates when stored, unprotected to visible light, due to a combination of the effects of water and light on the ketal bond. Therefore, P-SDA 1 must be stored long-term in the iodide salt form and ion-exchanged just prior to use.

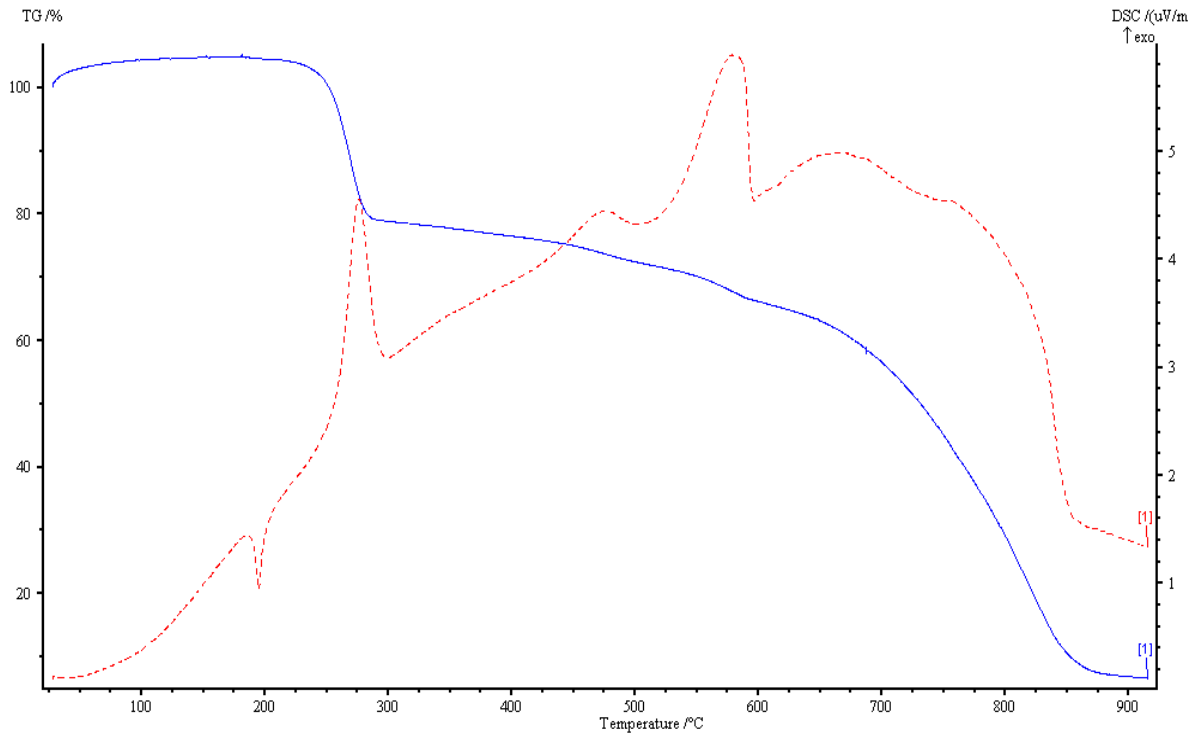

Figure 6.4 TGA data of P-SDA 1 prior to conversion of quaternary ammonium iodide salt form to quaternary ammonium hydroxide material

2.2 Photolysis of P-SDA 1

As with all members of the 2-nitrobenzyl group of photoactive molecules, P-SDA 1 cleaves with long-wave UV radiation through a hydrogen-abstraction mechanism (Figure 6.5). P-SDA 1, however, has not been reported in the literature; therefore, the molecule's photolytic ability must be confirmed. To do this, the ketal in its iodide salt form was dissolved in a variety of solvents (acetonitrile, N,N-dimethylformamide, dimethylsufloxide, water, benzene) and subjected to UV radiation with a wavelength of greater than 320 nm for various times following standard photo-cleavage procedures.[13,15,16] Unsurprisingly, it was found that protic solvents interfere with the cleavage of this molecule. Aprotic solvents, such as acetonitrile, however, allowed the complete cleavage of P-SDA 1 in its iodide salt form by irradiation after only one hour. The iodide salt form of the ketal was used in this case because the hydroxide form, when irradiated, completely decomposed due to the necessity of heavily concentrating the solution in order to follow standard photo-cleavage procedures, which led to the extremely basic solution destroying the molecule. The cleavage was followed using electrospray ionization mass spectroscopy (ESI MassSpec), which indicated the presence of the ketone cleavage fragment $[M^+] = 128.08$ and did not detect the intact ketal $[M^+] = 293.07$ after one hour.

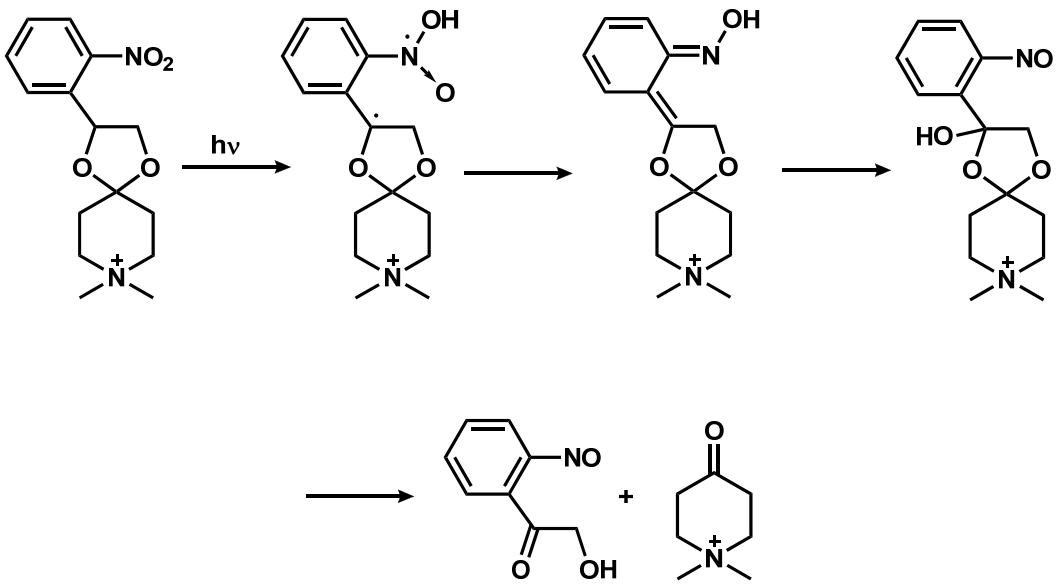

Figure 6.5 Photolysis mechanism of P-SDA 1, generating 2-hydroxy-1-(2-nitrosophenyl)ethanone and 1,1-dimethyl-4-oxopiperidinium

However, the cleavage of P-SDA 1 in a homogeneous solution does not serve as a perfect test of its ability to cleave within a zeolite framework, which is its final destination.[16] To determine the effectiveness of cleaving within a cage, and to find and to eliminate potential problems that may arise during cleavage, the ketal was then intercalated into a large cage, pure-silica zeolite (trade-name Tosoh 390-HUA, structure code FAU) donated by Chevron. Standard intercalation procedures called for activating 300 mg of this zeolite with heat and vacuum for 12 hours, then injecting a solution of 20 mg of the ketal iodide salt in 0.8 mL acetonitrile and stirring the solution for 24 hours. Solid-state ^{13}C cross-polarization magic-angle spinning nuclear magnetic resonance (CPMAS NMR, Figure 6.6) and TGA (Figure 6.7) were carried out on both the solid ketal (prior to

intercalation) and the zeolite sample (post-intercalation) to determine the success of the procedure. TGA data indicated that the zeolite was loaded with 16 wt % organic, and showed that the organic in the zeolite sample had the same characteristic curve as the pure iodide salt ketal. ^{13}C CPMAS NMR indicated peaks for the pure iodide salt ketal at 148.0, 140.5, 134.7, 130.1, 124.4, 123.3, 104.1, 74.3, 69.5, 60.2, 52.3, 42.9, 30.5, and 25.2. The corresponding crude spectrum for the loaded zeolite sample showed broad peaks whose width incorporated the 148.0 – 123.3 ppm peaks and the 74.3 – 25.2 peaks. A smaller peak corresponding to the ketal carbon at 104.1 ppm was also present.

Initial attempts to cleave the adsorbed molecule failed due to the use of procedures better suited to homogeneous solutions than molecules adsorbed within the zeolite cage (Figure 6.6c). If cleaved, the ^{13}C CPMAS NMR data would show a small peak at 200 ppm, due to the presence of a ketone. A modified procedure was then utilized. The new procedure called for the sample to be drop-coated in a thin layer onto glass slides, then irradiated. After photocleavage, the sample was scraped off the slides, and the P-SDA 1 fragments were extracted from the pore space using acetonitrile. The photocleavage was followed using infrared spectroscopy (IR), and yielded cleavage of the P-SDA 1 present in the zeolite material (Figure 6.8). This was demonstrated by the formation of the ketone carbon peak at 1790 cm^{-1}. In this case, IR was used to follow the photolysis rather than ^{13}C CPMAS NMR due to the very long experiment time required to obtain a good signal-to-noise ratio for this NMR spectrum.

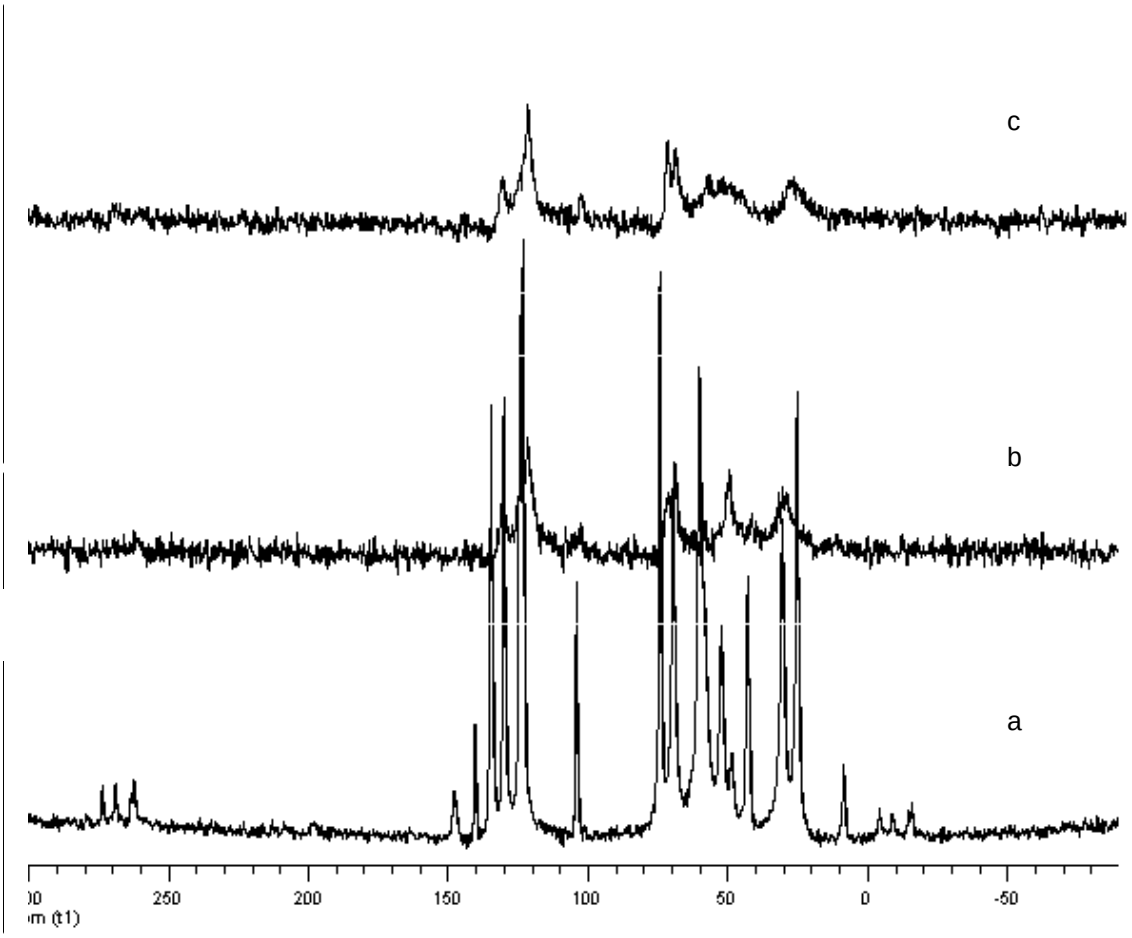

Figure 6.6 ^{13}C CPMAS NMR spectra of: (a) P-SDA 1 in the iodide salt form; (b) P-SDA 1 intercalated into the pure-silica zeolite with the FAU structure; (c) results of initial attempts to photocleave P-SDA 1 intercalated into the pure-silica FAU material demonstrate that cleavage did not occur, as the NMR data did not change

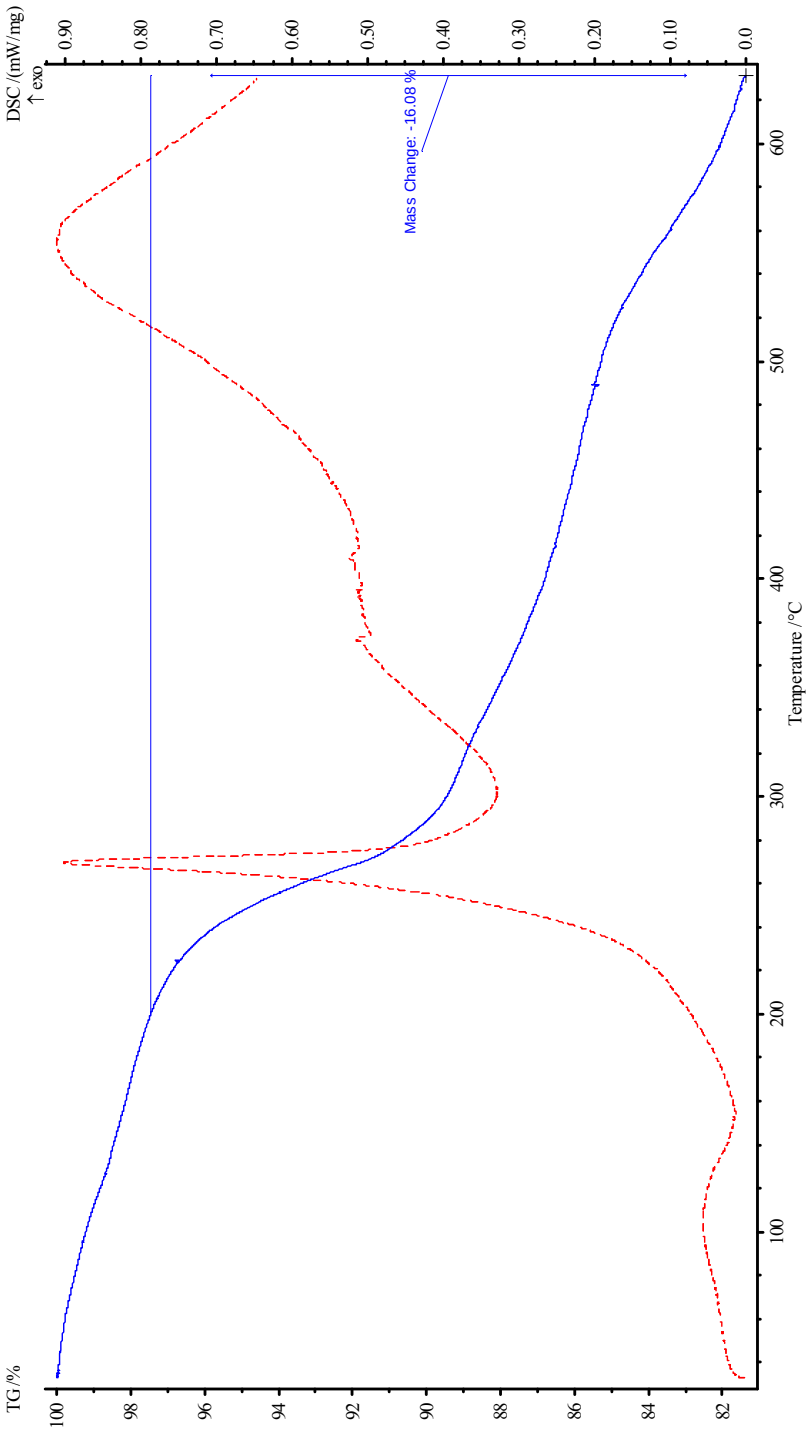

Figure 6.7 TGA data of P-SDA 1 intercalated in pure-silica zeolite FAU

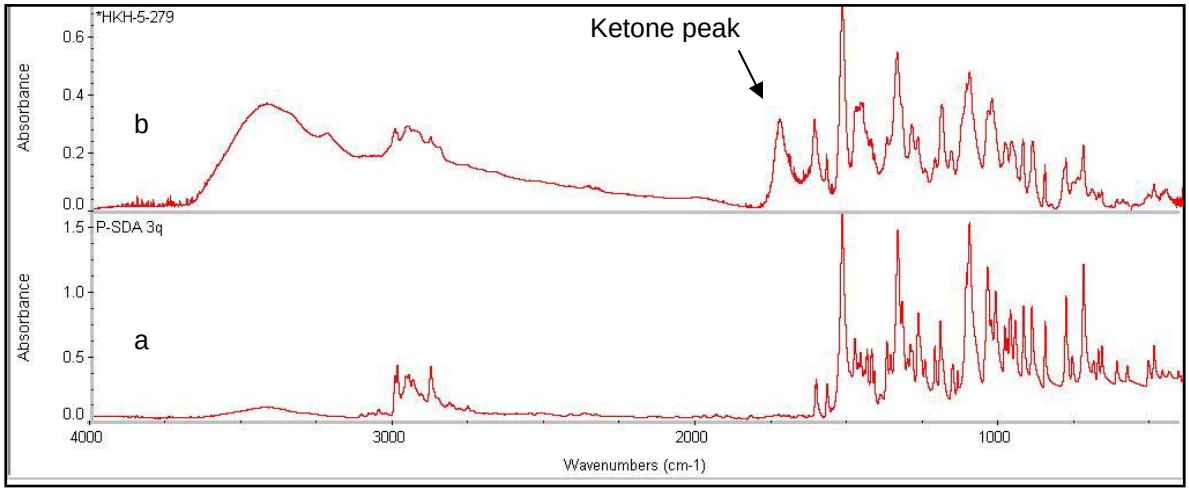

Figure 6.8 IR spectra of (a) P-SDA 1; (b) P-SDA 1 subjected to photolysis while intercalated in pure-silica zeolite FAU

2.3 Zeolite Synthesis Using P-SDA 1

Initial attempts to crystallize zeolite materials using P-SDA 1 were based on synthetic procedures that formed the zeolite MOR using the acid-cleavable equivalent molecule in Figure 6.1a. Unfortunately, these syntheses produced amorphous materials, even at extremely long crystallization times. It is likely that the addition of the nitro group to the molecule adversely affected zeolite nucleation, perhaps due to the slight change in electrostatic interactions caused by the electron-withdrawing nitro group on the aromatic portion of the molecule. Docking calculations that evaluate the stability of the ketal within a zeolite structure based on van der Waals interactions between the guest molecule and the zeolite host were performed by A. Burton at Chevron, to determine if another zeolite could be a more appropriate host. These simulations suggested that the zeolite beta (BEA*) would be an appropriate host for the photolabile molecule, given the

favorable stabilization energy of -12.0 kJ / mol of P-SDA 1, thus making it likely that the ketal could form BEA* given the correct synthesis conditions. The fit of the photolabile molecule inside the BEA* framework is shown in Figure 6.9.

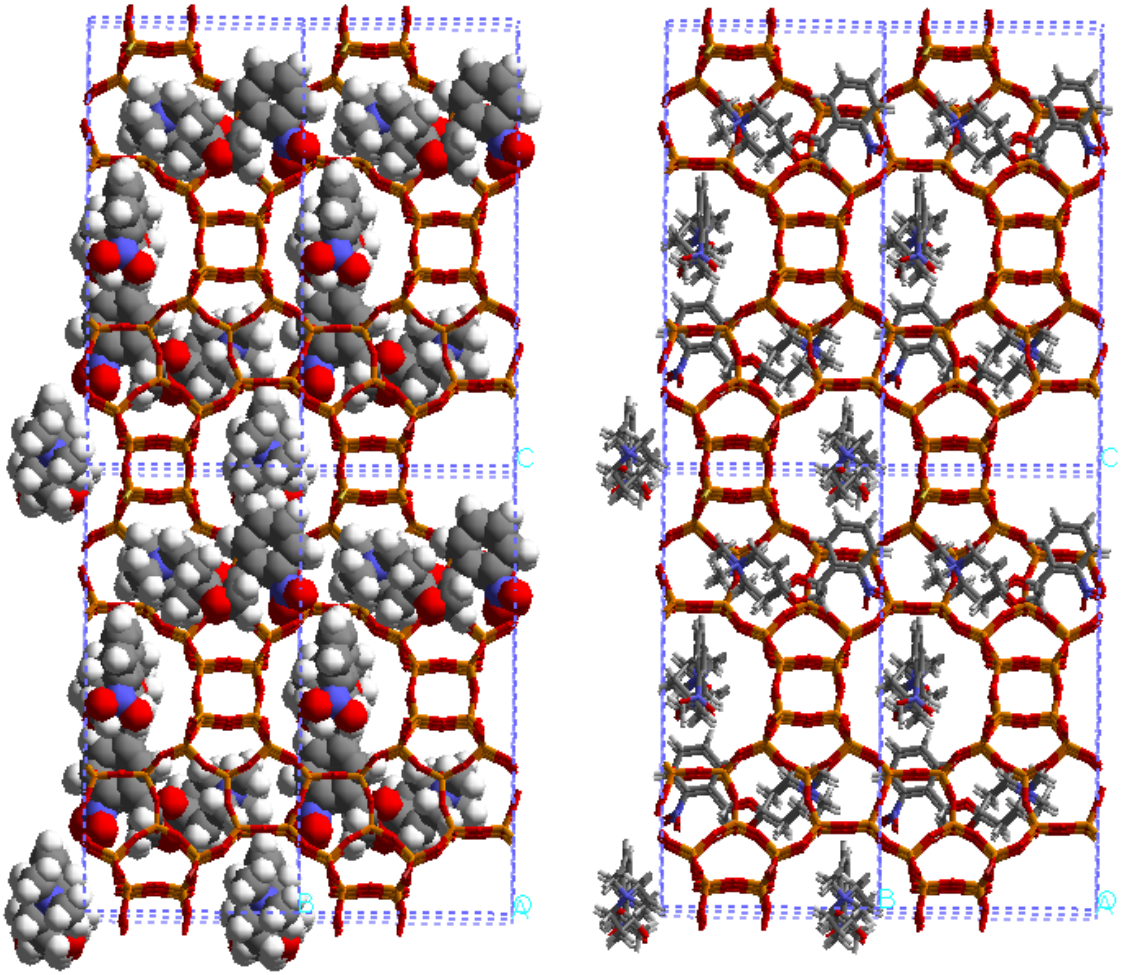

Figure 6.9 Schematic representation of P-SDA 1 in zeolite BEA* (docking calculations performed by A. Burton at Chevron)

Initial zeolite syntheses using P-SDA 1 as the structure-directing agent centered on standard aluminosilicate BEA*, and borosilicate BEA* (B-BEA*) syntheses. Table 6.1 shows the various reaction conditions attempted and their results. Interestingly, BEA* was never obtained, but a few of the BEA* recipes yielded small zeolite MFI crystals, as indicated by the low intensity of the diffraction patterns. This initiated a switch to the zeolite MFI family of recipes, to determine if this structure would more easily form using procedures specific to this material. The zeolite phase MFI is known to crystallize over a wide range of conditions with many different structure-directing agents; in some cases, it has been known to form without a structure-directing agent.[1,17,18,19,20,21] MFI-based syntheses, then, could be an excellent model system to demonstrate the structure-directing capabilities of P-SDA 1. Generally, the MFI recipes were based on silicalite (pure-silica zeolite with the MFI structure) recipes, and yielded the layered phase kanemite (due to high sodium content) as well as small MFI crystals. A seeded silicalite recipe using calcined silicalite seeds, however, resulted in a more crystalline sample with a larger crystal size, and a definite MFI structure. In these materials, ^{13}C CPMAS NMR spectra (Figure 6.10) showed that the occluded organics did not include a ketone-containing fragment of the P-SDA 1 molecule (represented by a peak at 200 ppm), showing that the organic was intact. The peaks in this data set were quite broad due to interactions with the inorganic species. Overall, however, this synthesis was found to be irreproducible after several attempts to repeat it.

Table 6.1 Synthesis conditions for zeolite synthesis using P-SDA 1 as the structure-directing agent

Recipe	Seed	Gel Composition	t, days	T, °C	Stir	Results
B-BEA	No	0.017 $Na_2B_4O_7$*10H_2O / 1 SiO_2 / 0.56 SDA / 23 H_2O	7	150	No	Amorphous
	No	0.034 $Na_2B_4O_7$*10H_2O / 1 SiO_2 / 0.56 SDA / 23 H_2O	7	150	No	Amorphous
	No	0.0039 $Na_2B_4O_7$*10H_2O / 1 SiO_2 / 0.074 SDA / 5.15 H_2O	15	150	No	MFI (low intensity)
BEA	No	60 SiO_2 / Al_2O_3 / 11 NaOH / 30 SDA / 1500 H_2O	4	165	No	Amorphous
	No	60 SiO_2 / Al_2O_3 / 11 NaOH / 30 SDA / 1500 H_2O	15	165	No	Amorphous
	No	60 SiO_2 / Al_2O_3 / 11 NaOH / 30 SDA / 1500 H_2O	12	165	Yes	MFI (low intensity)
	No	60 SiO_2 / Al_2O_3 / 11 NaOH / 30 SDA / 1500 H_2O	15	165	Yes	Amorphous
	No	60 SiO_2 / Al_2O_3 / 11 NaOH / 30 SDA / 1500 H_2O	15	165	Yes	Amorphous
	No	60 SiO_2 / Al_2O_3 / 11 NaOH / 30 SDA / 1500 H_2O	15	165	Yes	MFI
	No	60 SiO_2 / Al_2O_3 / 11 NaOH / 30 SDA / 1500 H_2O	15	165	Yes	Amorphous
	Yes	60 SiO_2 / Al_2O_3 / 11 NaOH / 30 SDA / 1500 H_2O	15	165	Yes	MFI (low intensity)
	Yes	60 SiO_2 / Al_2O_3 / 11 NaOH / 30 SDA / 1500 H_2O	15	165	Yes	Amorphous
	Yes	60 SiO_2 / Al_2O_3 / 11 NaOH / 30 SDA / 1500 H_2O	15	165	Yes	Amorphous
PSZ MFI	Yes	20 SiO_2 / 2 Na_2O / 2 SDA / 500 H_2O	20	150	No	Kanemite
	Yes	20 SiO_2 / 2 Na_2O / 2 SDA / 500 H_2O	20	150	No	MFI / Kanemite
	Yes	20 SiO_2 / 1 Na_2O / 2 SDA / 500 H_2O	15	150	No	MFI
	Yes	20 SiO_2 / 1.5 Na_2O / 2 SDA / 500 H_2O	15	150	No	MFI / Kanemite
	Yes	20 SiO_2 / 1 Na_2O / 2 SDA / 500 H_2O	15	150	No	Amorphous
	Yes	20 SiO_2 / 1 Na_2O / 2 SDA / 500 H_2O	15	150	No	Kanemite

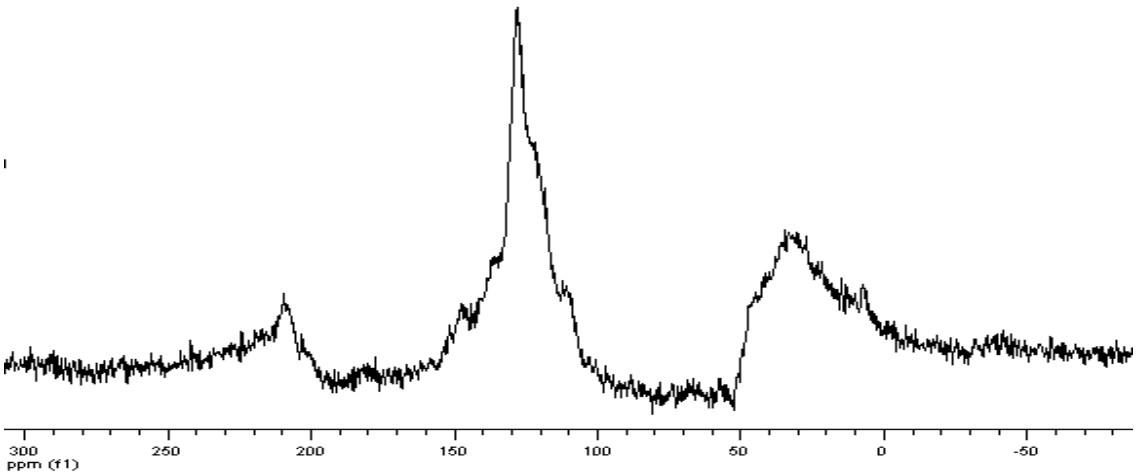

Figure 6.10 ^{13}C CPMAS NMR spectrum of P-SDA 1 in materials containing MFI crystals shows the molecule is still intact

After numerous attempts to reproducibly crystallize a zeolite material with a variety of synthetic conditions, it became apparent that the P-SDA 1 molecule, although capable of cleavage inside a large-cage zeolite, was inappropriate for use as a structure-directing agent under the conditions studied, despite the ability of its acid-cleavable counterpart to aid in the crystallization of MOR. This poor structure-directing ability could be due to many factors; among them could be, relative to its acid-cleavable counterpart, a change in the electrostatic interaction potential with the inorganic species due to the electron-withdrawing nature of the ring, a lower thermochemical stability in a zeolite gel at elevated temperatures compared, or the added bulk of the nitro group on the aromatic portion. Alternatively, the correct synthetic conditions for zeolite synthesis with this molecule may not have been evaluated. Although a combination of these is likely, it is

the last which may be the main culprit. The docking calculations of P-SDA 1 in zeolite BEA* indicate that the molecule has a rather tight fit in the pore structure, which may prevent formation of zeolites. Larger-pore zeolites could potentially be created via fluoride-mediated syntheses[22,23], but the presence of a strong acid like hydrofluoric acid would cause decomposition of the photolabile molecule, since it is also acid-cleavable. Lastly, the formation of the zeolite MFI in some of the syntheses could also be due to the presence of contaminants in the Teflon liners used for synthesis, or from some slight degradation of the P-SDA 1 molecules, undetected via NMR, to smaller molecules which could aid the formation of MFI crystals. This suggests that although low-intensity, very small crystals of MFI could be crystallized occasionally, P-SDA 1 does not have the structure-directing capabilities required to demonstrate the feasibility of the photolabile structure-directing agent route to zeolite synthesis.

3. Conclusions

Despite the ability of the photolabile molecule P-SDA 1 (8,8-dimethyl-2-(2-nitrophenyl)-1,4-dioxa-8-azoniaspiro[4.5]decane hydroxide) to undergo cleavage while occluded within the pore space of a large-cage zeolite, it has poor structure-directing ability over a range of synthetic conditions intended to produce such zeolite materials as BEA*, MFI, and MOR. Generally, these syntheses result in amorphous or layered materials after long crystallization times, but occasionally produce small amount of very small crystals of MFI material. These latter syntheses are unfortunately not reproducible. The inability of this molecule to produce a microporous, crystalline material is likely due to a combination of factors, including its large size, bulky aromatic group, and changed electrostatic interaction potential due to the nitro substituent's electron-withdrawing

nature when compared to the acid-cleavable equivalent of P-SDA 1. Although this particular molecule did not demonstrate the feasibility of the photolabile structure-directing agent route to zeolite syntheses, it did demonstrate the ability of the 2-nitrobenzyl class of molecules to cleave within a zeolite pore space when the material is in planar conformation. This suggests that this class of molecules could be useful for this route; future work should therefore focus on the development of smaller photolabile structure-directing agents, potentially with different synthetic conditions, such as the aluminophosphate zeolites, which could yield zeolitic material in shorter crystallization times to prevent degradation caused by exposure to elevated temperatures and caustic conditions over long periods of time.

4. Experimental

4.1 Synthesis of P-SDA 1

The synthesis of P-SDA 1 proceeds as shown in Figure 6.2, with a ketalization reaction followed by quaternization of the secondary amine.

4.1.1 Ketalization Reaction

4.00 g of 1-(2-nitrophenyl)ethane-1,2-diol (98%, Aldrich), 10.00 g of 4-piperidone monohydrate hydrochloride (98%, Aldrich), and 0.05 g p-toluenesulfonic acid monohydrate (99%, Aldrich) were suspended in 50 mL cyclohexane (EMD) in a round-bottom flask covered with aluminum foil. The suspension was refluxed under an N_2 atmosphere, while any water generated from the reaction was removed using a Dean-Stark apparatus. Yellow solids were produced. The solvent was evaporated using a

rotary evaporator. The solids were then re-suspended in 20 mL chloroform (EMD), and 1 mL of a saturated solution of potassium carbonate (Aldrich) in water was added to the solution to neutralize the p-toluenesulfonic acid. 5 mL water was then added to dissolve the excess 4-piperidone monohydrate hydrochloride. The product, 2-(2-nitrophenyl)-1,4-dioxa-8-azaspiro[4.5]decane, was recovered by extracting the aqueous phase several times with chloroform. The chloroform cuts were combined and evaporated to obtain the pure product in approximately 95% yield. ^{1}H NMR (dimethyl sulfoxide-d_6) data for this molecule before amine quaternization indicate peaks at 2.1, 3.1, 3.8, 4.6, 5.6, 7.6, 7.8, 8.1, and 8.3.

4.1.2 Amine Quaternization Reaction

4.15 g of 2-(2-nitrophenyl)-1,4-dioxa-8-azaspiro[4.5]decane (synthesis) and 2.89 g of triethylamine (Aldrich) were added to 30 mL methanol (EMD) in a round-bottom flask covered in aluminum foil while stirring. The round-bottom flask was capped with a rubber septum and placed in an ice bath. The solution was then placed under an Ar atmosphere. 10.15 g of methyl iodide (99.5%, Aldrich) was added drop-wise by injection over a period of 3 minutes. The mixture was stirred for 1 day at room temperature, producing yellow solids after a period of an hour. The solids were separated from the organic solution by centrifugation, and washed several times with diethyl ether (J.T. Baker). The solids were then recrystallized from chloroform (EMD) and diethyl ether to completely remove the triethylamine proton acceptor and to give the product, 8,8-dimethyl-2-(2-nitrophenyl)-1,4-dioxa-8-azoniaspiro[4.5]decane iodide in 50 – 70 % yield. ^{13}C CPMAS NMR indicated peaks for the pure iodide salt ketal at 148.0, 140.5,

134.7, 130.1, 124.4, 123.3, 104.1, 74.3, 69.5, 60.2, 52.3, 42.9, 30.5, and 25.2. The quaternary ammonium iodide salts, 8,8-dimethyl-2-(2-nitrophenyl)-1,4-dioxa-8-azoniaspiro[4.5]decane iodide, were converted to the corresponding hydroxide form in 97.9% yield using Bio-Rad AG1-X8 anion exchange resin.

4.2 Photocleavage of P-SDA 1

4.2.1 Homogeneous Cleavage of P-SDA 1

0.050 g of P-SDA 1 in its iodide salt form was dissolved in 2.5 mL of solvent (water, acetonitrile (EMD), N,N-dimethylformamide (EMD), dimethylsulfoxide (EMD), and benzene (EMD)), and placed in a quartz tube under stirring and Ar. A long-wave UV lamp (UVP Model B 100 AP) was positioned such that the lamp head was directed towards the side of the tube, and the head and the area surrounding the sample were enclosed with aluminum foil for safety reasons. The sample was irradiated for up to 24 h with UV radiation of wavelength 320 nm or greater UV lamp (UVP Model B 100 AP). After irradiation, the sample was investigated with either 1H NMR, Electrospray Ionization Mass Spectrometry (MassSpec), or Infrared Radiation Spectrometry (IR).

4.2.2 Photocleavage of P-SDA 1 Intercalated within Tosoh 390-HUA, a Dealuminated Zeolite X (Structure Code FAU)

0.300 g of Tosoh 390-HUA dealuminated zeolite X (structure code FAU) were activated to remove any water or organic materials accumulated within the pore space by heating, while under vacuum, the sample in a sealed quartz tube equipped with a stirbar at 140 °C for 12 h. The sample was then allowed to cool under vacuum, and then removed from

vacuum, maintaining a small (2 x 10^{-5} Torr) vacuum in the quartz tube. A solution of 0.020 g of P-SDA 1 in its iodide salt form in 0.8 mL acetonitrile was then slowly injected into the quartz tube, while stirring, and stirring the resulting mixture for 24 h. The solvent was then evaporated under argon flow, and the sample was dried to 2 x 10^{-5} Torr.[24] Solid-state ^{13}C cross-polarization magic-angle spinning nuclear magnetic resonance (CPMAS NMR) and TGA were carried out on both the solid P-SDA 1 iodide salt (prior to intercalation) and the FAU sample (post-intercalation) to determine the success of the procedure. The mixture was then slurried into 3 mL of water, sonicated to disperse the suspended particles, and drop-coated onto glass slides bounded with clear sticky tape to constrain the sample to a 2 x 2 cm^2 area on the slides. The slides were then dried at room temperature for 12 h to form a thin layer of zeolite and P-SDA 1 (iodide form) on the surface of the slides, and then placed in a glass petri dish for photolysis experiments. A long-wave UV lamp (UVP Model B 100 AP) was positioned such that the lamp head was directed above the layer, and the head and the area surrounding the sample were enclosed with aluminum foil for safety reasons. The sample was irradiated for up to 24 h with UV radiation of wavelength 320 nm or greater UV lamp (UVP Model B 100 AP). After irradiation, the P-SDA 1 fragments were extracted from the layer by scraping the layer off the slide, then washing with acetonitrile to separate the P-SDA 1 fragments from the zeolite. The organic solvent was removed, and the remaining fragments of P-SDA 1 were identified with either 1H NMR, MassSpec, or IR techniques.

4.3 Zeolite Synthesis with P-SDA 1

Silicate and aluminosilicate zeolite syntheses were attempted using P-SDA 1 as the structure-directing agent. The syntheses attempted (Table 6.1) were based on standard syntheses to produce silicate or aluminosilicate zeolites BEA* and MFI, and used the following general procedures. First, the sources of the charge-balancing cations and mineralizing agent were completely dissolved in distilled, de-ionized water in a small Teflon jar equipped with a screw-on lid and a stirbar. The alumina source (if required) was then dissolved in the solution while stirring for 30 – 75 min. An aqueous solution of P-SDA 1 was then added according to the required gel composition, and stirred for 10 – 30 min. The silica source (usually Cab-O-Sil fumed silica, Ludox colloidal silica, or tetraethylorthosilicate (Aldrich)) was then slowly added, and the solution was stirred for up to 16 h to ensure homogeneity. In some cases, calcined, previously prepared zeolite seeds were added (up to 5 wt % of the silica source) to the gel to encourage crystallization. The zeolite gel was then transferred into a Teflon-lined Parr Autoclave, which was placed in an oven and crystallized at 150 °C or 165 °C until phase separation occurred. In some cases, the autoclave was placed on a rotating spit inside the oven to decrease the crystallization time required. If, after 60 days, phase separation did not occur, the reaction was stopped. After removal from the oven, the solid material was collected from the autoclave by filtration and centrifugation, and washed exhaustively with water and acetone. The sample was then dried overnight in a 100 °C oven.

All of the attempted zeolite syntheses shown in Table 6.1 were not only run in duplicate, but also run without the SDA, and with 1,1-dimethyl-4-oxopiperidinium hydroxide (the

fragment resulting from photolytic cleavage of P-SDA 1) as controls to verify that a zeolite material could not crystallize unless the P-SDA 1 was intact. All the samples were characterized using X-ray diffraction (XRD), Thermogravimetric Analysis (TGA), and ^{13}C CPMAS NMR to verify crystallization and that the P-SDA 1 molecule was intact. If the molecule was intact, it was then cleaved using the procedures outlined above for the P-SDA 1 intercalated into Tosoh 390-HUA.

4.4 Characterization

The materials were characterized using a combination of liquid-state ^{1}H and solid-state ^{13}C nuclear magnetic resonance (NMR), infrared spectroscopy (IR), thermogravimetric analysis (TGA), and powder X-ray diffraction (XRD). NMR analysis was carried out with a Varian Mercury 300 MHz spectrometer (liquid state) and a Bruker AM 300 MHz spectrometer (solid-state). IR analysis was carried out on a Nicolet Nexus 470 FTIR spectrometer. TGA was performed on a NETZSH STA 449C analyzer in air using an aluminum sample pan. XRD was carried out on a Scintag XDS 2000 diffractometer operated at -45 kV and 40 mA using Cu K_α radiation (λ = 1.54056 Å) in the 2θ range of 2-40 at a step size of 0.5 ° / min.

5. References

[1] Lee, H., Zones, S. I. & Davis, M. E. A combustion-free methodology for synthesizing zeolites and zeolite-like materials. *Nature* **425**, 385-388 (2003).

[2] Lee, H., Zones, S. I. & Davis, M. E. Synthesis of molecular sieves using ketal structure-directing agents and their degradation inside the pore space. *Microporous Mesoporous Mat.* **88**, 266-274 (2006).

[3] Dong, J. H., Lin, Y. S., Hu, M. Z. C., Peascoe, R. A. & Payzant, E. A. Template-removal-associated microstructural development of porous-ceramic-supported MFI zeolite membranes. *Microporous Mesoporous Mat.* **34**, 241-253 (2000).

[4] Tosheva, L. & Valtchev, V. P. Nanozeolites: Synthesis, crystallization mechanism, and applications. *Chem. Mater.* **17**, 2494-2513 (2005).

[5] Wang, H. T., Wang, Z. B. & Yan, Y. S. Colloidal suspensions of template-removed zeolite nanocrystals. *Phys. Chem. Chem. Phys.* **2**, 2333-2334 (2000).

[6] Smaihi, M., Gavilan, E., Durand, J. O. & Valtchev, V. P. Colloidal functionalized calcined zeolite nanocrystals. *J. Mater. Chem.* **14**, 1347-1351 (2004).

[7] Gautier, B. & Smaihi, M. Template extraction from surface-functionalised zeolite beta nanoparticles. *New J. Chem.* **28**, 457-461 (2004).

[8] Boudreau, L. C. & Tsapatsis, M. A highly oriented thin film of zeolite A. *Chem. Mater.* **9**, 1705 (1997).

[9] Valtchev, V. & Mintova, S. Layer-by-layer preparation of zeolite coatings of nanosized crystals. *Microporous Mesoporous Mat.* **43**, 41-49 (2001).

[10] Liu, Y., Zhang, W. Z. & Pinnavaia, T. J. Steam-stable aluminosilicate mesostructures assembled from zeolite type Y seeds. *J. Am. Chem. Soc.* **122**, 8791-8792, doi:10.1021/ja001615z (2000).

[11] Platas-Iglesias, C. *et al.* Zeolite GdNaY nanoparticles with very high relaxivity for application as contrast agents in magnetic resonance imaging. *Chem.-Eur. J.* **8**, 5121-5131 (2002).

[12] Mintova, S. & Bein, T. Nanosized zeolite films for vapor-sensing applications. *Microporous Mesoporous Mat.* **50**, 159-166 (2001).

[13] Pillai, V. N. R. Photoremovable Protecting Groups in Organic Synthesis. *Synthesis* **1980**, 1-27 (1980).

[14] Guss, C. O. The Reactions Of Meta-Nitrostyrene And Ortho-Nitrostyrene Oxide With Phenol. *J. Org. Chem.* **17**, 678-684 (1952).

[15] Gravel, D., Hebert, J. & Thoraval, D. Ortho-Nitrophenylethylene Glycol As Photoremovable Protective Group For Aldehydes And Ketones - Syntheses, Scope, And Limitations. *Can. J. Chem.-Rev. Can. Chim.* **61**, 400-410 (1983).

[16] Gravel, D., Giasson, R., Blanchet, D., Yip, R. W. & Sharma, D. K. Photochemistry Of The Ortho-Nitrobenzyl System In Solution - Effects Of O-H Distance And Geometrical Constraint On The Hydrogen Transfer Mechanism In The Excited-State. *Can. J. Chem.-Rev. Can. Chim.* **69**, 1193-1200 (1991).

[17] Bein, T. Synthesis and applications of molecular sieve layers and membranes. *Chem. Mater.* **8**, 1636-1653 (1996).

[18] Lew, C. M., Li, Z. J., Zones, S. I., Sun, M. W. & Yan, Y. S. Control of size and yield of pure-silica-zeolite MFI nanocrystals by addition of methylene blue to the synthesis solution. *Microporous Mesoporous Mat.* **105**, 10-14 (2007).

[19] Li, S. A., Li, Z. J. & Yan, Y. S. Ultra-low-k pure-silica zeolite MFI films using cyclodextrin as porogen. *Adv. Mater.* **15**, 1528 (2003).

[20] Lee, H., Zones, S. I. & Davis, M. E. in *Recent Advances In The Science And Technology Of Zeolites And Related Materials, Pts A - C* Vol. 154 *Studies In Surface Science And Catalysis* 102-109 (2004).

[21] Flanigen, E. M. *et al.* Silicalite, A New Hydrophobic Crystalline Silica Molecular-Sieve. *Nature* **271**, 512-516 (1978).

[22] Corma, A., Rey, F., Rius, J., Sabater, M. J. & Valencia, S. Supramolecular self-assembled molecules as organic directing agent for synthesis of zeolites. *Nature* **431**, 287-290 (2004).

[23] Caullet, P., Paillaud, J. L., Simon-Masseron, A., Soulard, M. & Patarin, J. The fluoride route: a strategy to crystalline porous materials. *Comptes Rendus Chimie* **8**, 245-266 (2005).

[24] Turro, N. J., Lei, X. G., Li, W., Liu, Z. Q. & Ottaviani, M. F. Adsorption of cyclic ketones on the external and internal surfaces of a faujasite zeolite (CaX). A solid-state H-2 NMR, C-13 NMR, FT-IR, and EPR investigation. *J. Am. Chem. Soc.* **122**, 12571-12581 (2000).

Chapter 7: An Imidazole-Based, Photolabile Structure-Directing Agent for the Synthesis of Aluminophosphate Zeolites

Abstract

The synthesis, photocleavage, and structure-directing ability of the photolabile molecule 1-(2-nitrobenzyl)-1H-imidazole (P-SDA 2) is presented and discussed. The organic molecule is synthesized via photochemical protection of the imidazole functionality by the 2-nitrobenzyl photochemical protecting group, and results in P-SDA 2 in approximately 30% overall yield. Photolytic cleavage of the molecule proceeds via long-wave UV radiation with an Hg arc lamp to generate the unstable 2-nitrosobenzyl derivative of the 2-nitrobenzyl photochemical protecting group and imidazole. The structure-directing ability of P-SDA 2 was evaluated via synthetic attempts to produce aluminophosphate zeolites, using procedures based on the syntheses of $AlPO_4$-5 (structure code AFI), VPI-5 (structure code VFI), and MAPO-34 (structure code CHA). In this case, a control molecule, 1-benzyl-1H-imidazole, a non-photoactive molecule designated as SDA 2, was used to screen conditions for the synthesis of aluminophosphate zeolites, resulting in the production of $AlPO_4$-5 (structure code AFI) and $AlPO_4$-36 (structure code ATS). This control molecule was also used to demonstrate the synthesis of MAPO-36 (structure code ATS) under metal-substituted, aluminophosphate synthetic conditions. Attempts to synthesize aluminophosphate zeolites with P-SDA 2 using conditions that produced microporous crystalline material with SDA 2 yielded several unknown, and likely mixed, crystalline phases, although the primary results of these syntheses were dense phases and hydrated phases. The addition

of magnesium to the synthesis, using MAPO-34 procedures, also resulted in the synthesis of unidentified crystalline materials, with P-SDA 2 still intact inside the framework. Complete photocleavage of P-SDA 2 within the crystalline, aluminophosphate materials was also demonstrated.

1. Introduction

As the use of zeolite in non-traditional applications increases, the need for alternative methods to liberate the pore space of zeolites also increases.[1,2,3,4,5,6] Typically, thermal combustion processes are used to remove occluded organic molecules, but these processes destroy the often expensive structure-directing agent (SDA) within the zeolite pore space, and are frequently incompatible with either the end-use requirements or further fabrication steps of zeolites in nontraditional applications, like chemical sensors or electronic devices. Towards this end, the use of photolabile structure-directing agents for zeolite syntheses has been proposed, wherein the structure-directing agent can be removed post-synthesis via UV radiation and partially recycled.

To demonstrate the feasibility of the proposed route, a test molecule, 8,8-dimethyl-2-(2-nitrophenyl)-1,4-dioxa-8-azoniaspiro[4.5]decane hydroxide (P-SDA 1), a photo- and acid-cleavable organic molecule of the 2-nitrobenzyl family of photolabile molecules, was investigated in Chapter 6. This molecule was used to demonstrate that photocleavage of a molecule of the 2-nitrobenzyl family was possible in a large pore zeolite, such as a dealuminated zeolite with the FAU structure. Attempts to use this molecule to crystallize zeolites materials with the BEA* and MFI structures, using a wide

variety of synthesis conditions, however, resulted in only one of these syntheses producing a crystalline phase (MFI), which was not reproducible. The inability to reproducibly crystallize a zeolite might have been caused by the large structure of the P-SDA 1 molecule.

To address the problem of crystallization, a smaller member of the 2-nitrobenzyl family of photoactive compounds is proposed as a potential structure-directing agent: 1-(2-nitrobenzyl)-1H-imidazole (Figure 7.1a), known as P-SDA 2. Imidazole-based structure-directing agents have been used to synthesize a variety of zeolite phases, including zeolites with the ITW, MTT, TON, and MTW topologies, and other novel zeotype structures.[7,8,9] Like all members of the 2-nitrobenzyl family, P-SDA 2 undergoes photolytic cleavage via an intramolecular hydrogen abstraction mechanism (Figure 7.2) when irradiated with light of wavelength 320 nm or longer. Additionally, many variations of the synthesis of P-SDA 2 exist in the literature; generally, these syntheses are steps on the path to more complex, polyfunctional molecules.[10,11,12,13,14] Unlike P-SDA 1, P-SDA 2 is not acid-cleavable, making it suitable for acidic synthesis conditions, such as those used when crystallizing aluminophosphates zeolites, as well as basic synthesis conditions. Lastly, the non-photoactive equivalent of P-SDA 2, 1-benzyl-1H-imidazole (Aldrich, Figure 7.1b) is readily available and can be used to screen for the conditions that could potentially crystallize a zeolite material with P-SDA 2 (although previous work with P-SDA 1 has shown that the presence of a nitro substituent on the test molecule could affect its ability to act in a structure-directing role in comparison to the control molecule). For these reasons, the evaluation of the P-SDA 2 molecule in terms of

its structure-directing ability is of interest for the development of a photolabile route to zeolite synthesis.

a b

Figure 7.1 (a) 1-(2-nitrobenzyl)-1H-imidazole (P-SDA 2) ; (b) 1-benzyl-1H-imidazole (SDA 2)

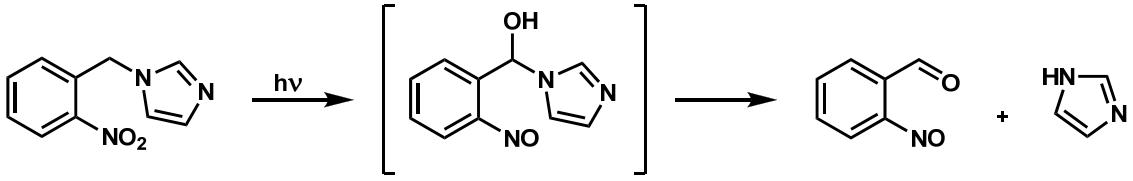

Figure 7.2 Photolysis of P-SDA 2 proceeds via an intramolecular hydrogen abstraction from the carbon-hydrogen bond ortho to the nitro group to yield carbonyl and nitroso groups in the ortho position

The stability of both P-SDA 2 and SDA 2 with respect to strong acids makes it possible to evaluate the molecules' potential structure-directing ability using the aluminophosphate class of zeolites, which crystallizes under acidic conditions. This family of crystalline, microporous materials is unusual in that crystallization of these

materials can occur in a matter of hours, rather than days, as with aluminosilicate zeolites.[15] Aluminophosphate molecular sieves ($AlPO_4$'s) are generally crystallized from reactive gels of composition 1.0 Al_2O_3 / 1.0 (± 0.2) P_2O_5 / x SDA / y H_2O, where x is generally 1.0 – 3.0, and y is 20 – 100. The primary alumina source for these gels is pseudo-boehmite, a reactive, dense-phase, hydrated alumina powder; while the phosphorous source is o-phosphoric acid. Framework substitution of phosphorous for silicon, or metals such as magnesium, manganese, and iron for aluminum can also occur if the correct precursor gel and reaction conditions are used. Like aluminosilicate zeolites, the $AlPO_4$ materials crystallize at temperatures between 125 °C and 200 °C, but there are also notable differences. First, $AlPO_4$ materials have a neutral framework, due to the Al^{3+} and P^{5+} ions, consisting of alternating aluminum and phosphorous oxides, and therefore do not require charge-balancing cations. Instead, only water or organic molecules are present within the pore space. Second, $AlPO_4$ materials require the presence of an organic additive in the precursor gel in order to promote crystallization of stable, microporous materials. Third, the organic additive is generally less specific in its structure-directing role than for aluminosilicate zeolites in that a single aluminophosphate structure can be crystallized using an assortment of different structure-directing agents of various sizes, shapes, and solubility, while a single structure-directing agent can promote crystallization of a variety of aluminophosphate zeolite phases. For example, the aluminophosphate zeolite with the $AlPO_4$-5 structure can be synthesized with over 20 different nitrogen-containing organic additives.[15] These additives can be primary, secondary, or tertiary amines, or the typical quaternary ammonium cations used for aluminosilicate zeolite synthesis. Fourth, dense aluminophosphate phases tend to form at

low crystallization temperatures in addition to high crystallization temperatures over long periods of time. These differences present three primary benefits for using the aluminophosphate zeolite system to evaluate the structure-directing ability of SDA 2 and P-SDA 2: (1) the fast crystallization time, (2) the ease of crystallization with a wide variety of structure-directing agents' sizes, shapes, etc., and (3) the standard precursor gel recipe, which reduces the variable space to be examined to variations of only two reagents (the structure-directing agent and water), in addition to crystallization time and temperature. In this chapter, the ability of SDA 2 and P-SDA 2 to synthesize aluminophosphate materials is examined and discussed. Additionally, a short study of the effects of gel composition and reaction temperature on the ability of SDA 2 to promote the crystallization of $AlPO_4$-36, the aluminophosphate zeolite with the ATS structure, is presented. Lastly, the ability of P-SDA 2 to undergo photolytic cleavage within crystalline aluminophosphate materials is demonstrated using procedures determined in Chapter 6.

2. Results and Discussion

2.1 P-SDA 2 Synthesis

The synthesis of P-SDA 2 was carried out according to literature procedures, generating the molecule in approximately 30% overall yield; general literature procedures reported yields of 17 – 30%.[16] P-SDA 2 has several characteristic features in its infrared (IR) spectrum (Figure 7.3) and its ^{13}C cross-polarization, magic angle spinning, nuclear magnetic resonance (CPMAS NMR) spectrum (Figure 7.4). For instance, in the IR spectrum, the absorbances at 1530 and 1375 cm^{-1} are characteristic of the nitro group, and

in the ^{13}C spectrum, the peaks at 50 ppm and 145 ppm represent, respectively, the carbon attached to both the phenyl ring and the imidazole, and the carbon with the nitro substituent. These characteristic peaks may be used to verify that the molecule is still intact after crystallization. The thermogravimetric analysis (TGA) data indicate that there are two decomposition events, one beginning at 200 °C and the other beginning at 550 °C (Figure 7.5).

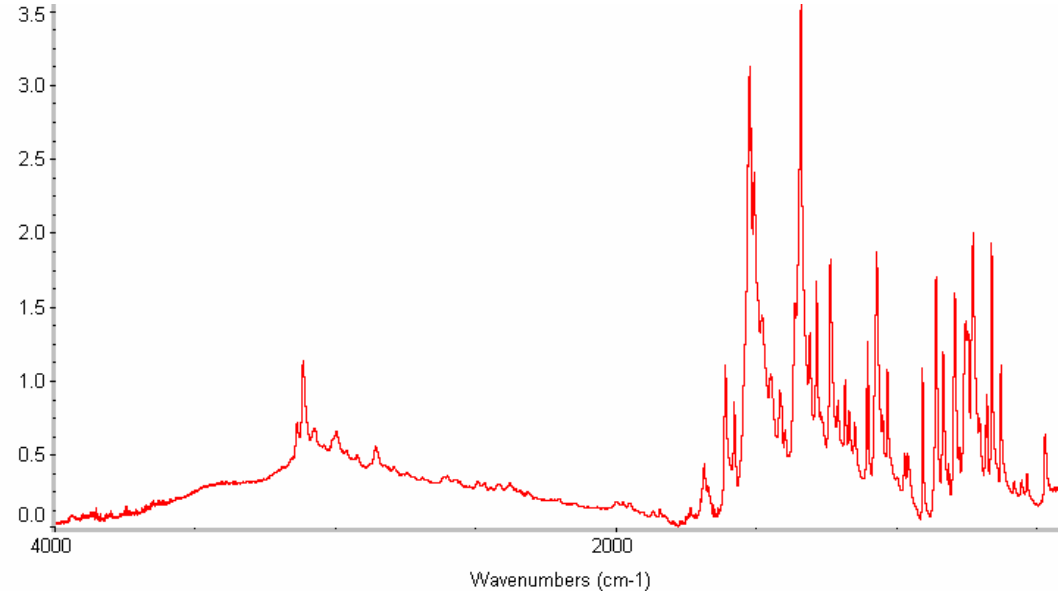

Figure 7.3 IR absorbance spectrum of P-SDA 2

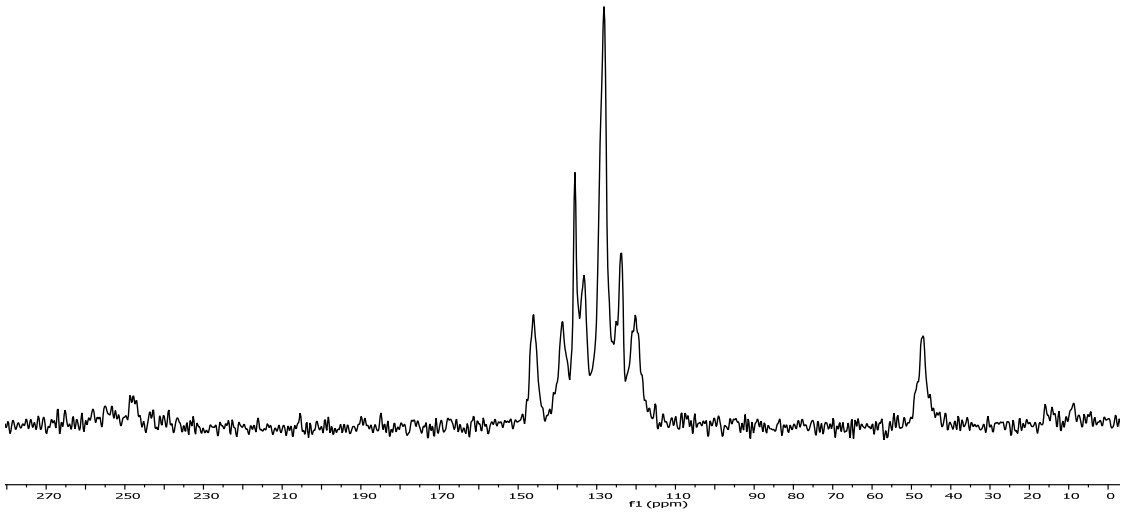

Figure 7.4 ^{13}C CP MAS NMR spectrum of P-SDA 2 at a spin rate of 6,000

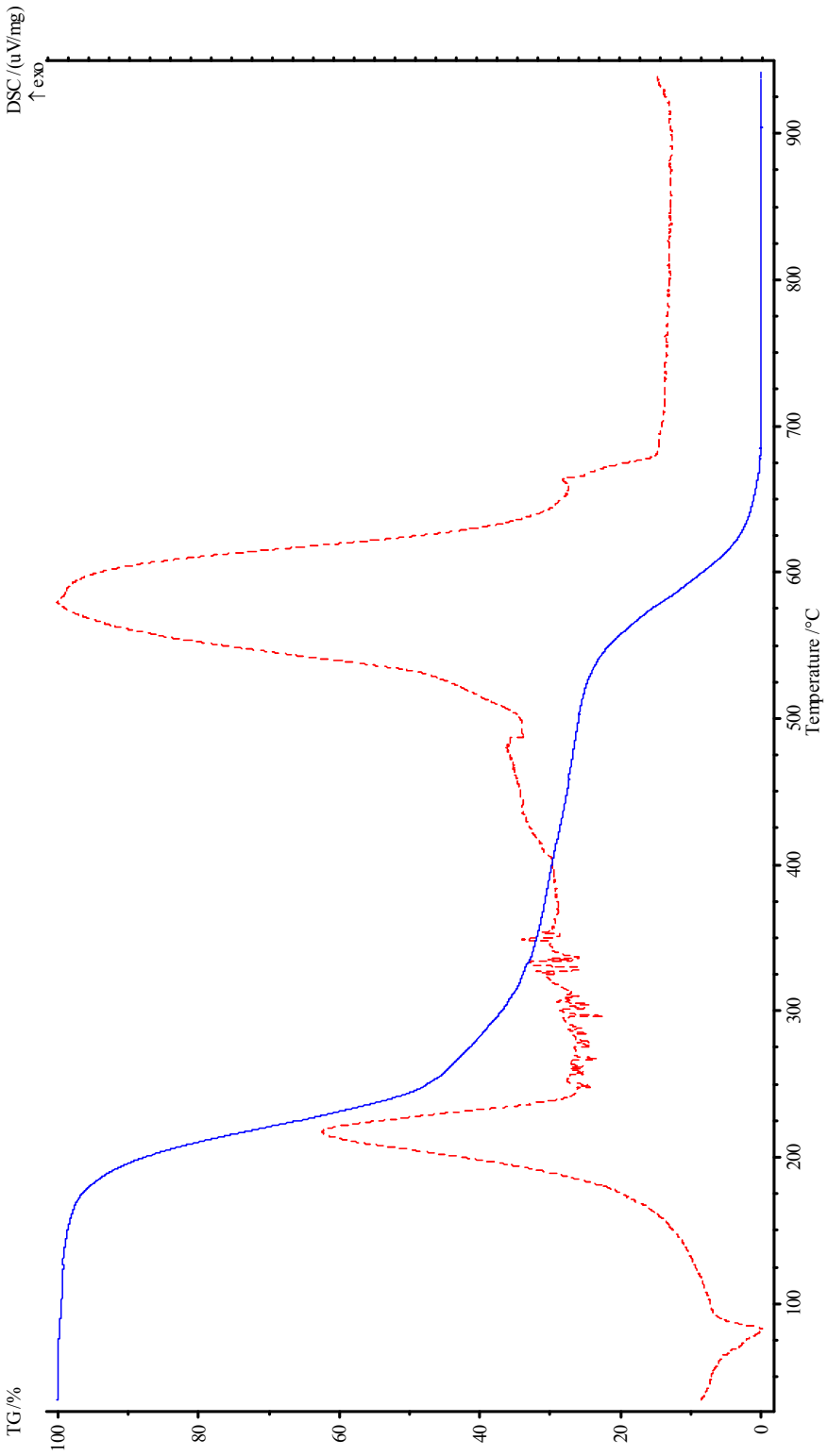

Figure 7.5 TGA data for P-SDA 2

2.2 Aluminophosphate Zeolite Synthesis Using SDA 2

The $AlPO_4$ control syntheses were designed to evaluate temperature, amount of structure-directing agent, and gel dilution, using molar gel compositions of 1 Al_2O_3 / x SDA / 1 P_2O_5 / y H_2O (x = 1 – 3, y = 40, 60, 80) and temperatures of 140, 150, and 200 °C. These procedures were based on the syntheses of $AlPO_4$-5 (structure code AFI) and VPI-5 (structure code VFI). The results of the $AlPO_4$ syntheses attempted with SDA 2 are given in Table 7.1. The XRD patterns of the two phases obtained, AFI and ATS, are shown in Figure 7.6 (their corresponding structures are shown in Figure 7.7); in the XRD patterns both are mixed with other phases (a dense phase known as tridymite in the case of AFI, and an unknown phase for ATS). Interestingly, these phases formed only at 150 °C, and higher or lower temperatures yielded amorphous or dense phases.

To help guide the syntheses to a more conclusive crystalline phase, rather than a mixed phase, magnesium sulfate was introduced into the reactive aluminophosphate gel. The substitution of metals, such as magnesium, for the Al^{3+} atoms in the framework yields a more negatively charged framework, and can induce a "harder" positive charge on the amine functionality in the structure-directing agent.[17] Several syntheses were run with a final molar gel composition of 0.8 Al_2O_3 / 1 P_2O_5 / x SDA / y H_2O / z MgO where x = 1 – 2, y = 10 – 100, and z = 0.2 – 0.4, with the structure-directing agent being SDA 2. Table 7.2 shows the results of the various metal-substituted, aluminophosphate runs with SDA 2, and Figure 7.8 shows the XRD pattern that corresponds to the phases described in Table 7.2.

Table 7.1 Results of $AlPO_4$ syntheses attempted with SDA 2 (A = amorphous, DP = dense phase, #1 = ATS / unknown phase, #2 = AFI / tridymite)

Gel Composition	140 °C	150 °C	200 °C
1.0 Al_2O_3 / 1.0 P_2O_5 / 1.0 SDA / 40.0 H_2O	A	1	DP
1.0 Al_2O_3 / 1.0 P_2O_5 / 1.0 SDA / 60.0 H_2O	A	2	DP
1.0 Al_2O_3 / 1.0 P_2O_5 / 1.0 SDA / 80.0 H_2O	A	2	DP
1.0 Al_2O_3 / 1.0 P_2O_5 / 1.5 SDA / 40.0 H_2O	A	2	DP
1.0 Al_2O_3 / 1.0 P_2O_5 / 1.5 SDA / 60.0 H_2O	A	2	DP
1.0 Al_2O_3 / 1.0 P_2O_5 / 1.5 SDA / 80.0 H_2O	A	2	DP
1.0 Al_2O_3 / 1.0 P_2O_5 / 2.0 SDA / 40.0 H_2O	A	2	A
1.0 Al_2O_3 / 1.0 P_2O_5 / 2.0 SDA / 60.0 H_2O	A	2	A
1.0 Al_2O_3 / 1.0 P_2O_5 / 2.0 SDA / 80.0 H_2O	A	2	A
1.0 Al_2O_3 / 1.0 P_2O_5 / 2.5 SDA / 40.0 H_2O	A	A	A
1.0 Al_2O_3 / 1.0 P_2O_5 / 2.5 SDA / 60.0 H_2O	A	A	A
1.0 Al_2O_3 / 1.0 P_2O_5 / 2.5 SDA / 80.0 H_2O	A	2	A
1.0 Al_2O_3 / 1.0 P_2O_5 / 3.0 SDA / 40.0 H_2O	A	2	DP
1.0 Al_2O_3 / 1.0 P_2O_5 / 3.0 SDA / 60.0 H_2O	A	2	A
1.0 Al_2O_3 / 1.0 P_2O_5 / 3.0 SDA / 80.0 H_2O	A	2	A

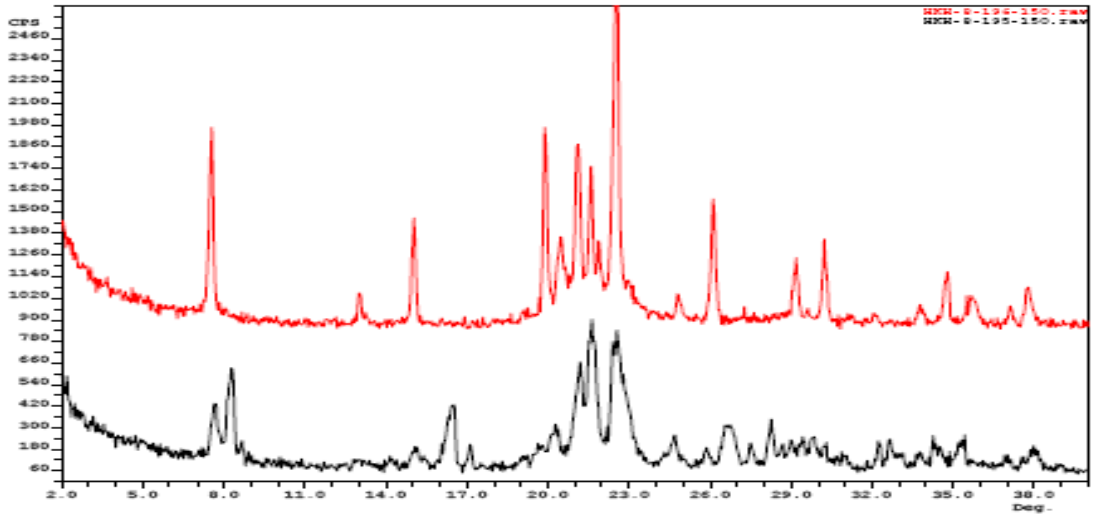

Figure 7.6 XRD patterns of aluminophosphate zeolites made with SDA 2: (bottom) ATS / unknown phase; (top) AFI / tridymite dense phase

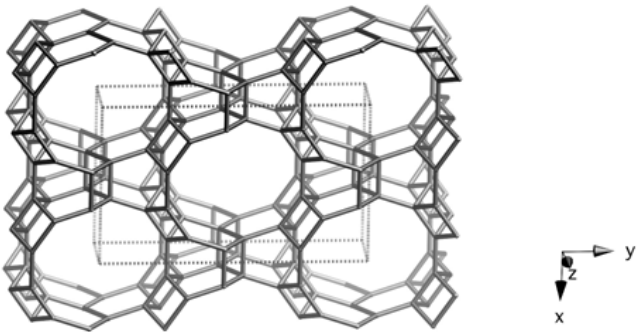

a

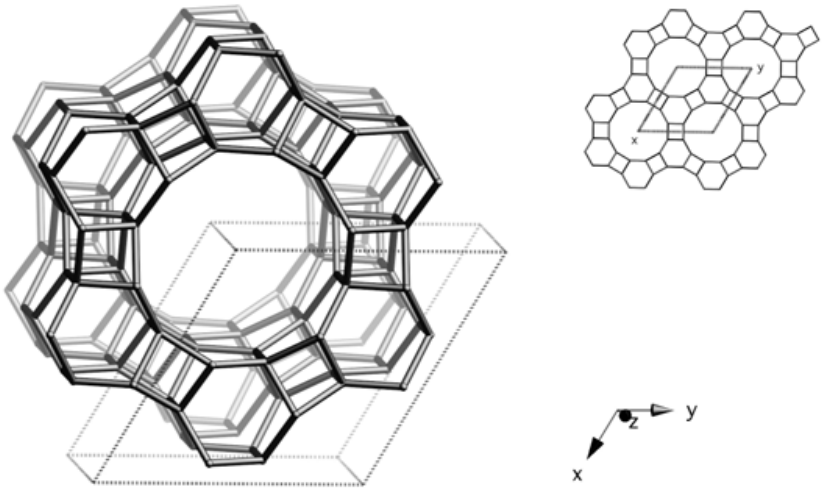

b

Figure 7.7 Framework schematic of the aluminophosphate zeolites phases: (a) ATS, viewed along the [001] axis; (b) AFI, viewed along the [001] axis with projection down the [001] axis on the upper right[18]

Table 7.2 Results of magnesium-substituted aluminophosphate runs using SDA 2 at 150, 175, and 200 °C (A = Amorphous)

Gel Composition	150 °C	175 °C	200 °C
0.8 Al_2O_3 / 1.0 P_2O_5 / 1.0 SDA / 10.0 H_2O / 0.2 MgO	ATS	ATS	A
0.8 Al_2O_3 / 1.0 P_2O_5 / 1.0 SDA / 10.0 H_2O / 0.4 MgO	ATS	ATS	ATS
0.8 Al_2O_3 / 1.0 P_2O_5 / 1.0 SDA / 47.0 H_2O / 0.2 MgO	ATS	ATS	ATS
0.8 Al_2O_3 / 1.0 P_2O_5 / 1.0 SDA / 47.0 H_2O / 0.4 MgO	ATS	ATS	A
0.8 Al_2O_3 / 1.0 P_2O_5 / 1.0 SDA / 100.0 H_2O / 0.2 MgO	ATS	ATS	ATS
0.8 Al_2O_3 / 1.0 P_2O_5 / 1.0 SDA / 100.0 H_2O / 0.4 MgO	ATS	ATS	ATS
0.8 Al_2O_3 / 1.0 P_2O_5 / 1.5 SDA / 10.0 H_2O / 0.2 MgO	ATS	ATS	ATS
0.8 Al_2O_3 / 1.0 P_2O_5 / 1.5 SDA / 10.0 H_2O / 0.4 MgO	ATS	ATS	ATS / AFI
0.8 Al_2O_3 / 1.0 P_2O_5 / 1.5 SDA / 47.0 H_2O / 0.2 MgO	ATS	ATS	ATS
0.8 Al_2O_3 / 1.0 P_2O_5 / 1.5 SDA / 47.0 H_2O / 0.4 MgO	ATS	ATS	A
0.8 Al_2O_3 / 1.0 P_2O_5 / 1.5 SDA / 100.0 H_2O / 0.2 MgO	ATS	ATS	A
0.8 Al_2O_3 / 1.0 P_2O_5 / 1.5 SDA / 100.0 H_2O / 0.4 MgO	ATS	ATS	ATS
0.8 Al_2O_3 / 1.0 P_2O_5 / 2.0 SDA / 10.0 H_2O / 0.2 MgO	ATS	A	A
0.8 Al_2O_3 / 1.0 P_2O_5 / 2.0 SDA / 10.0 H_2O / 0.4 MgO	ATS	ATS	AFI
0.8 Al_2O_3 / 1.0 P_2O_5 / 2.0 SDA / 47.0 H_2O / 0.2 MgO	A	ATS	ATS
0.8 Al_2O_3 / 1.0 P_2O_5 / 2.0 SDA / 47.0 H_2O / 0.4 MgO	ATS	ATS	ATS
0.8 Al_2O_3 / 1.0 P_2O_5 / 2.0 SDA / 100.0 H_2O / 0.2 MgO	ATS	ATS	A
0.8 Al_2O_3 / 1.0 P_2O_5 / 2.0 SDA / 100.0 H_2O / 0.4 MgO	ATS	ATS	ATS

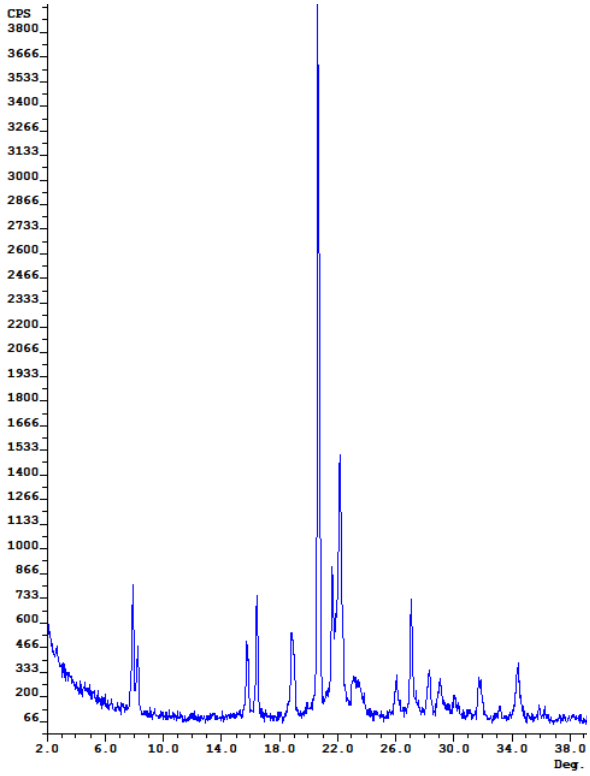

Figure 7.8 XRD pattern of the ATS phase from the compositions in Table 7.2

Some general trends can be seen in the results of the syntheses. (a) Aluminophosphate materials with the zeolite structure ATS are the preferred crystallization product of these syntheses with SDA 2. (b) Gels that were crystallized at 200 °C yielded approximately 1/3 of the crystalline material as the 175 °C runs, and were more frequently amorphous. (c) A shift between the production of aluminophosphate materials with the zeolite structures of ATS and AFI can be seen at 200 °C for higher amounts of magnesium in the synthesis. (d) At 150 °C, higher magnesium content in the zeolite gel leads higher crystallinity in the resulting materials, as the diffraction patterns of those materials are more intense with sharper peaks, but otherwise does not appear to change the structure that is crystallized. Given this data, it is apparent that attempts to synthesize aluminophosphate zeolites with P-SDA 1 could lead to the production of materials with

the ATS zeolite structure at 150 °C; additionally, using the lower temperature conditions would minimize the possibility of thermal decomposition of the P-SDA 2 molecule.

2.3 Aluminophosphate Zeolite Synthesis Using P-SDA 2

After identifying the synthesis conditions likely to produce aluminophosphate zeolite materials with SDA 2, the reactive precursor gels were modified to utilize P-SDA 2 as the structure-directing agent. Four different crystalline materials were produced from the syntheses (Table 7.3, Figure 7.9). These phases were designated as phases 3, 4, 5, 6, and 7. Phase 3 was a hydrated phase that collapses on dehydration to form a dense material. The other three phases were not readily identifiable as known crystalline materials, and were likely the result of mixed phases; phase 5, however, could potentially be a combination of ATS and another unknown phase. Interestingly, on calcination, phase 5 transformed into an aluminophosphate material with the zeolite structure ATV, in addition to some slight dense phase impurities. From these data, the following conclusions were reached regarding the production of the hydrate phase (phase 3): (a) gels containing higher P_2O_5 / Al_20_3 ratios were more likely to yield a hydrated phase or dense phases, (b) at low P_2O_5 / Al_2O_3 ratios in the gel, a lower P-SDA 2 content will more likely result in a hydrated phase than a non-hydrate, crystalline phase, and (c) generally, gels that are more dilute are more likely to produce hydrated phases, while more concentrated phases will produce a non-hydrate, crystalline phase.

Table 7.3 Results of attempted aluminophosphate zeolite syntheses with P-SDA 2 as the structure-directing agent (3 = unknown hydrated phase, 4 = unknown phase, 5 = unknown phase, 6 = ATS / unknown phase, 7 = ATV / dense phase, DP = dense phase)

Gel Composition	150 °C	Calcined
1.0 Al_2O_3 / 1.0 P_2O_5 / 1.0 SDA / 40.0 H_2O	3	DP
1.0 Al_2O_3 / 1.0 P_2O_5 / 1.0 SDA / 50.0 H_2O	DP	DP
1.0 Al_2O_3 / 1.0 P_2O_5 / 1.0 SDA / 60.0 H_2O	3	DP
1.0 Al_2O_3 / 1.0 P_2O_5 / 1.0 SDA / 80.0 H_2O	3	DP
1.0 Al_2O_3 / 1.0 P_2O_5 / 1.5 SDA / 40.0 H_2O	3	DP
1.0 Al_2O_3 / 1.0 P_2O_5 / 1.5 SDA / 60.0 H_2O	3	DP
1.0 Al_2O_3 / 1.0 P_2O_5 / 1.5 SDA / 80.0 H_2O	3	DP
1.0 Al_2O_3 / 1.0 P_2O_5 / 2.0 SDA / 40.0 H_2O	4	4
1.0 Al_2O_3 / 1.0 P_2O_5 / 2.0 SDA / 40.0 H_2O	5	7
1.0 Al_2O_3 / 1.0 P_2O_5 / 2.0 SDA / 60.0 H_2O	4	4
1.0 Al_2O_3 / 1.0 P_2O_5 / 2.0 SDA / 60.0 H_2O	5	7
1.0 Al_2O_3 / 1.0 P_2O_5 / 2.0 SDA / 80.0 H_2O	4	4
1.0 Al_2O_3 / 1.0 P_2O_5 / 2.0 SDA / 80.0 H_2O	5	7
1.0 Al_2O_3 / 1.0 P_2O_5 / 2.5 SDA / 40.0 H_2O	4	4
1.0 Al_2O_3 / 1.0 P_2O_5 / 2.5 SDA / 60.0 H_2O	4	4
1.0 Al_2O_3 / 1.0 P_2O_5 / 2.5 SDA / 80.0 H_2O	5	7
1.0 Al_2O_3 / 1.0 P_2O_5 / 3.0 SDA / 40.0 H_2O	4	4
1.0 Al_2O_3 / 1.0 P_2O_5 / 3.0 SDA / 60.0 H_2O	4	4
1.0 Al_2O_3 / 1.0 P_2O_5 / 3.0 SDA / 80.0 H_2O	4	4
1.0 Al_2O_3 / 1.5 P_2O_5 / 0.5 SDA / 40.0 H_2O	3	DP
1.0 Al_2O_3 / 1.5 P_2O_5 / 0.75 SDA / 10.0 H_2O	5	7
1.0 Al_2O_3 / 1.5 P_2O_5 / 0.75 SDA / 40.0 H_2O	6	-
1.0 Al_2O_3 / 1.5 P_2O_5 / 0.75 SDA / 50.0 H_2O	3	DP

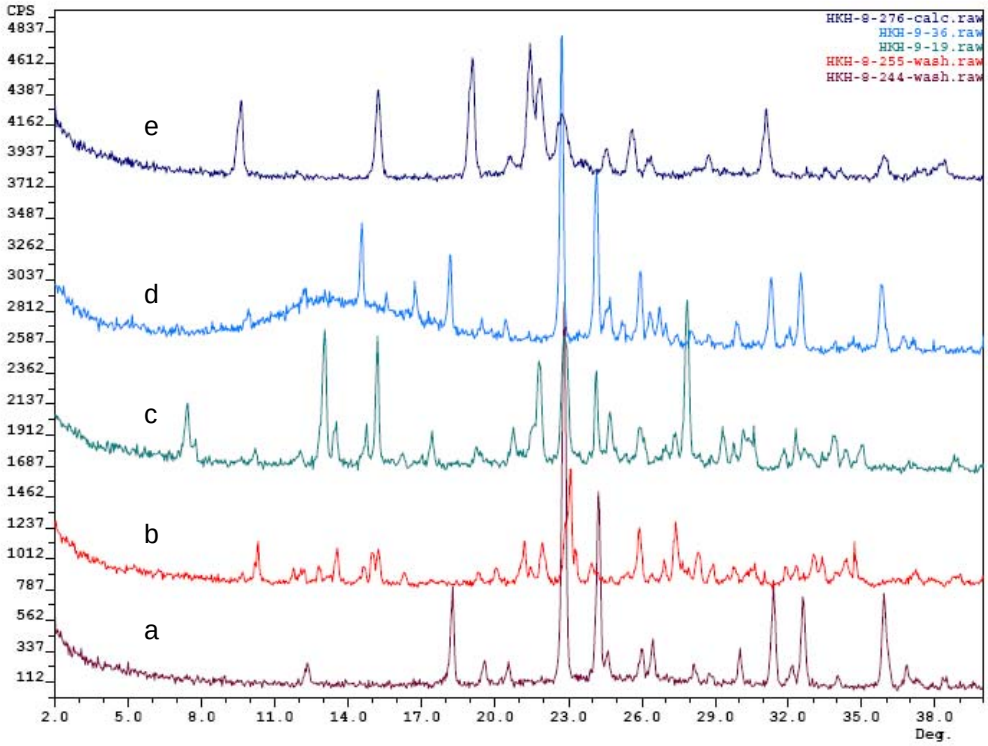

Figure 7.9 XRD patterns of as-made aluminophosphate materials produced using P-SDA 2 as the structure-directing agent: (a) phase 3; (b) phase 4; (c) phase 5; (d) phase 6; and calcined phase 5: (e) ATV / dense phase

Of the conditions in Table 7.3, those that produced phases 4 and 5 appeared most likely to promote the reproducible crystallization of known aluminophosphate zeolite phases rather than dense phases, so the resulting crystalline material was further investigated. According to the ^{13}C CP MAS NMR spectrum of the phase 5 material (Figure 7.10), P-SDA 2 is still intact. TGA data of the phase (Figure 7.11) show similar decomposition events as the P-SDA itself, with a reasonable organic content for an aluminophosphate material.

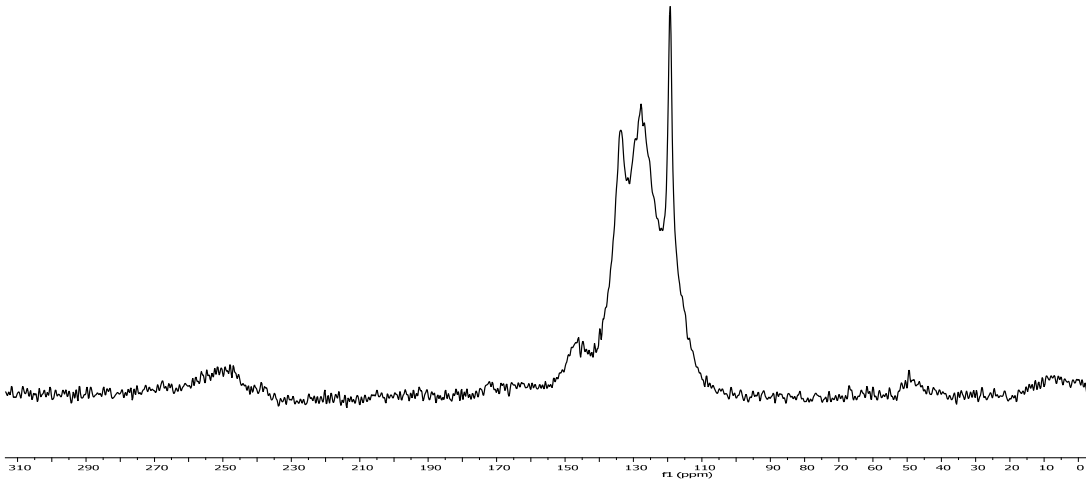

Figure 7.10 ^{13}C CPMAS NMR spectrum of the as-made, crystalline, aluminophosphate phase 5 produced using P-SDA 2 as the structure-directing agent

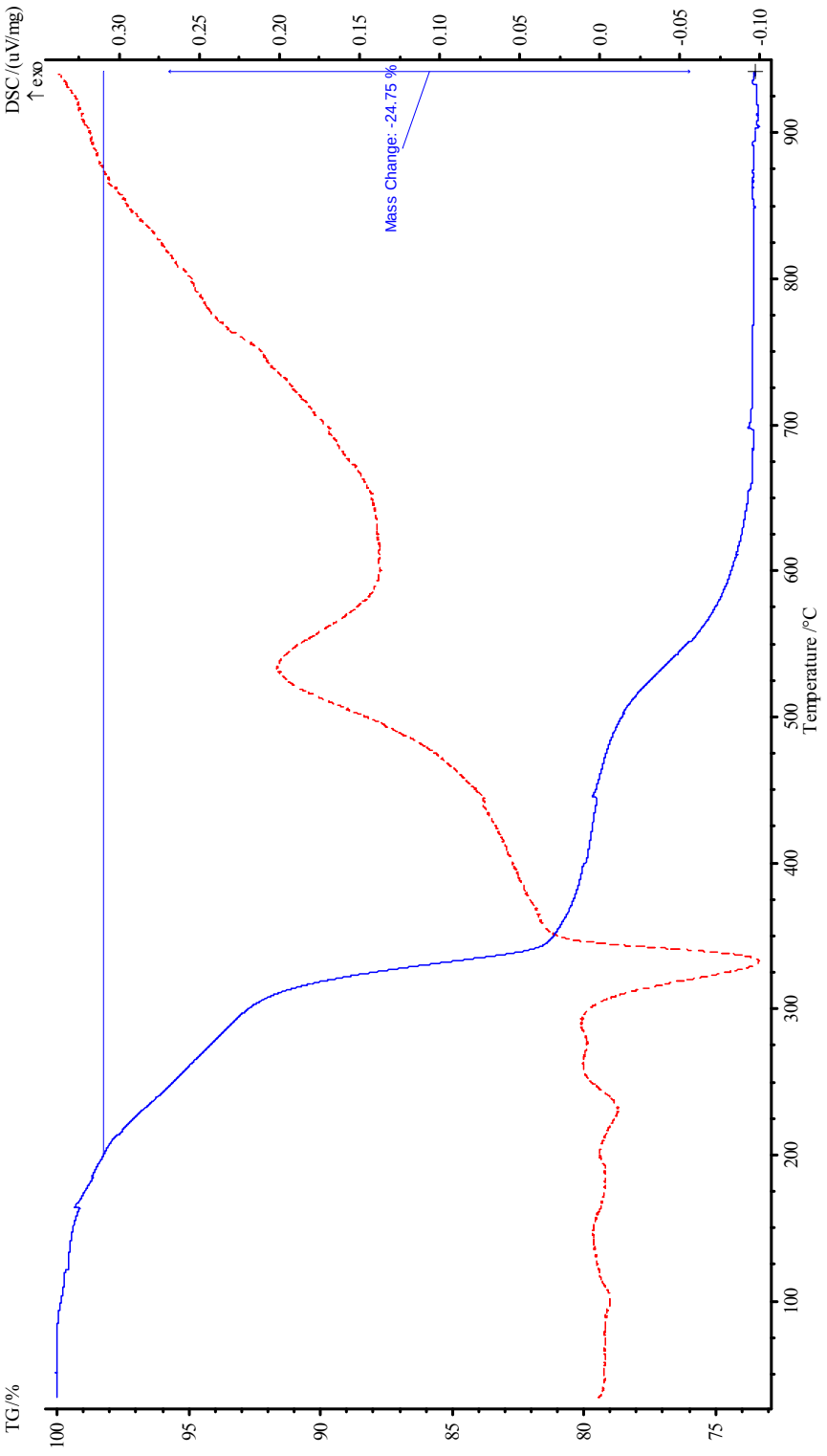

Figure 7.11 TGA data of the as-made, aluminophosphate phase 5, produced using P-SDA 2 as the structure-directing agent

The results shown above demonstrate that P-SDA 2 is indeed capable of acting in a structure-directing role for the synthesis of crystalline, aluminophosphate materials and withstanding the conditions of an aluminophosphate zeolite synthesis. However, the results also demonstrate its lack of specificity towards any one phase; interestingly, the same reaction conditions produced both phase 4 and phase 5. In order to guide the synthesis of aluminophosphate materials in such a way that a more definite crystalline material is formed using P-SDA 2 as the structure-directing agent, the synthetic conditions were modified to include metal substitution. As with SDA 2, metal-substituted aluminophosphates were synthesized with a final molar gel composition of 0.8 Al_2O_3 / x SDA / 1 P_2O_5 / y H_2O / z MgO where x = 1 – 2, y = 47 – 100, and z = 0.2 – 0.4 using P-SDA 2 as the structure-directing agent, at temperatures of 150 and 175 °C. The results of these synthetic attempts are shown in Table 7.4

These results demonstrate that a crystallization temperature of 150 °C results in the production of crystalline material using P-SDA 2 as the structure-directing agent, compared to higher temperatures. Additionally, the magnesium substitution does not appear to promote the crystallization of a specific phase or known material, and instead narrows the results to phases 4 and 5 (Figure 7.9). Lastly, the difference in water content greatly affects the results, as more dilute gels produced dense phases with greater regularity than concentrated gels. Therefore, aluminophosphate materials can be produced using relatively mild synthetic conditions and P-SDA 2 as the structure-directing agent; however, these aluminophosphates are not known zeolite phases.

Table 7.4 Results of attempted metal-substituted, aluminophosphate zeolite syntheses with P-SDA 2 as the structure-directing agent

Gel Composition	150 °C	175 °C
0.8 Al_2O_3 / 1.0 P_2O_5 / 1.0 SDA / 47.0 H_2O / 0.2 MgO	5	A
0.8 Al_2O_3 / 1.0 P_2O_5 / 1.0 SDA / 100.0 H_2O / 0.2 MgO	DP	DP
0.8 Al_2O_3 / 1.0 P_2O_5 / 1.5 SDA / 47.0 H_2O / 0.2 MgO	5	4
0.8 Al_2O_3 / 1.0 P_2O_5 / 1.5 SDA / 100.0 H_2O / 0.2 MgO	DP	5
0.8 Al_2O_3 / 1.0 P_2O_5 / 2.0 SDA / 47.0 H_2O / 0.2 MgO	5	A
0.8 Al_2O_3 / 1.0 P_2O_5 / 2.0 SDA / 100.0 H_2O / 0.2 MgO	DP	DP
0.8 Al_2O_3 / 1.0 P_2O_5 / 1.0 SDA / 47.0 H_2O / 0.4 MgO	DP	DP
0.8 Al_2O_3 / 1.0 P_2O_5 / 1.0 SDA / 100.0 H_2O / 0.4 MgO	DP	DP
0.8 Al_2O_3 / 1.0 P_2O_5 / 1.5 SDA / 47.0 H_2O / 0.4 MgO	A	DP
0.8 Al_2O_3 / 1.0 P_2O_5 / 1.5 SDA / 100.0 H_2O / 0.4 MgO	4 / 5	4 / 5
0.8 Al_2O_3 / 1.0 P_2O_5 / 2.0 SDA / 47.0 H_2O / 0.4 MgO	A	4
0.8 Al_2O_3 / 1.0 P_2O_5 / 2.0 SDA / 100.0 H_2O / 0.4 MgO	DP	DP

2.4 Photocleavage of P-SDA 2 within Aluminophosphate Material

Samples of the aluminophosphate materials generated using P-SDA 2 were subjected to UV radiation in an attempt to photolytically cleave P-SDA 2 in the pores, using thin layer procedures developed previously. The ^{13}C CP MAS NMR spectrum (Figure 7.12) showed that the P-SDA 2 material was completely cleaved, as evidenced by the disappearance of the peak at 50 ppm. Additionally, the spectrum contained only those peaks that would correspond to the imidazole fragment.

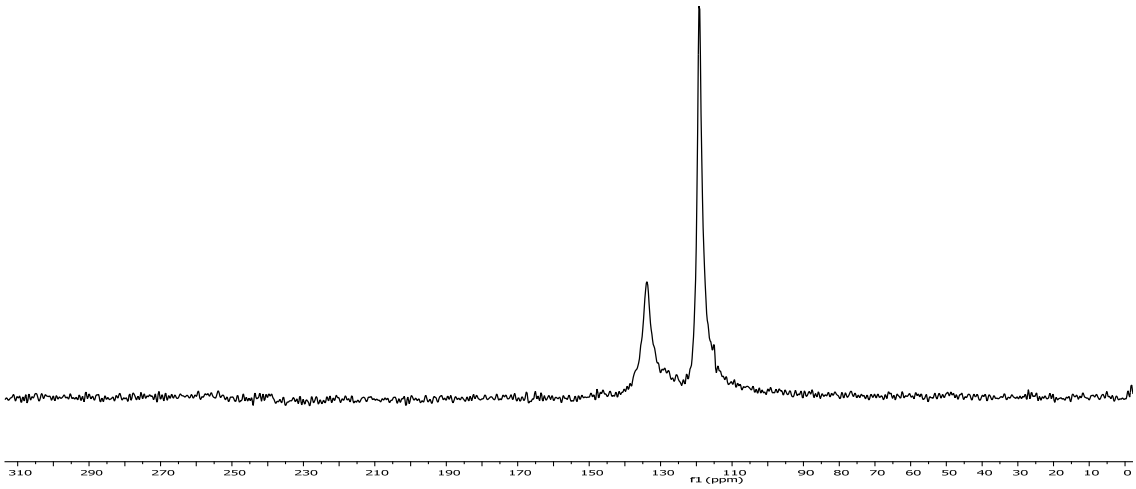

Figure 7.12 ^{13}C CPMAS NMR spectrum of as-made, aluminophosphate material produced using P-SDA 2 as the structure-directing agent, after UV irradiation

Initial attempts to extract the cleaved fragment were partially successful, as the color of the sample lightened from a deep red / brown to a light tan, however, further testing via NMR revealed that organic was still present in the irradiated sample. Further extraction processes, such as soxhlet extraction with polar solvents such as acetone, ethylacetate, and water, completely removed approximately 35% of the remaining imidazole fragment according to TGA data (Figure 7.13). XRD analysis of the cleaved and extracted material showed that the phase remained intact after these processing steps (Figure 7.14). The inability to completely remove the imidazole fragment suggests that, if the material is porous, the pore apertures of the structure may be too small to allow access to the imidazole fragment. Alternatively, the imidazole fragment could be protonated and bound to the framework via electrostatic interactions to charge-balance defects in the structure. Protonated imidazoles generally show broad features in the 3000-3500 cm^{-1} region of their IR spectra; these can be seen in the remaining imidazole fragments in the

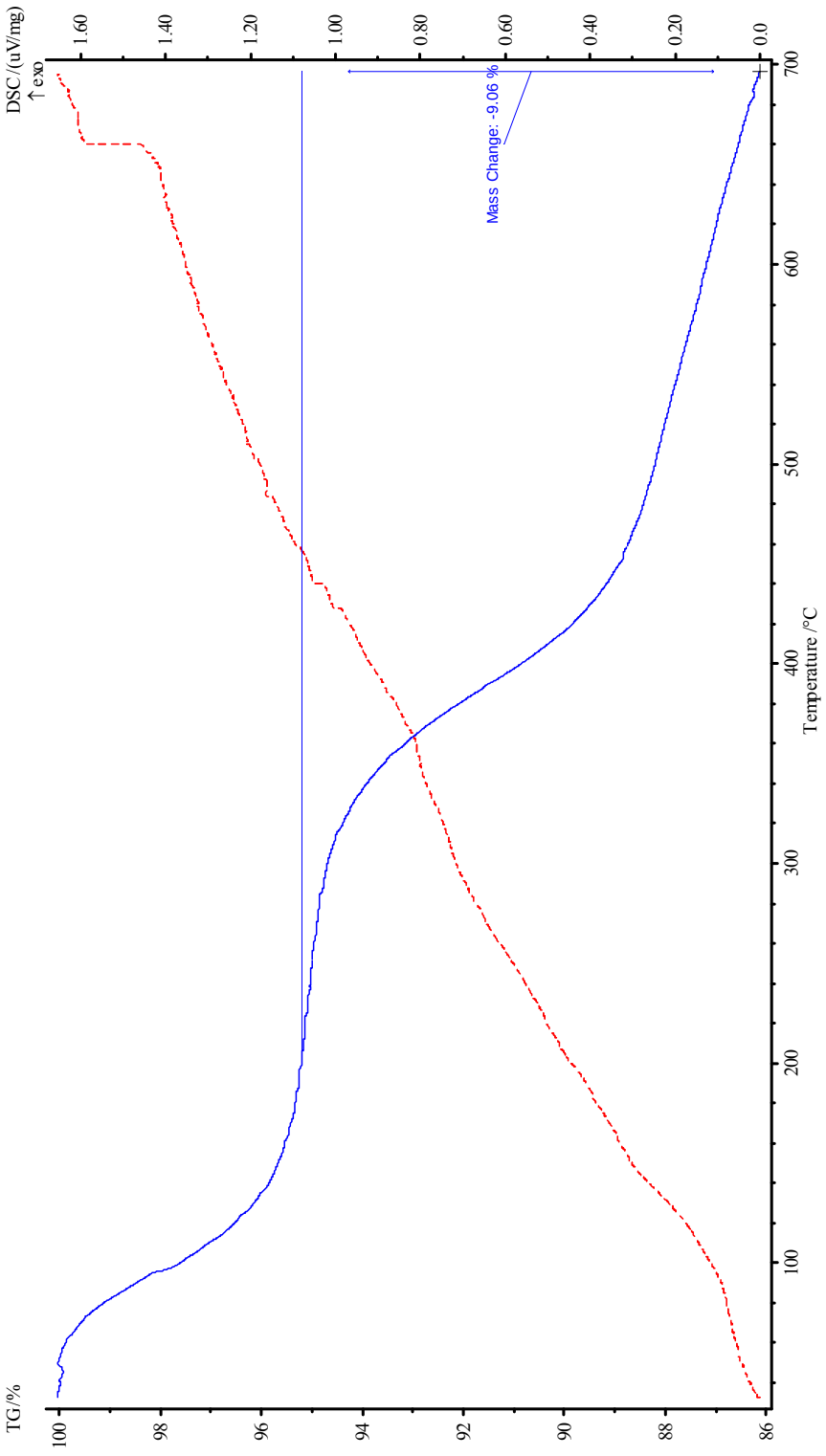

Figure 7.13 TGA data of the cleaved and extracted aluminophosphate material

extracted phase 5 material (Figure 7.15), suggesting that this is the case.

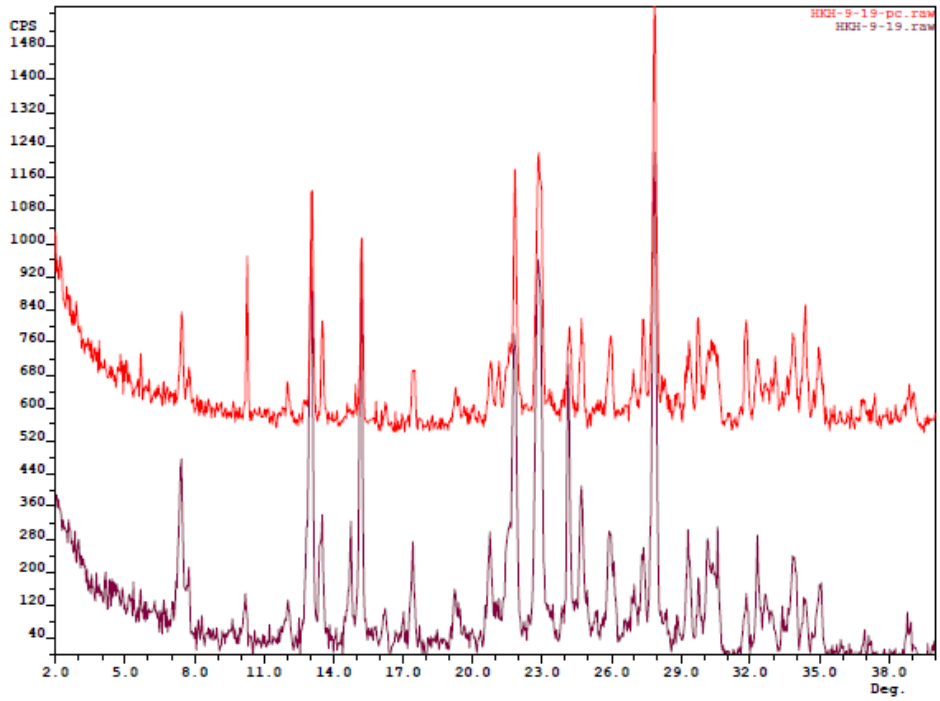

Figure 7.14 XRD patterns of: (bottom) the as-made phase 5 sample; (top) the photocleaved phase 5 sample

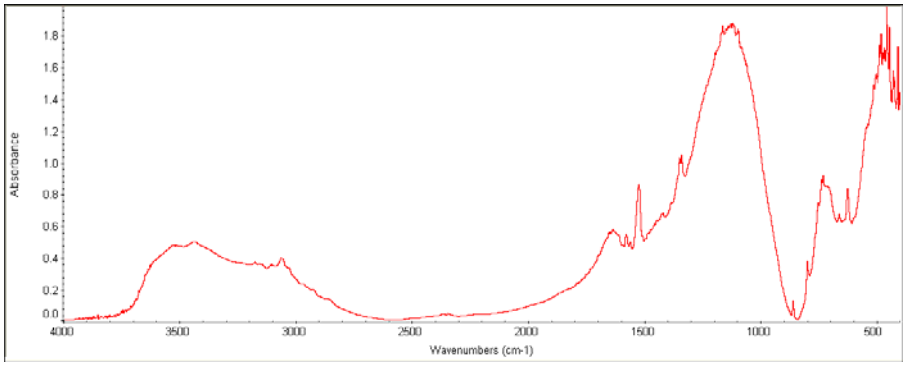

Figure 7.15 IR spectra of photocleaved and extracted phase 5 sample

Given that the as-made material undergoes a transformation to an ATV / dense phase material upon high temperature calcination, but remains in the as-made crystalline structure on photocleavage, we were interested in comparing the resulting materials. The phase transformation of an aluminophosphate material to ATV on high temperature calcination is not unusual, as this typically occurs during the calcination of $AlPO_4$-21 (structure code AWO). Scanning electron microscope micrographs of the photocleaved material (Figure 7.16a) and the ATV-like material that is formed on high-temperature calcination (Figure 7.16b) show that the crystals do not have an obvious crystal habit, with crystal sizes ranging from sub-micron to tens of microns. It is, of course, possible that the phase 5 material is a mixed phase, thus accounting for the range of crystal sizes and lack of definite crystal habit; in fact, many of the sub-micron to micron-sized crystals appear to be in a flat plate conformation. The calcined ATV / dense phase material looks very similar to the phase 5 material, in that there is no obvious crystal habit, although on the whole, the crystals for this phase are larger than that of the phase 5 material. Nitrogen adsorption measurements of the ATV / dense phase sample showed that the sample has 0.034 cc pore / g sample, of which 0.009 cc / g is due to microporosity, which is very low for zeolite materials. Interestingly, literature reports of the porosity of ATV materials state that the apertures of the ATV structure (3.0 Å by 4.9 Å) are either too distorted or too small to readily adsorb N_2, which explains the low porosity obtained.[19]

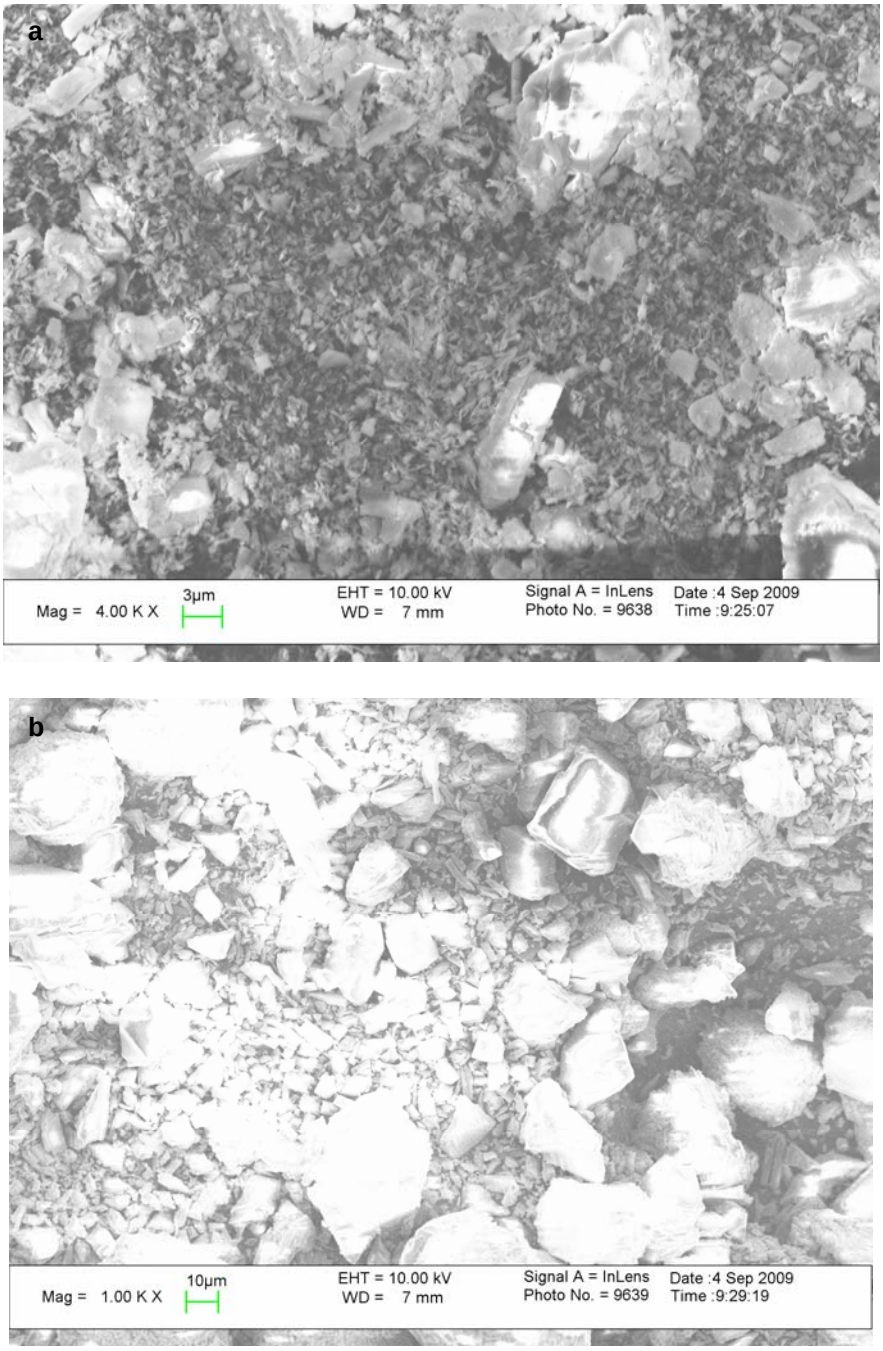

Figure 7.16 SEM micrographs of: (a) photocleaved phase 5 crystals and aggregates; (b) calcined ATV / dense phase material crystals and aggregates

3. Conclusions

The use of the photolabile molecule 1-(2-nitrobenzyl)-1H-imidazole (P-SDA 2) as a structure-directing agent in aluminophosphate and metal-substituted aluminophosphate zeolite syntheses resulted in the formation of crystalline aluminophosphate materials with unknown structures, potentially including the zeolite structure ATS. In general, the ability of this molecule to act in a structure-directing role for the production of aluminophosphate materials was confirmed; however, its ability to act as a structure-directing agent for aluminophosphate zeolites was not confirmed. Unlike many structure-directing agents, this molecule does not promote the crystallization of only one crystalline phase, rather, it can promote crystallization of a variety of materials. The addition of magnesium to the aluminophosphate reactive gels, however, narrowed the range of aluminophosphate phases produced to only two: phase 4 and phase 5. The latter of these could include material with the zeolite structure ATS. On calcination, the crystalline aluminophosphates with phase 5 produced materials with the zeolite structure ATV. The complete photocleavage of P-SDA 2 within the aluminophosphate materials was also demonstrated. Overall, the feasibility of a photolabile structure-directing agent route to the synthesis of crystalline aluminophosphates, rather than aluminophosphate zeolites, was demonstrated. This method could therefore provide a reasonable substitute for calcination for materials that require an organic additive to be crystallized, and can be formed with photolabile organic additives.

4. Experimental

4.1 Synthesis of P-SDA 2

P-SDA 2 was synthesized following literature procedures using standard S_N2 chemistry to protect the amino functionality of imidazole (Figure 7.14).[12]

Figure 7.17 Synthesis of P-SDA 2 via photochemical protection of the amino functionality of the imidazole

13.44 g of 2-nitrobenzylchloride (Aldrich) and 7.05 g of imidazole (sodium derivative, Acros) were combined in a 500 mL round-bottom flask equipped with a stirbar and covered in aluminum foil. A condenser was placed in the flask, which was then placed under an Ar atmosphere in an oil bath. Approximately 250 mL of anhydrous 1,2-dimethoxyethane (EMD) was added via syringe techniques to the flask, and the solution was refluxed at 90 °C for up to 12 h. The solution was filtered to remove the NaCl evolved, as well as unreacted reagents, and the solids were washed thoroughly with chloroform to fully remove any product in the solids. The filtrate was then rotovapped to remove the solvent, and 30 mL distilled, deionized (DDI) H_2O was added to dissolve the solids. The crude product was extracted from the aqueous phase with four washings of 50 mL ethyl acetate each, using a separation funnel. The organic phase was collected and evaporated using a rotovap to give a viscous orange to deep red liquid. The crude

product was recrystallized from ether, or toluene / ether to produce red crystals in approximately 30% yield.

4.2 Synthesis of Aluminophosphate Zeolites with SDA 2 and P-SDA 2

Aluminophosphates were synthesized with a final molar gel composition of 1 Al_2O_3 / x SDA / 1 P_2O_5 / y H_2O where x = 1, 1.5, 2, 2.5, and 3 and y = 40, 60, and 80. The structure-directing agent for these syntheses was either 1H-benzylimidazole (Aldrich, SDA 2), or 1-(2-nitrobenzyl)-1H-imidazole (P-SDA 2). These gels were created by first dissolving o-phosphoric acid (85 wt%, Fisher) in DDI H_2O (~ 30 wt % of the total DDI H_2O added) in a Teflon jar and adding the stirred solution to a suspension of Al_2O_3 • $2H_2O$ (Catapal Alumina Vista) in DDI H_2O (~ 70 wt% of the total DDI H_2O added) that had been stirred for 10 m. After combining, the slurry was stirred at room temperature for 2 h. The SDA was then added to the slurry, and the gel was then stirred for at least 1.5 h. The homogeneous gel was then crystallized, until phase separation at 140, 150, 175, or 200 °C in a Teflon-lined Parr autoclave, usually 48 – 96 hours. After removing the autoclave from the oven, the product was slurried in 35 mL of DDI H_2O in a 50 mL centrifuge tube, and the solution was centrifuged and decanted. The resulting solids were slurried with 35 mL of acetone (Fisher), and centrifuged several times, until the supernatant was clear. The solids were then air-dried at 100 °C overnight.

4.3 Synthesis of Metal-Substituted Aluminophosphate Zeolites with SDA 2 and P-SDA 2

Metal-substituted aluminophosphates were synthesized with a final molar gel composition of 0.8 Al_2O_3 / x SDA / 1 P_2O_5 / y H_2O / z MgO where x = 1 – 2, y = 10 – 100, and z = 0.2 – 0.4. The structure-directing agent for these syntheses was either 1H-benzylimidazole (Aldrich, SDA 2), or 1-(2-nitrobenzyl)-1H-imidazole (P-SDA 2). These gels were created by first dissolving o-phosphoric acid (85 wt%, Fisher) in DDI H_2O (~ 30 wt % of the total DDI H_2O added) in a Teflon jar and adding to the stirred solution $Al_2O_3 \bullet 2H_2O$ (Catapal Alumina Vista). After combining, the slurry was stirred at room temperature for 2 h. The SDA was then added to the slurry, and the gel was then stirred for another 2 h. The metal (anhydrous magnesium sulfate) was added, and the gel was stirred again for 2 h. The homogeneous gel was then crystallized, until phase separation at 150, 175, or 200 °C in a Teflon-lined Parr autoclave, usually 24 - 72 h. After removing the autoclave from the oven, the product was slurried in 35 mL of DDI H_2O in a 50 mL centrifuge tube, and the solution was centrifuged and decanted. The resulting solids were slurried with 35 mL of acetone (Fisher), and centrifuged several times, until the supernatant was clear. The solids were then air-dried at 100 °C overnight.

4.4 Photocleavage of P-SDA 2 in As-Made Aluminophosphate and Metal-Substituted Aluminophosphate Materials

The as-made, crystalline, aluminophosphate and metal-substituted aluminophosphate materials were suspended in DDI H_2O via sonication for 5 min. and drop-coated onto glass slides bounded by sticky tape, and allowed to air-dry for 24 h. Using a UVP Blak-

Ray long-wave mercury arc lamp, the samples were irradiated for 6 h. After cleavage, the samples were scraped off the glass slides, and stirred for 2 h each with acetone (Fisher), chloroform (EMD), and ethyl acetate (EMD), filtering between each step, to extract the organic fragments.

4.5 Characterization

The materials were characterized using a combination of liquid-state ^{1}H and solid-state ^{13}C nuclear magnetic resonance (NMR), infrared spectroscopy (IR), thermogravimetric analysis (TGA), and powder X-ray diffraction (XRD). NMR analysis was carried out with a Varian Mercury 300 MHz spectrometer (liquid state) and a Bruker AM 300 MHz spectrometer (solid-state). IR analysis was carried out on a Nicolet Nexus 470 FTIR spectrometer. TGA was performed on a NETZSH STA 449C analyzer in air using an aluminum sample pan. XRD was carried out on a Scintag XDS 2000 diffractometer operated at -45 kV and 40mA using Cu K_α radiation (λ = 1.54056 Å) in the 2θ range of 2-40 at a step size of 0.5 ° / min. Porosity measurements were carried out on using nitrogen adsorption techniques with a Micromeritics ASAP 2000.

5. References

[1] Lee, H., Zones, S. I. & Davis, M. E. A combustion-free methodology for synthesizing zeolites and zeolite-like materials. *Nature* **425**, 385-388 (2003).

[2] Lee, H., Zones, S. I. & Davis, M. E. in *Recent Advances In The Science And Technology Of Zeolites And Related Materials, Pts A - C* Vol. 154 *Studies In Surface Science And Catalysis,* 102-109 (2004).

[3] Lee, H., Zones, S. I. & Davis, M. E. Zeolite synthesis using degradable structure-directing agents and pore-filling agents. *J. Phys. Chem. B* **109**, 2187-2191 (2005).

[4] Lee, H., Zones, S. I. & Davis, M. E. Synthesis of molecular sieves using ketal structure-directing agents and their degradation inside the pore space. *Microporous Mesoporous Mat.* **88**, 266-274 (2006).

[5] Clark, T. *et al.* A new application of UV-ozone treatment in the preparation of substrate-supported, mesoporous thin films. *Chem. Mater.* **12**, 3879-3884 (2000).

[6] Li, Q. H., Amweg, M. L., Yee, C. K., Navrotsky, A. & Parikh, A. N. Photochemical template removal and spatial patterning of zeolite MFI thin films using UV/ozone treatment. *Microporous Mesoporous Mat.* **87**, 45-51 (2005).

[7] Cooper, E. R. *et al.* Ionic liquids and eutectic mixtures as solvent and template in synthesis of zeolite analogues. *Nature* **430**, 1012-1016, doi:10.1038/nature02860 (2004).

[8] Yang, X. B., Camblor, M. A., Lee, Y., Liu, H. M. & Olson, D. H. Synthesis and crystal structure of As-synthesized and calcined pure silica zeolite ITQ-12. *J. Am. Chem. Soc.* **126**, 10403-10409 (2004).

[9] Zones, S. I. & Burton, A. W. Diquaternary structure-directing agents built upon charged imidazolium ring centers and their use in synthesis of one-dimensional pore zeolites. *J. Mater. Chem.* **15**, 4215-4223, doi:10.1039/b500927h (2005).

[10] Il'ichev, Y. V., Schworer, M. A. & Wirz, J. Photochemical reaction mechanisms of 2-nitrobenzyl compounds: Methyl ethers and caged ATP. *J. Am. Chem. Soc.* **126**, 4581-4595, doi:10.1021/ja039071z (2004).

[11] Piggott, A. M. & Karuso, P. Synthesis of a new hydrophilic o-nitrobenzyl photocleavable linker suitable for use in chemical proteomics. *Tetrahedron Lett.* **46**, 8241-8244, doi:10.1016/j.tetlet.2005.09.077 (2005).

[12] Pillai, V. N. R. Photoremovable Protecting Groups in Organic Synthesis. *Synthesis* **1980**, 1-27 (1980).

[13] Cuberes, M. R., Morenomanas, M. & Trius, A. Alpha-Lithiation of N-arylmethylimidazoles and Triazoles - A General Method for the Synthesis of 1,2-diaryl-1-(N-azolyl)-ethanes. *Synthesis-Stuttgart*, 302-304 (1985).

[14] Utzinger, G. E. N-substituierte Arylhydroxylamine und deren Umwandlungsprodukte. *Justus Liebigs Annalen der Chemie* **556**, 50-64 (1944).

[15] Szostak, R. *Molecular Sieves: Principles of Synthesis and Identification*. 2nd ed., (Blackie Academic & Professional, 1998).

[16] Greene, T. W. *Protective Groups in Organic Synthesis*. (John Wiley & Sons, Inc., 1981).

[17] Morris, R. E., Burton, A. W., Bull, L. M. & Zones, S. I. SSZ-51 - A New Aluminophosphate Zeotype: Synthesis, Crystal Structure, NMR and Dehydration Properties. *Chem. Mater.* **16**, 2844-2851 (2004).

[18] Baerlocher, C., Meier, W. M. & Olson, D. H. *Vol. 2006*. (International Zeolite Association, 2006).

[19] Chen, J. S. *et al.* Cobalt-substituted Aluminophosphate Molecular-Sieves - X-Ray Absorption, Infrared Spectroscopic, and Catalytic Studies. *Chem. Mater.* **4**, 1373-1379 (1992).

Chapter 8: Summary and Conclusions

1. Summary and Conclusions

This thesis is the result of two separate pieces of zeolite science research that address different issues in the development of new synthetic routes to zeolite thin films. Part I of this thesis presents the development of a new route to the synthesis of fluoride-mediated, pure-silica zeolite thin films, with a particular emphasis on the application of these films as low dielectric constant (low-*k*) materials. Past efforts to utilize pure-silica zeolite thin films in applications such as chemical sensors, membrane reactors, and microelectronic devices have been limited by the number of pure-silica zeolite materials that can be accessed via current zeolite thin film synthetic approaches. These approaches include *in situ* crystallization (a process where the zeolite films is grown in situ onto a bare substrate from a dilute precursor solution that is free from preformed crystals), and the spin-on of zeolite nanoparticle suspensions. Of the 19 zeolite topologies with pure-silica compositions, only 4 (structure codes MFI, MEL, *MRE, and BEA*) have been prepared into films for zeolite low-*k* applications. A facile method that could produce films of this type – and therefore extend the library of pure-silica zeolite materials available for use – would be of great use.

Two methods for the synthesis of fluoride-mediated, zeolite thin films were examined to determine if they could overcome the limitations of fluoride-mediated zeolite syntheses, which render them incompatible with standard film synthesis techniques. The first method utilised a seeding and dilution modification to typical *in situ* film syntheses. The

second method applied the vapor phase transport method to the zeolite mineralizing agent, fluoride, to crystallize a precursor film deposited by dip-coating techniques. These methods were investigated using fluoride-mediated zeolites with the LTA topology, which is potentially useful as a low-*k* material when synthesized in the pure-silica composition, due to its low framework density. Although the modification of typical *in situ* synthesis procedures by seeding and diluting the zeolite precursor gel resulted in the ability to obtain germanosilicate and silicate zeolites with the LTA topology within a greatly increased composition range, the modification did not yield films of these materials. This was due in part to the degradation of the substrate materials used due to direct contact with the fluoride mineralizing agent. However, using the vapor phase transport of fluoride (VPTF) method, thin films of silicate and germanosilicate zeolites with the LTA topology were obtained on a variety of substrates, which included (100) silicon, glass, and quartz materials. This method also used chemical techniques to modify the surface of the substrates was used to promote good adhesion of the resulting films to the surface of the substrate. The films were characterized by a combination of X-ray diffraction, field emission scanning electron microscopy, X-ray energy dispersive analyses, and mechanical testing via nanoindentation to determine their quality. From these analyses, the films were determined to be polycrystalline, intergrown, continuous, and well-adhered to their substrates. Additionally, the silicate films were determined to have mechanical properties capable of withstanding the chemical-mechanical polishing techniques used in fabrication of microelectronic devices, one of the potential applications for pure-silica zeolite thin film materials.

To evaluate if the vapor phase transport of fluoride method could further expand the library of pure-silica zeolite materials available as thin films, the thin film synthesis of the pure-silica zeolite systems CHA, ITW, STT, and -SVR were attempted using the vapor phase transport of fluoride method. These attempts yielded thin films of each type of material on surface-modified, (100) silicon wafers. Like the pure-silica zeolite LTA thin films, the CHA, STT, ITW, and -SVR films were polycrystalline, intergrown, continuous, and well-adhered to their substrates. The films are characterized by a combination of techniques, including X-ray diffraction and field emission scanning electron microscopy.

As mentioned above, the development of pure-silica zeolite thin films as low dielectric constant (low-*k*) materials is of particular interest to the semiconductor industry. In order to decrease the feature size in integrated, without potentially increasing cross-talk noise and energy dissipation, the industry must develop an ultra-low-*k* (between 2.3 – 2.6) material to replace nonporous silica ($k = 4.0$) as the dielectric film insulating the wiring between transistors. Pure-silica zeolites have *k*-values that are tunable based on the selection of topologies with different porosities, which are functions of their framework density. For instance, the LTA topology has the lowest framework density (FD = 14.2) among all available pure-silica zeolites, and therefore could have the lowest dielectric constant. Additionally, zeolites could be useful as low-*k* materials due to their high mechanical strength, high heat conductivity, high thermal stability, and high chemical stability. For these reasons, the exploration of low-framework density, pure-silica zeolites as low-*k* materials has generated great interest.

The fluoride-mediated, pure-silica LTA, CHA, STT, ITW, and -SVR zeolite powders and films were investigated for low dielectric constant (low-*k*) material applications. The pure-silica ITQ-29 (LTA) films synthesized in Chapter 3 using this method were demonstrated to have a *k*-value of 1.69 via parallel-plate capacitance measurements, which is the lowest value experimentally obtained on any zeolite film. The pure-silica zeolite powders crystallized in conjunction with the film syntheses of these materials were examined via Time Domain Reflectometry at high frequencies to determine their dielectric properties. This investigation demonstrated that these materials were appropriate for low-*k* applications, especially the LTA topology, which has the lowest intrinsic dielectric constant of all the pure-silica zeolites. Consistent with our previous studies, all the zeolites investigated here, except STT, gave *k*-values lower than predicted from their porosities using the Bruggeman effective medium model, which has been commonly used and found valid for correlating dielectric constants of amorphous porous silicas with their porosities. Comparison of the dielectric data to the k-values of other pure-silica zeolites measured using this technique also showed interesting dielectric behavior with respect to porosity. These data demonstrated that the dielectric properties of zeolites are affected by their pore structures, even though they are still primarily a function of porosity. Generally, materials with low framework density *and* high symmetry structures were shown to have low relative permittivities.

Part I of this thesis demonstrates that there is an inherent difference between zeolites and other porous silicas with respect to the relationship between porosity and relative

permittivity, and suggests that by using zeolites, the dielectric properties can be tailored based on not only porosity, but also pore architecture. Using this general relationship between the dielectric constant, and the porosity / pore structure of the zeolite, it is possible to tune the final values of the dielectric properties of the materials. Additionally, Part I shows that the vapor phase transport of fluoride is a facile and general method for the synthesis of fluoride-mediated, zeolite thin films, specifically those with the pure-silica composition. Lastly, the techniques demonstrated here could expand the current library of zeolite films available for a variety of applications.

Part II of this thesis focuses on the development of a photolabile structure-directing agent that could be used to promote zeolite crystallization. This technique would enable the removal of the structure-directing agent from within the zeolite pore space via photolysis and extraction, rather than thermal calcination, which can be incompatible with nontraditional zeolite applications that require the synthesis of thin films, membranes, and nanoparticles of various sizes. Additionally, calcination results in the complete destruction of the structure-directing agent, which can be very expensive and therefore cost-prohibitive for use on an industrial scale. A photolysis technique that selectively cleaves the photolabile molecule could allow for the partial recycling of the structure-directing agent, thus reducing overall costs. Towards this end, the development of partially recyclable, photo-cleavable structure-directing agents is investigated using molecules in the 2-nitrobenzyl family of photoactive molecules, which have been used extensively in the organic synthesis of polyfunctional materials, and undergo photolysis

via long-wave UV radiation with a Hg arc lamp to generate the unstable 2-nitrosophenyl derivative of the 2-nitrobenzyl photochemical protecting group.

The first photolabile structure-directing agent (designated as P-SDA 1) developed was a derivative of 8,8-dimethyl-2-phenyl-1,4-dioxa-8-azoniaspiro[4,5]decane hydroxide, an acid-cleavable molecule that has been demonstrated to produce the zeolite known as mordenite (structure code MOR). The synthesis of P-SDA 1, 8,8-dimethyl-2-(2-nitrophenyl)-1,4-dioxa-8-azoniaspiro[4.5]decane hydroxide, had not previously been reported in literature, but was synthesized via standard ketalization reaction procedures, where a diol is used to protect the ketone functionality of a molecule, followed by the production of a water molecule. This reaction was followed by quaternization of the amine present, and ion exchange to the final hydroxide form, generating P-SDA 1 in approximately 50% overall yield. Cleavage of the photolytic P-SDA 1 was first demonstrated in a homogeneous solution of acetronitrile, and then demonstrated while intercalated into a dealuminated zeolite with the FAU structure, which is an open-framework zeolite used as a model to evaluate the ability of P-SDA 1 to undergo photolysis while confined within the pore system of a zeolite framework. The structure-directing ability of P-SDA 1 was evaluated via attempts to synthesize silicate and aluminosilicate zeolites through procedures similar to those that result in the crystallization of various compositions of the BEA* and MFI zeolite structures. These syntheses resulted in the formation of primarily amorphous and layered materials. One synthesis did yield crystalline material with the MFI zeolite topology; however, this synthetic result was not reproducible. The inability of this molecule, when compared to

its acid-cleavable equivalent that could produce crystalline material with the zeolite structure MOR, to produce a zeolite material was likely due to a combination of factors. These included its larger size, bulkier aromatic group, and changed electrostatic interaction potential due to the presence of the nitro substituent's electron-withdrawing nature when compared to the acid-cleavable equivalent of P-SDA 1. Although this particular molecule did not demonstrate the feasibility of the photolabile structure-directing agent route to zeolite syntheses, it did demonstrate the ability of the 2-nitrobenzyl class of molecules to cleave within a zeolite pore space when the material is in planar conformation. This suggested that this class of molecules could be useful for this route; further investigation of this route was therefore focused on the development of smaller photolabile structure-directing agents.

The second photolabile structure-directing agent (designated P-SDA 2) developed was 1-(2-nitrobenzyl)-1H-imidazole. Imidazole-based structure-directing agents have been used to synthesize a variety of zeolite phases, including zeolites with the ITW, MTT, TON, and MTW topologies, and other novel zeotype structures. The organic molecule was synthesized according to literature procedures via the photochemical protection of the imidazole functionality by the 2-nitrobenzyl photochemical protecting group, which resulted in P-SDA 2 in 30% overall yield. The structure-directing ability of P-SDA 2 was evaluated via synthetic attempts to produce aluminophosphate zeolites, using procedures based on the syntheses of $AlPO_4$-5 (structure code AFI), VPI-5 (structure code VFI), and MAPO-34 (structure code CHA). The aluminophosphate class of zeolites, which crystallizes under acidic conditions, is unusual in that crystallization of these materials

can occur in a matter of hours, rather than days, as with aluminosilicate zeolites. In this case, a control molecule, 1-benzyl-1H-imidazole, a non-photoactive molecule designated as SDA 2, was used to screen conditions for the synthesis of aluminophosphate zeolites, resulting in the production of $AlPO_4$-5 (structure code AFI) and $AlPO_4$-36 (structure code ATS). This control molecule was also used to demonstrate the synthesis of MAPO-36 (structure code ATS) under metal-substituted, aluminophosphate synthetic conditions. Attempts to synthesize aluminophosphate zeolites with P-SDA 2 using conditions that produced microporous crystalline material with SDA 2 yielded several unknown, and likely mixed, crystalline phases, although the primary results of these syntheses were dense phases and hydrated phases. The addition of magnesium to the synthesis, using MAPO-34 procedures, also resulted in the synthesis of unidentified crystalline materials. In all of these materials, P-SDA 2 was shown to be intact by ^{13}C cross-polarization magic-angle spinning nuclear magnetic resonance (CPMAS NMR) as well as infrared spectroscopy (IR). Complete photocleavage of P-SDA 2 within the crystalline, aluminophosphate materials was also demonstrated by ^{13}C CPMAS NMR; photolysis was carried out on the as-made crystalline samples deposited in a thin layer via drop-coating techniques onto glass slides. Extraction of the imidazole fragment that was produced by photolysis was carried out via soxhlet extraction.

Overall, the feasibility of the photolabile structure-directing agent route to zeolite synthesis was unfortunately not completely demonstrated. P-SDA 1 was unable to reproducibly promote the crystallization of any stable crystalline phase, likely due to its large size; potentially, it could still be useful as a structure-directing agent using other

reactive gel compositions or reaction conditions. P-SDA 2, on the other hand, was very capable of producing crystalline aluminophosphate materials, which were easily reproduced. However, none of the crystalline materials was a known zeolite phase. It is likely that one of the phases crystallized with P-SDA 2 contained a zeolite (probably ATS) combined with an unknown phase; however, repeated syntheses were unable to selectively promote the crystallization of only the ATS phase. Additionally, on calcination, some of the crystalline aluminophosphate material produced with P-SDA 2 was structurally transformed to a known aluminophosphate zeolite phase, ATV; however, this transformation was only seen at high temperatures, which also resulted in the destruction of P-SDA 2. P-SDA 2 was obviously capable of acting in a structure-directing role, even though it did not result of the production of known zeolite materials. It is possible that, under other conditions, P-SDA 2 could produce a known zeolite phase. Lastly, even though neither photolabile structure-directing agent was demonstrated to reproducibly crystallize a known zeolite material, both molecules were shown to be capable of photolysis while confined in a crystalline material. This suggests that this route could still be feasible if the photolabile structure-directing agent is appropriately matched to the synthetic conditions.

2. Future Directions

Micropatterned zeolite films and membranes are potential candidates for use in or development of chemical sensor micro-arrays, nanoreactors, molecular storage, and catalysis. Additionally, the ability to directly manage the spatial zoning of open- and closed-pore zeolites is of intrinsic interest to the design of optical and semiconductor

devices. The vapor phase transport of fluoride route to fluoride-mediated, pure-silica zeolite thin films developed here could be useful for a number of applications involving micropatterning. First, given that the method is used to crystallize an amorphous precursor gel adhered to a substrate by various coating techniques, the possibility exists to coat the surface with a micropattern using inkjet technology. When crystallized, this could result in novel, nanostructured materials that could be useful to the development of zeolite-coated cantilever sensors, for example. The ability to precisely control where the zeolite is deposited could be very beneficial. Second, this method could be used to synthesize patterned zeolite films, or more precisely, synthesize micropillars of continuous zeolite crystals, via lithographic techniques. Here, we can envision the use of standard lithography techniques to pattern a silicon substrate with a gold grid, with empty spaces that could be later filled in with a zeolite precursor gel that is then crystallized using the vapor phase transport of fluoride route. The gold grid could then be removed using standard lift-off procedures, resulting in the production of a micro-array of zeolite pillars on a surface. These pillars could then be used to evaluate the mechanical properties of the zeolites via nanoindentation techniques. This would be useful, as the mechanical properties of only a few zeolites have been studied to this point, due in part to the difficulty of producing large enough single crystals to evaluate. Lastly, it could be possible to combine the thin film synthesis techniques developed here with the photolabile structure-directing agent route to zeolite crystallization if the appropriate photoactive organic molecule was found. Some spatial patterning of microporous materials has been done using UV irradiation / ozonolysis and physical masks, but it results in the destruction of the structure-directing agent used to synthesize the zeolite

films. Using a photolabile structure-directing agent to generate zeolite thin films would allow patterning and pore functionalization of the zeolite pore space in conjunction with patterning of the zeolite film itself. Overall, the techniques developed here could be very useful for the development of micropatterned zeolite films and membranes.